U.S. Department of Transportation

Federal Railroad Administration

Investigation of the Relationship between Crashworthiness Performance and Weight for High-Speed Train Operations in the U.S.

Office of Research,
Development
and Technology
Washington, DC 20590

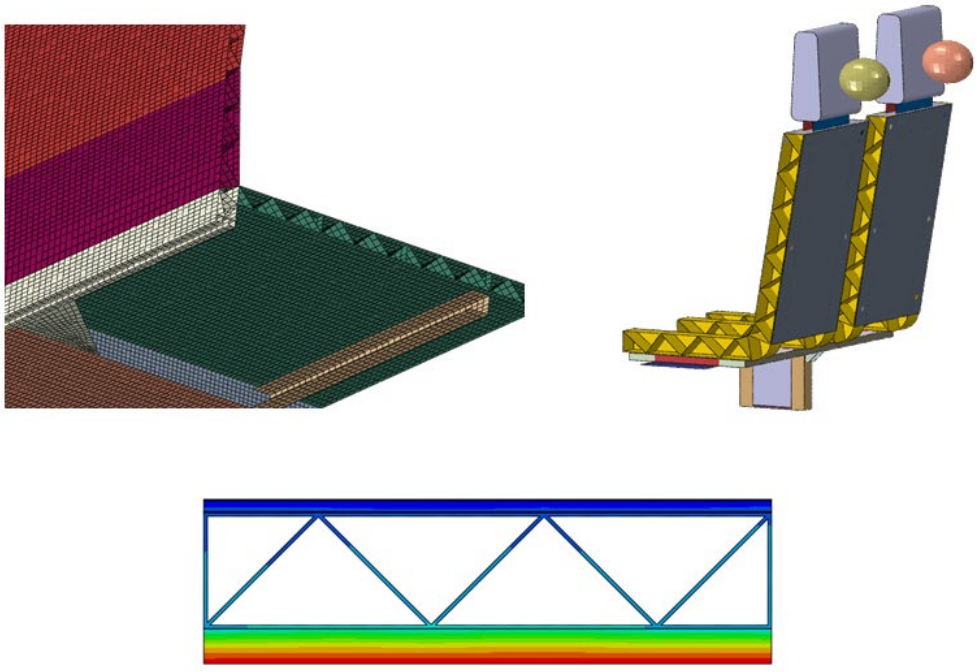

DOT/FRA/ORD-20/36

Final Report
August 2020

REPORT DOCUMENTATION PAGE

Form Approved
OMB No. 0704-0188

1. AGENCY USE ONLY (Leave blank)	2. REPORT DATE	3. REPORT TYPE AND DATES COVERED
	August 2020	Technical Report, 08/09/2012 to 12/13/2013

4. TITLE AND SUBTITLE
Investigation of the Relationship between Crashworthiness Performance and Weight for High-Speed Train Operations in the U.S.

5. FUNDING NUMBERS
DTFR53-12-C-00021

6. AUTHOR(S)
Ronald A. Mayville, Richard G. Stringfellow, Nicholas D. Catella, Kevin J. LaMalva

7. PERFORMING ORGANIZATION NAME(S) AND ADDRESS(ES)
Simpson Gumpertz & Heger Inc.
41 Seyon Street
Waltham, MA 02453

TIAX, LLC
35 Hartwell Ave.
Lexington, MA 02421

8. PERFORMING ORGANIZATION REPORT NUMBER

9. SPONSORING/MONITORING AGENCY NAME(S) AND ADDRESS(ES)
U.S. Department of Transportation
Federal Railroad Administration
Office of Railroad Policy and Development
Office of Research, Development and Technology
Washington, DC 20590

10. SPONSORING/MONITORING AGENCY REPORT NUMBER
DOT/FRA/ORD-20/36

11. SUPPLEMENTARY NOTES
COR: Jeff Gordon

12a. DISTRIBUTION/AVAILABILITY STATEMENT
This document is available to the public through the FRA website.

12b. DISTRIBUTION CODE

13. ABSTRACT (Maximum 200 words)
This report describes an evaluation of the effects of increased crashworthiness performance on high-speed train weight. The crashworthiness features investigated include occupied volume strength, energy absorption systems, seats, and fire protection systems. In each case, a baseline model was developed to represent the high-speed train subsystem. The baseline models were then modified to improve crashworthiness, and the incremental weight associated with these changes was also calculated. Finite element analysis was used to conduct the calculations. The results indicated that significant weight increases would occur by imposing the 8g/250 ms American Public Transportation Association crash pulse requirement for seat testing. Changes to the other features resulted in weight increases, but these were not as substantial as for seats.

14. SUBJECT TERMS
High-speed train, crashworthiness, weight, seats, structural fire protection, energy absorber, occupant volume strength

15. NUMBER OF PAGES
88

16. PRICE CODE

17. SECURITY CLASSIFICATION OF REPORT	18. SECURITY CLASSIFICATION OF THIS PAGE	19. SECURITY CLASSIFICATION OF ABSTRACT	20. LIMITATION OF ABSTRACT
Unclassified	Unclassified	Unclassified	

NSN 7540-01-280-5500

Standard Form 298 (Rev. 2-89)
Prescribed by
ANSI Std. 239-18
298-102

METRIC/ENGLISH CONVERSION FACTORS

ENGLISH TO METRIC	METRIC TO ENGLISH
LENGTH (APPROXIMATE)	**LENGTH (APPROXIMATE)**
1 inch (in) = 2.5 centimeters (cm)	1 millimeter (mm) = 0.04 inch (in)
1 foot (ft) = 30 centimeters (cm)	1 centimeter (cm) = 0.4 inch (in)
1 yard (yd) = 0.9 meter (m)	1 meter (m) = 3.3 feet (ft)
1 mile (mi) = 1.6 kilometers (km)	1 meter (m) = 1.1 yards (yd)
	1 kilometer (km) = 0.6 mile (mi)
AREA (APPROXIMATE)	**AREA (APPROXIMATE)**
1 square inch (sq in, in^2) = 6.5 square centimeters (cm^2)	1 square centimeter (cm^2) = 0.16 square inch (sq in, in^2)
1 square foot (sq ft, ft^2) = 0.09 square meter (m^2)	1 square meter (m^2) = 1.2 square yards (sq yd, yd^2)
1 square yard (sq yd, yd^2) = 0.8 square meter (m^2)	1 square kilometer (km^2) = 0.4 square mile (sq mi, mi^2)
1 square mile (sq mi, mi^2) = 2.6 square kilometers (km^2)	10,000 square meters (m^2) = 1 hectare (ha) = 2.5 acres
1 acre = 0.4 hectare (he) = 4,000 square meters (m^2)	
MASS - WEIGHT (APPROXIMATE)	**MASS - WEIGHT (APPROXIMATE)**
1 ounce (oz) = 28 grams (gm)	1 gram (gm) = 0.036 ounce (oz)
1 pound (lb) = 0.45 kilogram (kg)	1 kilogram (kg) = 2.2 pounds (lb)
1 short ton = 2,000 pounds (lb) = 0.9 tonne (t)	1 tonne (t) = 1,000 kilograms (kg) = 1.1 short tons
VOLUME (APPROXIMATE)	**VOLUME (APPROXIMATE)**
1 teaspoon (tsp) = 5 milliliters (ml)	1 milliliter (ml) = 0.03 fluid ounce (fl oz)
1 tablespoon (tbsp) = 15 milliliters (ml)	1 liter (l) = 2.1 pints (pt)
1 fluid ounce (fl oz) = 30 milliliters (ml)	1 liter (l) = 1.06 quarts (qt)
1 cup (c) = 0.24 liter (l)	1 liter (l) = 0.26 gallon (gal)
1 pint (pt) = 0.47 liter (l)	
1 quart (qt) = 0.96 liter (l)	
1 gallon (gal) = 3.8 liters (l)	
1 cubic foot (cu ft, ft^3) = 0.03 cubic meter (m^3)	1 cubic meter (m^3) = 36 cubic feet (cu ft, ft^3)
1 cubic yard (cu yd, yd^3) = 0.76 cubic meter (m^3)	1 cubic meter (m^3) = 1.3 cubic yards (cu yd, yd^3)
TEMPERATURE (EXACT)	**TEMPERATURE (EXACT)**
[(x-32)(5/9)] °F = y °C	[(9/5) y + 32] °C = x °F

QUICK INCH - CENTIMETER LENGTH CONVERSION

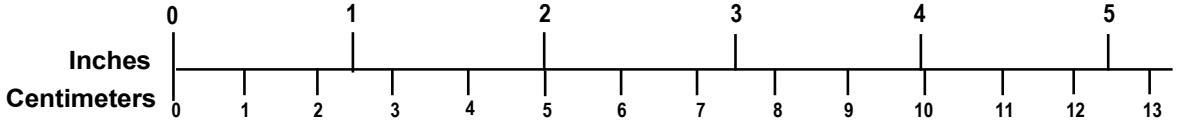

QUICK FAHRENHEIT - CELSIUS TEMPERATURE CONVERSIO

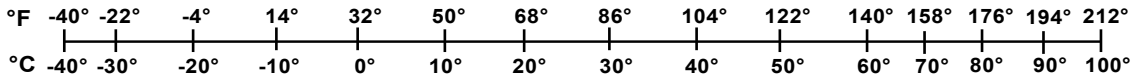

For more exact and or other conversion factors, see NIST Miscellaneous Publication 286, Units of Weights and Measures. Price $2.50 SD Catalog No. C13 10286

Updated 6/17/98

Acknowledgements

The authors would like to acknowledge Jeffrey Gordon of the Federal Railroad Administration for his technical and programmatic input for this project.

Contents

Illustrations

Tables

Executive Summary

The objective of this report was to determine the effect of increased crashworthiness performance on the weight of high-speed trains. Weight is a particularly critical factor for high-speed trains because of its effects on acceleration and the overall wear-and-tear of both rail vehicles and infrastructure, each of which are finely tuned in high-speed operations to provide safe and comfortable service to customers.

Between August 2012 and December 2013, researchers at SGH, Inc. and TIAX, LLC focused the weight assessment on four vehicle subsystems: occupied volume (car shell), energy absorbers, seats, and structural fire protection systems. In each case, researchers generated a baseline model approximately representative of current high-speed trains. They selected this model to meet the recently proposed Tier III requirements, but with little or no margin. The research team generated variations on this baseline model to provide greater crashworthiness performance and determine the weight associated with the changes. They used finite element analysis to evaluate the performance in each case, except for energy absorbers.

Among the key results, researchers found that for an aluminum extrusion occupied volume, increasing the strength by 25 percent increases carbody weight by about 1,500 lbs.

The estimated weight penalty associated with increasing the required collision scenario speed by 5 mph is comparable to that required to increase the occupied volume strength by 25 percent. However, this assessment is complicated by a few factors. A substantially lower increase in absorber weight could be achieved if carbon fiber-reinforced polymers were used instead of metal, but the cost would be much higher and it would be more difficult to ensure repeatable behavior.

The weight penalty estimated for seats is based on occupant compartmentalization and, effectively, seat strength measures of crashworthiness improvement; the results suggest that the injury measures are probably not controlling. In effect, seat stiffness in this study was modified by simply increasing the thickness of the model elements. Seat stiffness could be modified with a lower weight penalty by changing the depth of sections or using alternative materials, such as fiber-reinforced polymers. Such changes affect meeting spatial and cost requirements. Higher seat attachment strength is also required with more severe crashworthiness requirements, but these can likely be accommodated without a substantial weight penalty.

The results pertaining to the study of fire protection supports the general belief that it is difficult for cars built from aluminum extrusions to meet the current U.S. structural fire resistance requirements, particularly if a 30-minute duration is specified. Nevertheless, it seems likely that the requirements could be met with the addition of a layer of fire protection material on the underside of the aluminum floor structure. The additional weight in this case could be as low as 350 lbs/car if a mineral wool blanket system were used and if the attachment approach were sufficiently robust.

Researchers noted that a methodology of simply changing a baseline configuration to meet new requirements and calculating weight differentials ignores the elements of the actual design process. In reality, a high-speed train will have limitations on weight, usually expressed in terms of axle load, and the systems incorporated into the train must be adjusted to meet this weight budget. Such changes promote innovation and the pursuit of alternate equipment. Thus, one

may also view the results of this study as indicative of the degree of difficulty created by requiring higher crashworthiness performance.

1. Introduction

This report describes the results of a research program to investigate the relationship between weight and crashworthiness performance for high-speed trains.

A desired characteristic of high-speed trains is low weight. Weight not only influences the ability to propel the train to high speeds, but it also affects the design, weight, and maintenance of many subsystems. These subsystems include the trucks and equipment needed to brake the train and track infrastructure. The suppliers of high-speed equipment have spent considerable time and effort to keep the weight of their trains as low as possible while accommodating the other systems needed for safety, operation, and convenience. Table 1 lists the axle load of typical high-speed trains compared to conventional U.S. trains.

Table 1. Typical axle loads for U.S. and high-speed trains

Train	Typical Axle Load (tons*){tonnes}
U.S. light rail	8.3 {7.5}
U.S. transit	10.5 {9.5}
U.S. commuter	16 {14.5}
U.S. intercity	17 {15.4}
European high speed	14-17 {12.7-15.4}
Japanese high speed	12 {10.9}

*Empty weight: 1 ton = 2,000 lbs

Note that the weight of European high-speed trains is not substantially different from U.S. commuter and intercity trains, which comply with U.S. structural requirements. Nevertheless, the concern raised by car builders on increasing crashworthiness is that it would result in weight penalties that would render the service-proven equipment considerably less reliable. The very light weight of Japanese trains can be attributed in part to significantly less stringent crashworthiness requirements, which is justified through an intense focus on crash avoidance.

1.1 Background

The Federal Railroad Administration (FRA) and the railroad industry have been active over the last few years in developing structural standards for high-speed trains in the U.S. There have been many discussions regarding the differences between conventional U.S. Tier I equipment and the high-speed equipment operating in Europe and Asia. The structural standards for each are very different; high-speed train car builders maintain that the requirement to have their trains possess the crashworthiness characteristics of U.S. Tier I trains would result in heavier components, heavier vehicles, with an adverse effect on their service-proven equipment. The work reported here is intended to provide some information to judge the accuracy of the car builders' contention.

1.2 Objectives

This report includes a review of existing and proposed crashworthiness requirements, and then, an analysis of the effect of higher crashworthiness performance on weight for each of the following subsystems:

- Occupied volume structure
- Energy absorption systems
- Seats
- Fire protection systems

1.3 Overall Approach

Researchers at SGH, Inc. and TIAX, LLC focused the weight assessment on four vehicle subsystems: occupied volume (car shell), energy absorbers, seats, and structural fire protection systems. In each case, they generated a baseline model approximately representative of current high-speed trains. This model was selected to meet the recently proposed Tier III requirements, but with little or no margin. The research team generated variations on this baseline model to provide greater crashworthiness performance and determine the weight associated with the changes. They used finite element analysis to evaluate the performance in each case, except for energy absorbers.

1.4 Scope

The focus in this report is on Tier III passenger equipment, defined as equipment that can run up to 220 mph on dedicated rights-of-way, which can also run in mixed traffic (e.g., with freight trains) at speeds below 125 mph. The proposed crashworthiness requirements for this train class differ from the conventional Tier I requirements, which will be summarized in the next section and described in greater detail in the individual sections dedicated to the subsystems.

Table 2 lists high-speed traincar builders reviewed for this report.

Table 2. Manufacturers of high-speed trains

Train	Manufacturer
Velaro	Siemens
AGV, ETR	Alstom
250	Talgo
Zefiro	Bombardier
N700	Nippon-Sharyo
E5	Kawasaki

1.5 Organization of the Report

The report is organized as follows:

Section 2 provides a summary of current U.S. carbody crashworthiness requirements for conventional (Tier I) and high-speed trainsets (Tier III). An objective of this study is to determine the changes in weight required to achieve higher crashworthiness performance than that required for Tier III.

Section 3 describes the results of analyses to estimate the weight increase associated with increasing the crashworthiness of the occupied volume (the space normally occupied by the

passengers and operators also referred to as occupied volume integrity or OVI) for high-speed trains.

Section 4 discusses various components of the crush zone, including energy absorbers. Most high-speed trains with crush zones incorporate several elements to provide energy absorption and each contributes to the overall weight of the crush zone which varies substantially depending on the particular design approach and the amount of energy to be absorbed.

Section 5 includes discussion on passenger seats, which represent a significant component of weight of high speed trains. Calculations were conducted to obtain an approximate relationship between seat crashworthiness performance and seat weight.

Section 6 provides an analysis of the influence on railcar weight of various fire protection strategies. This is an important consideration, as high-speed train car manufacturers have reported difficulty meeting the U.S. CFR structural fire resistance requirements for their lightweight aluminum structures.

Section 7 contains a summary of the major findings from the analyses of the four subject high-speed train subsystems in terms of incremental weight increase (on a per car basis) and overall conclusions. It is noted that none of these incremental increases in weight are substantial compared to the overall weight of a high speed rail car.

Section 8 contains the references cited in this report.

2. Summary of Current U.S. Carbody Crashworthiness Requirements

Current crashworthiness requirements for high-speed trains in the U.S. are under development. The FRA Railroad Safety Advisory Committee (RSAC) Engineering Task Force (ETF) has recently proposed structural requirements for the new high-speed Tier III category that are substantially different than the requirements for conventional U.S. trains. The new regulation went into effect on November 20, 2018. Comparable changes have also been proposed for Tier I equipment, which is equipment that always runs at speeds below 125 mph, possibly in mixed operation. All regulatory proposals have been made with the goal of achieving crashworthiness performance equivalent to or exceeding that of current U.S. equipment. Table 3 provides a comparison between the new requirements and those for conventional Tier I trains. Part of the objective of the study is to determine the changes in weight required to achieve higher crashworthiness performance than those listed for Tier III found in Table 3.

Table 3. Comparison of rail vehicle crashworthiness requirements (kip = 1000 lbs; anthropomorphic test device (ATD)

Parameter	Current CFR requirement	Proposed ETF Tier III requirement
Buff strength	800 kips	337 kips, but with additional crash energy management requirements
Occupied volume strength	800-kip buff strength	Strength on the load path of the crush zone elements of either: a) 800 kips (no yield) b) 1,000 kips (< 5% plastic strain) c) 1,200 kips (ultimate strength not reached)
Collision energy absorption (train-to-train collision)	None	20 mph collision with a freight locomotive-led train*
Collision energy absorption (grade crossing collision)	120,000 ft-lbf (corner post); 135,000 ft-lbf (collision post)	Same
Passenger seats	8/4/4 g static; 8g-250 ms pulse; maintain seat structural integrity; satisfy certain ATD* injury measures	5g-100 ms pulse with min. $\Delta V = 5$ m/s and pulse more severe than determined in train-to-train collision simulation; maintain seat structural integrity; satisfy certain ATD injury measures
Structural fire resistance	Satisfy E 119 test for at least 15 minutes.	Satisfy E 119 test for at least 15 minutes; may include bottom cover.

* Cab-led high-speed train consists are assumed in this study. The RSAC ETF also proposes a 25-mph collision speed for other consist configurations.

3. Occupied Volume

The occupied volume corresponds to the space normally occupied by the passengers and operators. Occupied volume integrity (OVI), or strength, is a measure of a railcar's ability to resist intrusion into the occupied space in the event of a collision. The primary measure of OVI in the U.S. has been the traditional buff strength, in which the carbody is required to carry a longitudinal compression load applied through the buff stops of the couplers at each end without causing yielding of the structural members. The new Tier III requirements permit an alternate definition of OVI as described below.

Introduction

This section describes the results of analyses to estimate the weight increase associated with increased OVI for high-speed trains. A summary of the requirements is provided, followed by a general description of high-speed train occupied volume design. The results of analyses are then presented to provide an approximate relationship between occupied volume strength and carbody weight.

3.1 OVI Requirements

OVI requirements for Tier III equipment are specified in two categories:

1. The ability to resist intrusion in a defined train-to-train collision.
2. Static longitudinal strength

To meet the Tier III collision scenario requirement—a collision between two trains at 20 mph without significant deformation of the occupied volume (described in greater detail in Section 4)—it is necessary to have an energy-absorbing crush zone at least at the cab ends of the train if not at all coupled or connected interfaces. The static strength requirements are specified in terms of the collision load path and at the coupler connection point. The collision load path at the cab end will include the points at which individual energy absorbers are connected to the carbody. It may also include the pushback coupler connection to the car if the coupler does not have a shear-off mechanism that separates it from the load path after pushback.

The collision load path at coupled or connected interfaces may also be through crushable energy absorber locations, or it may be restricted to the coupler, if the coupler is intended to absorb all the energy at these locations. In either case, each Tier III car is also required to sustain a minimum load of 337 kips (1,500 kN) along the line of the couplers without yielding (without the simultaneous action of other loads.) The collision load path in conventional U.S. rail cars is through the coupler only, since these have generally not been designed to push back.

The Tier III static strength requirements applied to the collision load path are as follows (see also Table 4):

- No permanent deformation of the carbody at an applied load of 800 kips
- Limited permanent deformation (less than 5 percent plastic strain) of the carbody at an applied load of 1,000 kips
- No crippling (exceedance of ultimate load-carrying capacity) at an applied load of 1,200 kips.

If the collision load path were only through the coupler, the first of these options would be equivalent to the current conventional buff strength requirement.

The collision load path for cab ends that have crush zones including energy absorbers usually comprises several locations so that the static load would be applied at these locations in proportion to the load from the individual absorbers. These locations are usually at the floor level, but are also at some level above the floor. This leads to a more uniform load distribution over the carbody cross section than the conventional buff load.

Most high-speed train car builders have shown evidence they can meet two or more of these criteria, as shown in Table 4 (as of 2011).

Table 4. Survey of car builders' compliance with ETF Tier III occupied volume strength criteria (from ETF meetings)

Criterion	Car Builder			
	Alstom	Bombardier	Siemens	Talgo
800 kips	Y	Y	N	Y*
1000 kips	Y	Y	Y	Y
1200 kips	Y	Y	Y	Y

*Talgo indicated that a "minor modification" to standard car design is required to meet the 800 kip criterion.

Technically, occupied volume strength is also assured by requiring side, roof and end frame strength, with the latter to mitigate the effects of grade crossing collisions. However, these measures are not treated in this report.

3.2 High-Speed Train Carbody Design

To evaluate the relationship between carbody structural weight and occupied volume strength, it is necessary to determine materials and geometric configurations typically used in high speed train carbody design. However, due to their proprietary nature, high-speed train car builders do not make carbody design details available to the public. Therefore, typical high-speed train carbody designs were determined based on a review of published research, publicly available patent literature, and discussions with high-speed train car builders.

All the high-speed train car builders listed in Table 4 use aluminum extrusions. This structural approach yields a light-weight car shell that is relatively easy to fabricate. The extrusion sections forming the overall cross section are usually less than 3.3 feet (1 m) wide and over 66 feet (20 m) in length and are connected by longitudinal welds; openings for windows, doors, hatches, and other needs are machined into the extrusions. Other aluminum pieces are welded onto the extrusions or into openings to form items such as the bolsters and reinforcements for doors and windows. An example carbody cross-section of aluminum extrusions is shown in Figure 1.

Aluminum extrusions are hollow, thin-shelled elements that generally consist of a top and bottom flange connected by diagonal web members, as shown in Figure 2. Because the welding of these extrusion alloys leads to significant reduction in the yield strength (by nearly 50 percent in the heat affected zones), it is common to include local reinforcement in the welded zone to compensate for this effect, which is shown in Figure 3.

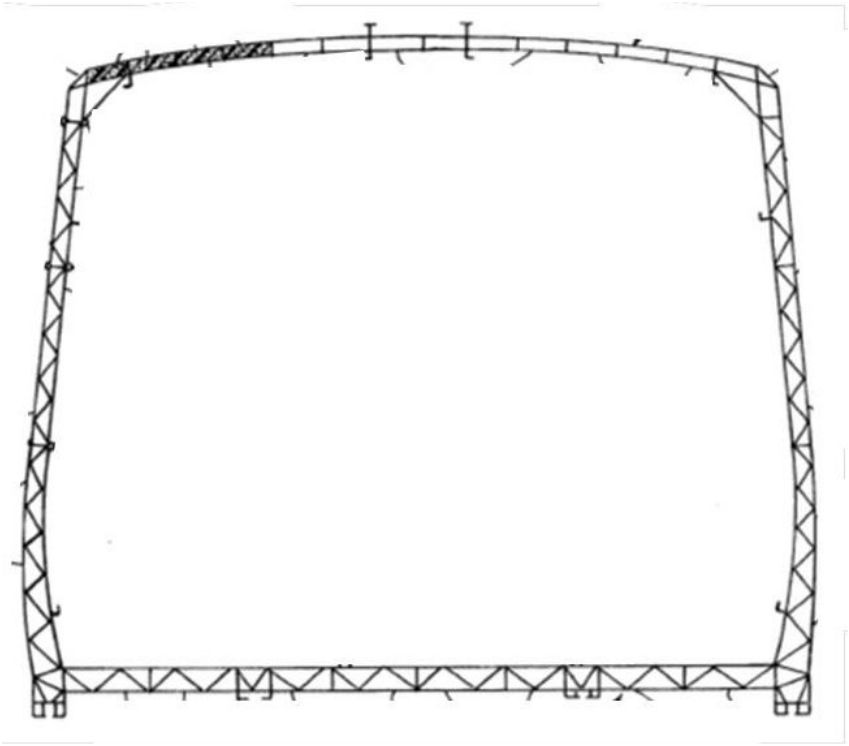

Figure 1. High-speed rail carbody constructed of aluminum extrusions [1]

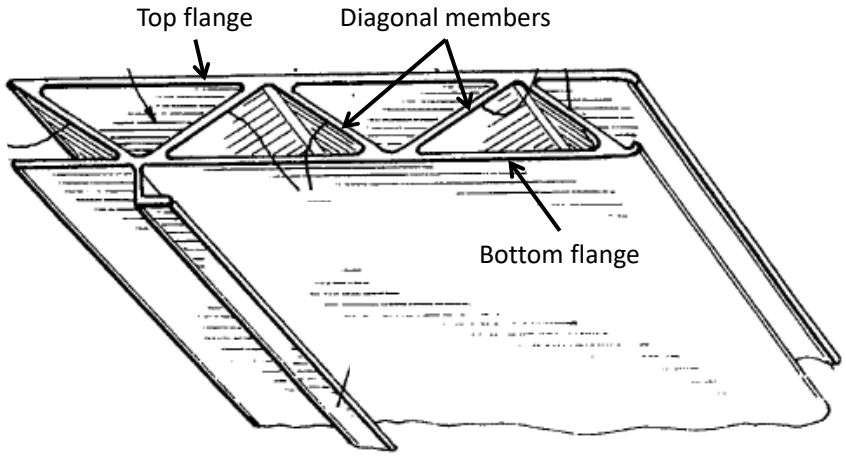

Figure 2. Typical aluminum extrusion element used for side wall construction [1]

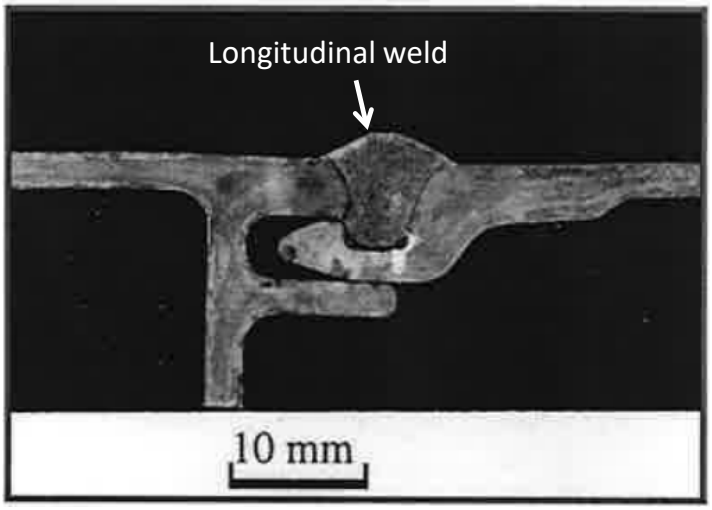

Figure 3. Section cut of an aluminum extrusion showing the longitudinal weld detail between the top flange of adjacent elements [2]

Some Japanese high-speed train car builders use an integrally stiffened carbody approach to car shell design [3]. Carbodies composed of integrally stiffened panels have an appearance similar to sheet and stringer construction. However, in the case of these carbodies, the members and skin are extruded as a single unit. An example carbody composed of integrally stiffened panels is shown in Figure 4. As with the aluminum extrusions described earlier, the welded regions of integrally stiffened panels must be detailed so that the heat-affected zone does not control section strength. Figure 5 shows a weld detail between two integrally stiffened panel elements in which the thickness of the panels is increased in the heat-affected zone.

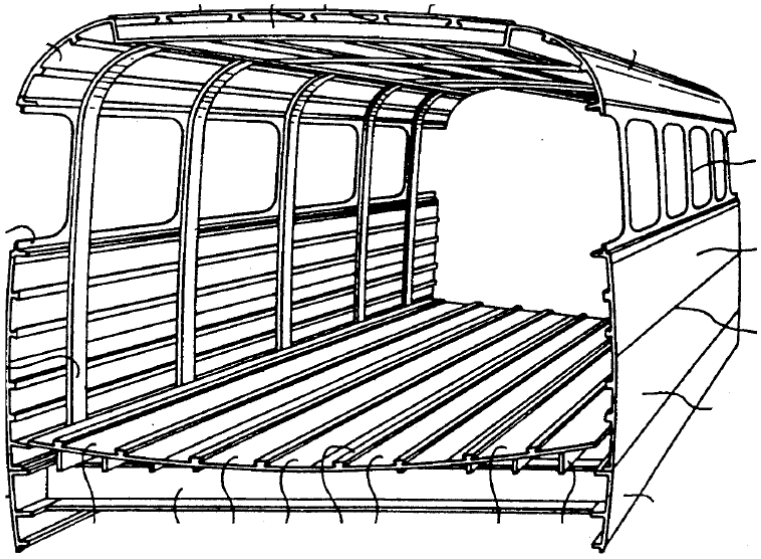

Figure 4. High-speed rail carbody of integrally stiffened panel construction [3]

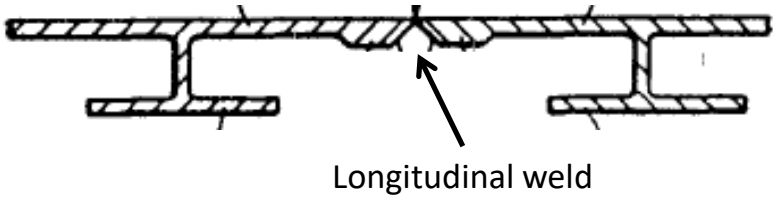

Figure 5. Weld detail between two integrally stiffened panel elements [3]

Geometric discontinuities play an important role in determining carbody strength. Common geometric discontinuities include:

- Transition from the cab end structural frame to the main carbody structure
- Door and window openings in side walls
- Connections between the floor and sides and the body bolster
- Abrupt changes in depth, cross-sectional area, or stiffness of structural members

First yield typically occurs at the stress concentrations associated with discontinuities. After yielding, structural elements subjected to compressive forces are also more prone to local buckling and, eventually, crippling.

3.3 Selection of Baseline Carbody Model

A baseline carbody design was needed to determine the effects of modifications on occupied volume strength and weight. It was not possible to obtain specifics of typical details of structural discontinuities, and the model eventually used was based on the authors' general knowledge of railcar design and fabrication. Given the unavailability of a specific design that is public, and in order to generalize across car builders, a generic carbody model was developed that included some of the key features common to high-speed trains. The intent was to create a model with an occupied volume strength of about 800 kips based on the no-yield criterion. The model assumed aluminum extrusion construction and includes some of the more significant structural discontinuities, since these generally control strength.

The baseline model for the study presented here had a substantial length of uniform cross section, with some openings, and a simulated operators' compartment, as shown in Figure 6. There are two planes of symmetry. The aluminum extrusions of the end portion of uniform cross section were modeled in detail and a central section was modeled with shell elements of equivalent stiffness properties to the extrusions as discussed below. The portion of uniform cross section corresponded to a carbody that is approximately 3 m (9.8 feet) tall by 3 m (9.8 feet) wide and 21 m (68.9 ft) long. A cross-section of the detailed segment, with section definitions, is shown in Figure 7. These same sections were used in both the detailed and simplified segments.

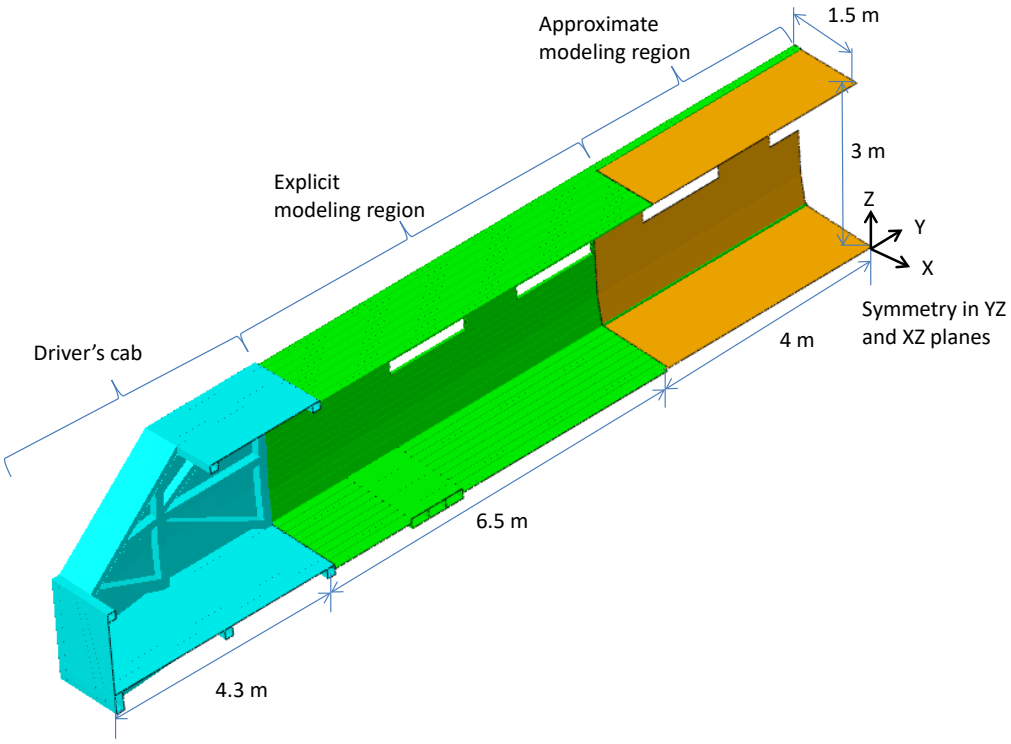

Figure 6. Schematic of the overall baseline finite element model

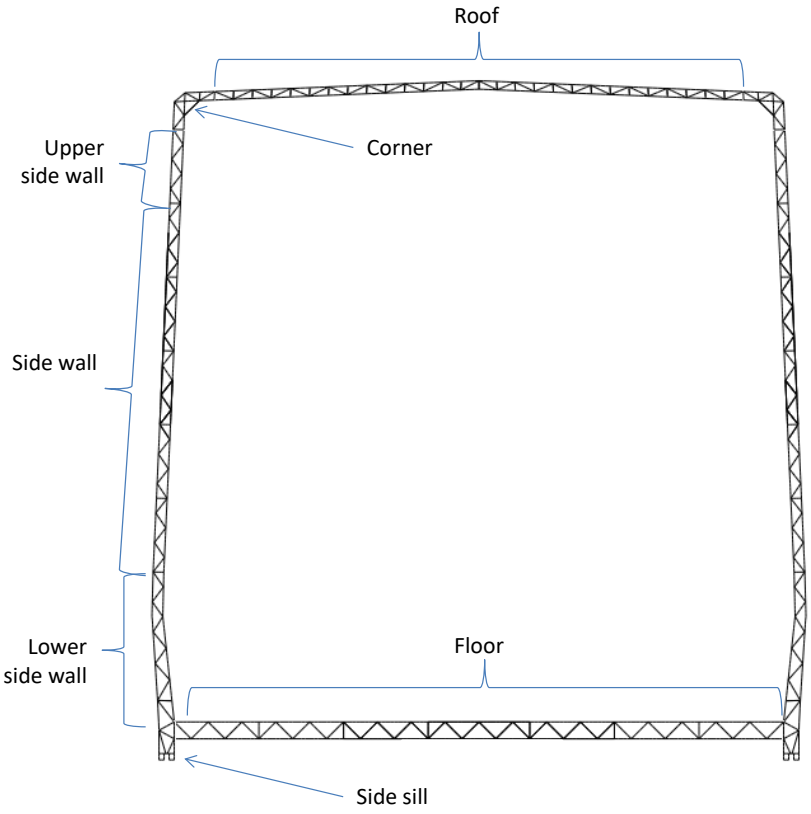

Figure 7. Baseline model cross section showing longitudinal aluminum extrusions

The dimensions of aluminum extrusions in the detailed cross section are listed in Table 5 with reference to Figure 8. For simplicity, the thickness of the upper and lower flanges and the diagonal webs are equal for a particular section. In reality, it is common for the webs to be thinner than the flanges. Additional dimensions of the side sill and corner profiles are shown in Figure 9. Comments from European high-speed rail car builders indicated that the thicknesses used in the baseline model here were lower than they use in practice. This was likely due to the need to accommodate elements such as discontinuities and attachments. The focus of the work here was only on longitudinal strength and did not capture all of these other effects.

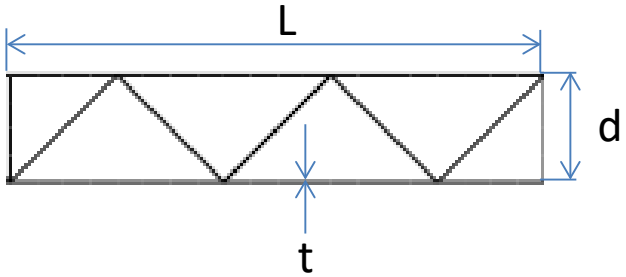

Figure 8. Dimensions of a generic aluminum extrusion cross section

Table 5. Aluminum extrusion section dimensions for the baseline model (see Figure 8 for definition of parameters; 1 mm = 0.040 in.)

Section	Dimension from Figure		
	t (mm)	d (mm)	L (mm)
Floor	2.5	80	400
Side sill	2.0	n.a.	n.a.
Center sill	4.0	n.a.	n.a.
Side wall	2.0 (flanges) 1.0 (diagonals)	90-63	750
Corner	2.0	n.a.	n.a.
Roof	2.0 (flange) 1.0 (diagonals)	60	360
Bolster box beam flanges	8.0	n.a.	n.a.
Bolster box beam webs	8.0	n.a.	n.a.
Bolster stiffeners	8.0	n.a.	n.a.
Bolster gusset plates	3.0	n.a.	n.a.

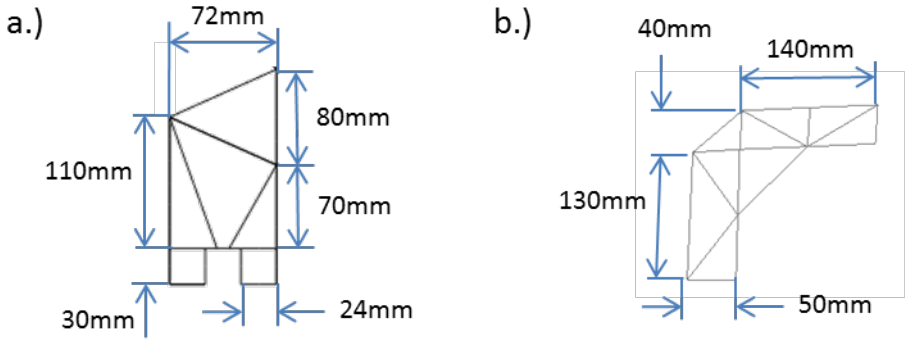

Figure 9. Cross-section from the finite element model of a.) side sill extrusion, b.) corner member extrusion (see also Table 5)

An image of two of the geometric discontinuities incorporated into the baseline carbody model is shown in Figure 10. The body bolster (referred to as "bolster" in this section) spanned between the side sills and interrupted the continuity of the floor extrusions, which caused redistribution of forces and stresses from the floor to the bolster and sides. The window opening caused redistribution of forces and stresses in the side wall. The redistribution of stresses in the floor and side wall was expected to result in stress concentrations in these locations. The window and bolster provided representative discontinuities and so a door opening was not included in the model.

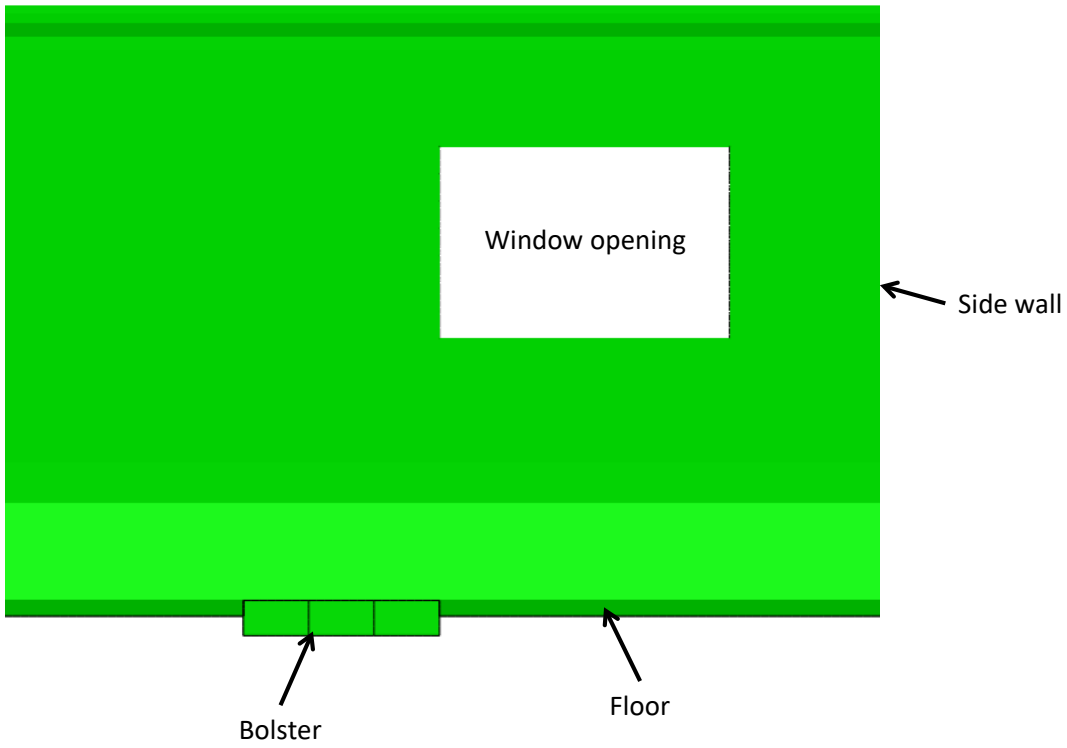

Figure 10. Schematic from the finite element model of geometric discontinuities

Figure 11 shows details of the model bolster region. A center member extended from the operator's cab to the bolster and is primarily intended to provide additional load carrying capacity for loads associated with buff and draft forces. This center member consisted of a channel shape with depth and width equal to 100 mm (3.94 in.). The centerline of the bolster was located 2 m (6.6 feet) from the point at which the operator's cab connects to the section of uniform cross-section. The bolster was composed of three box beams running in the transverse direction. The connection between the box beams and the longitudinal floor members was reinforced by stiffeners within the box beams. The connection between the bolsters and the side included triangular gusset plates. Member thicknesses and other key section dimensions for the bolsters and center sills are provided in Table 5.

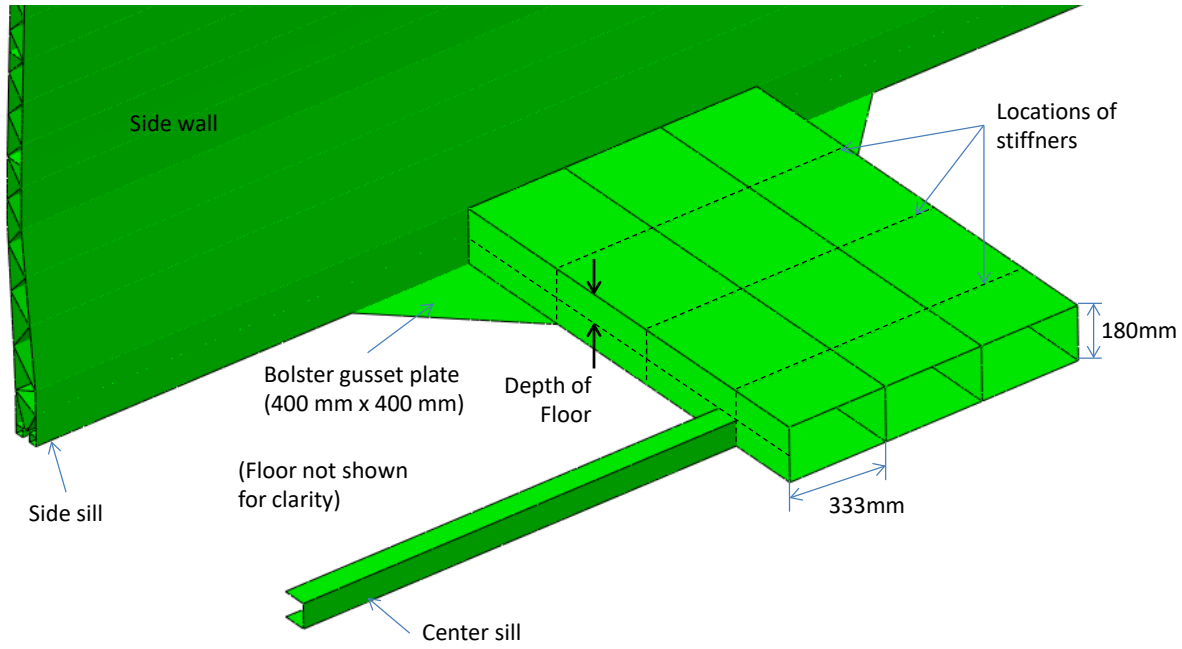

Figure 11. Section cut through center of the carbody finite element model showing bolster and center member details

The operator's compartment was included in the baseline carbody design, but the section properties were selected to ensure that strength was not controlled by this region. The purpose of including it was to obtain a more realistic distribution of load to the primary occupied volume. The model consisted of sheet and tube aluminum construction and is shown in Figure 12. It was recognized that the effect of having the transverse plane of symmetry resulted in a simulated car with a cab at each end. This was not a realistic situation, but it was felt that the essence of the occupied volume strength and the effect of section changes could still be captured by this approach while providing a simplified and efficient computational model.

The weight of the structural members within the model occupied volume of uniform cross section (that is, excluding the operator's cab) for the baseline was 4,300 kg (9,440 lbs).

a.)

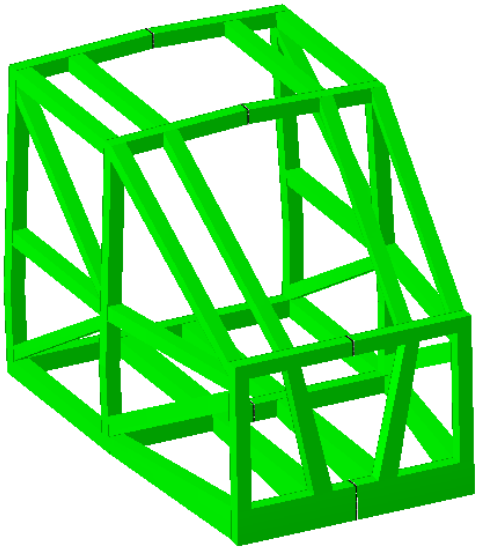

b.)

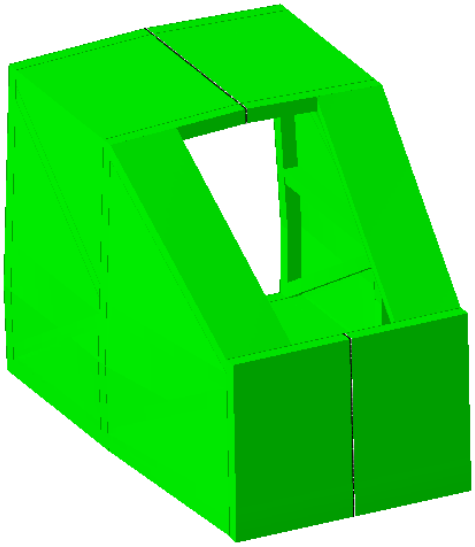

Figure 12. Schematic of the finite element model driver's cab a.) without structural skin, b.) with structural skin

3.4 Finite Element Analysis

Finite element analysis (FEA) was used to calculate occupied volume strength for the baseline model and its variants. The computer program Abaqus 6.13 was used for this purpose. Dimensions of the baseline carbody structural members were adjusted to approximately meet the 800 kip no-yield criterion. Results from the baseline carbody FEA were used to create iterative analysis models, in which the compressive strength of the carbody was increased by selectively adding material to highly stressed structural elements. Results from the iterative FEA models were used to develop a relationship between occupied volume strength and structural carbody weight.

An overall view of the carbody finite element model is shown in Figure 6. Again, the model used two planes of symmetry for computational efficiency. The aluminum extrusions (flanges and webs) were modeled explicitly with shell elements for the 6.5 m (21.3 foot) length of passenger occupied volume closest to the driver's cab. The remaining 4 m (13.1 feet) of passenger occupied volume were modeled with a single layer of shell elements, but utilizing the composite section property of Abaqus. The section property was selected to closely match the axial and flexural stiffness of the floor, roof, and side sill extrusions in the linear range of deformation. It was subsequently verified that this 4 m section remains elastic in the analyses conducted here. The tubes and sheet components of the operators' cab region were also modeled with shell elements. Aluminum extrusion detailing was simplified, as was shown in Figure 8; for example, diagonal members were assumed to intersect with the flanges at a single point.

Views of the finite element model mesh in a few locations are shown in Figure 13 and Figure 14. Note that, in general, there were eight elements in each flange section between diagonal webs, and there were four elements in the diagonal webs; there were some exceptions to this for some shorter segments. Window corner radii were not explicitly modeled, but a structural window frame was included.

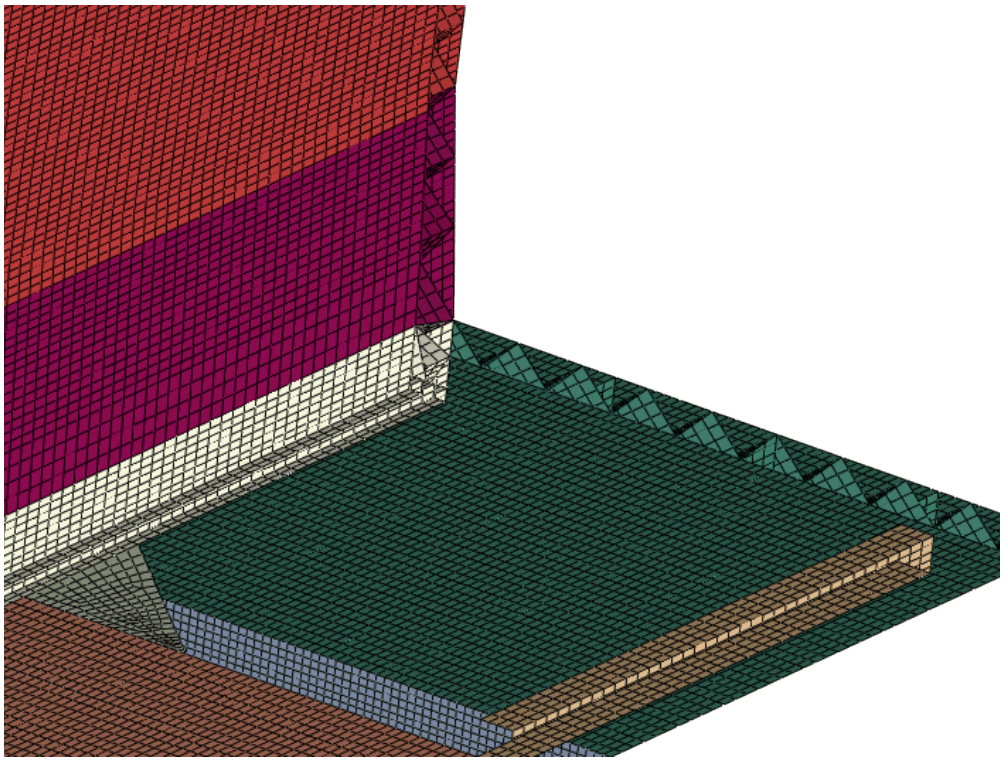

Figure 13. View of the finite element model mesh in the floor area

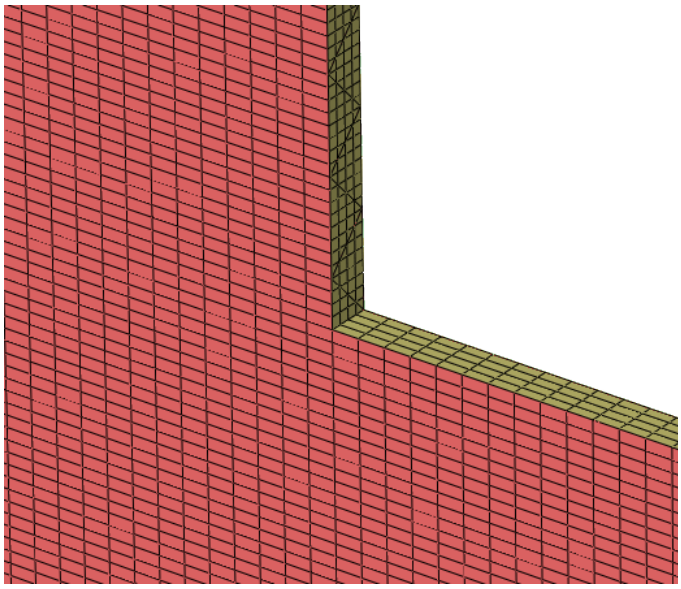

Figure 14. View of the finite element model mesh in the window area

All structural members in the model were assigned the material properties corresponding to the 6005A-T6 aluminum alloy, a common alloy used for aluminum railcar construction. (Note that this material is mainly used for the long extrusions; other aluminum alloys are used for other components.) The stress-strain curve used in the FEA was based on test data obtained from published research [2] and is shown in Figure 15; other material properties are shown in Table 6.

For simplification, heat-affected zones and weld details were omitted in the model. This was effectively an assumption that the welds did not control the various failure criteria.

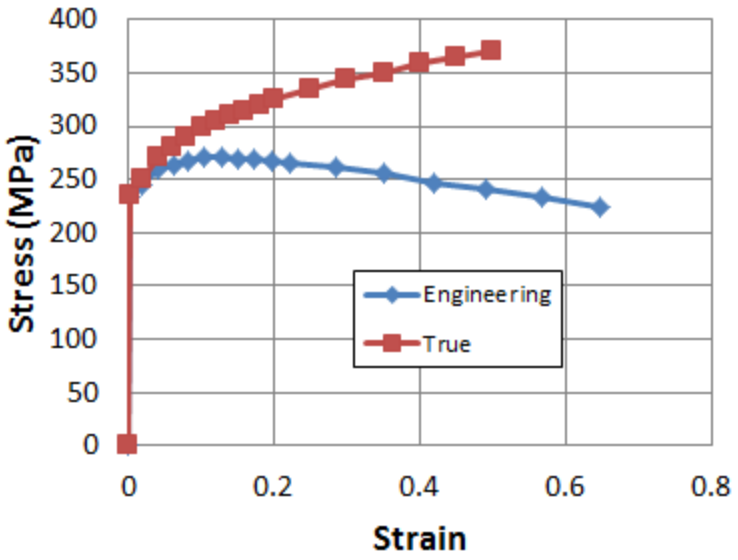

Figure 15. Stress-strain curve for 6005A-T6 aluminum alloy [2]

Table 6. Material properties for 6005A-T6 aluminum alloy [2]

Property	Value
Density	2700 kg/m^3 (0.1 lb/in^3)
Yield strength	235 MPa (34.1 ksi)
Tensile strength	270 MPa (39.2 ksi)
Elongation	8%

All analyses were performed using the Abaqus/Explicit solver under pseudo-static loading conditions. The longitudinal compressive load was applied to the front of the driver's cab through a rigid plate that had only a longitudinal degree of freedom. This approach permitted simulation of local and global buckling effects. The compressive load was applied by specifying the velocity versus time history of the rigid plate with a maximum rate of 0.4 m/s (1.3 ft/s). To ensure pseudo-static conditions were properly simulated, the kinetic energy of the model was verified to be less than 5 percent of the model's internal energy (an ETF criterion).

3.4.1 Results from Baseline Model

The results of the FEA suggested that the occupied volume strength of the baseline model met the Tier III requirements. The load-displacement curve obtained for this case is shown in Figure 16. Note that both load and displacement calculated from analysis of the baseline model have been multiplied by two in this plot to account for symmetry. The initial region of the curve showed essentially elastic behavior. The load remained relatively stable after the maximum load (crippling) was reached then dropped off sharply. The shape and magnitude of the load-

displacement curve from the baseline model was consistent with those reported in the ETF by high-speed railcar builders.

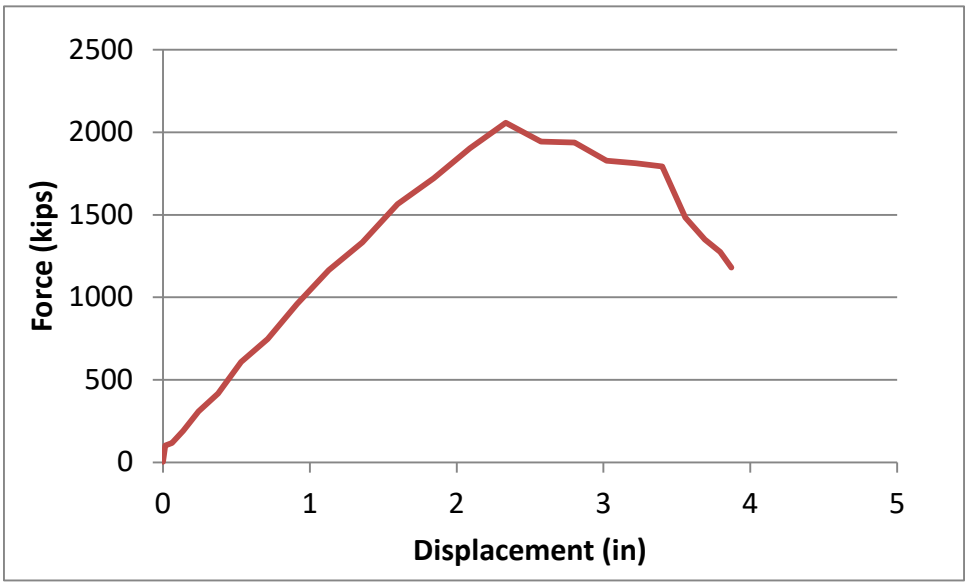

Figure 16. Load-displacement curve obtained from analysis of the baseline finite element model

First yield for the baseline model occurred at a load of 847 kips (3,767 kN), which was close to but greater than the Tier III minimum yield load of 800 kips. First yield occurred in the bottom flange of the floor adjacent to the bolsters (Figure 17). Yielding adjacent to an element such as the bolster was consistent with the expectation that occupied volume strength would be controlled by geometric discontinuities. Plastic strain of 5 percent (ETF criterion b) was also first reached in the bottom flange of the floor adjacent to the bolsters.

Figure 18 shows stress contours in the carbody at the moment when 5 percent plastic strain was reached. Note that at this point in the analysis, the stress contours appeared to undulate due to the local buckling mode shapes in the floor and side wall. Local buckling is discussed in greater detail below. The load at 5 percent plastic strain was 1,976 kips (8,789 kN), which was greater than the load required by Tier III (1,000 kips). The maximum compressive load for the baseline model was 2,058 kips (9,154 kN), which was greater than the load required by Tier III (1,200 kips). Crippling occurred along the floor and side wall just inboard of the bolster. Figure 19 shows stress contours in the carbody at the point of maximum compressive load.

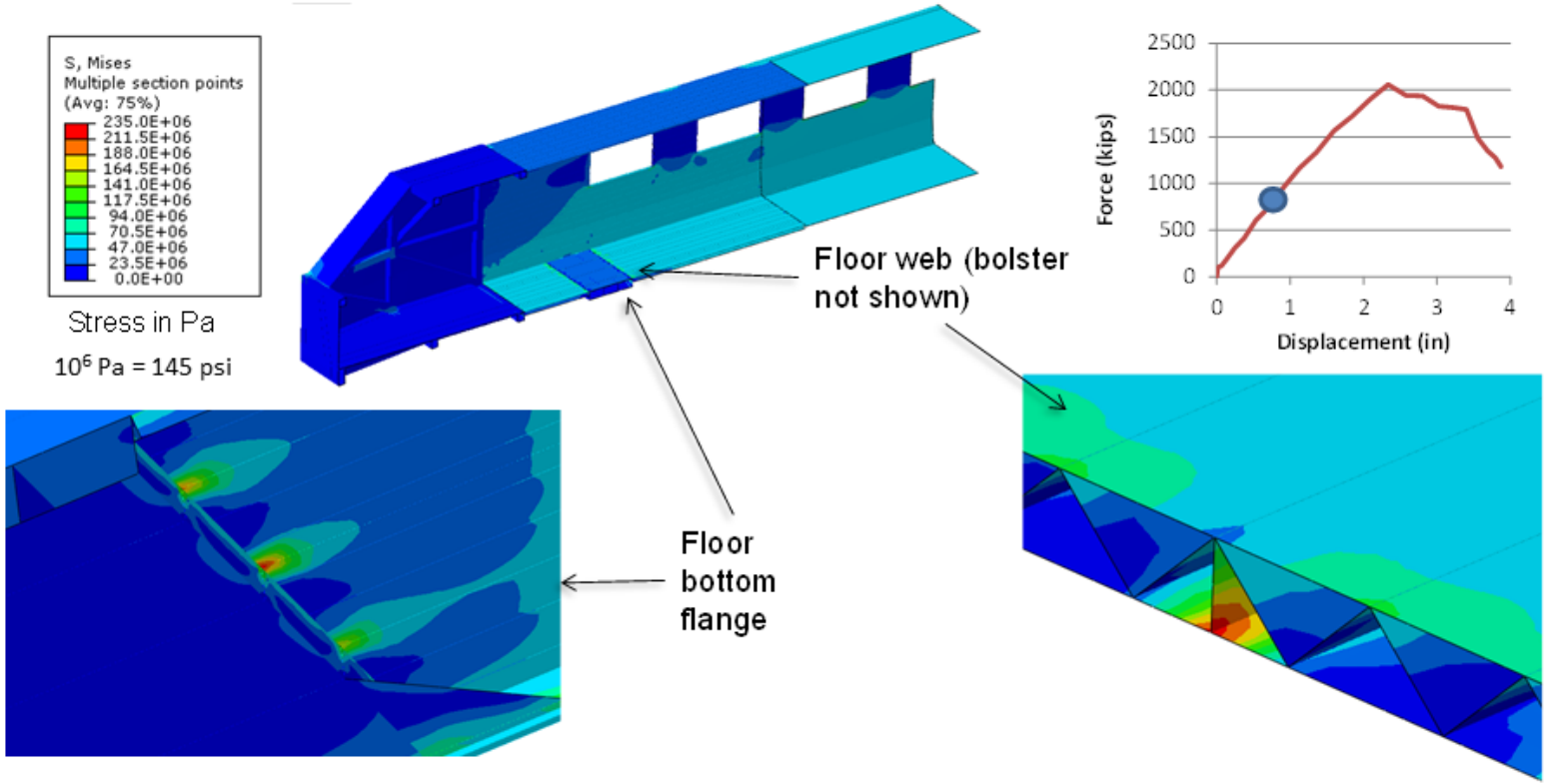

Figure 17. Stress contours of the baseline carbody model at first yield

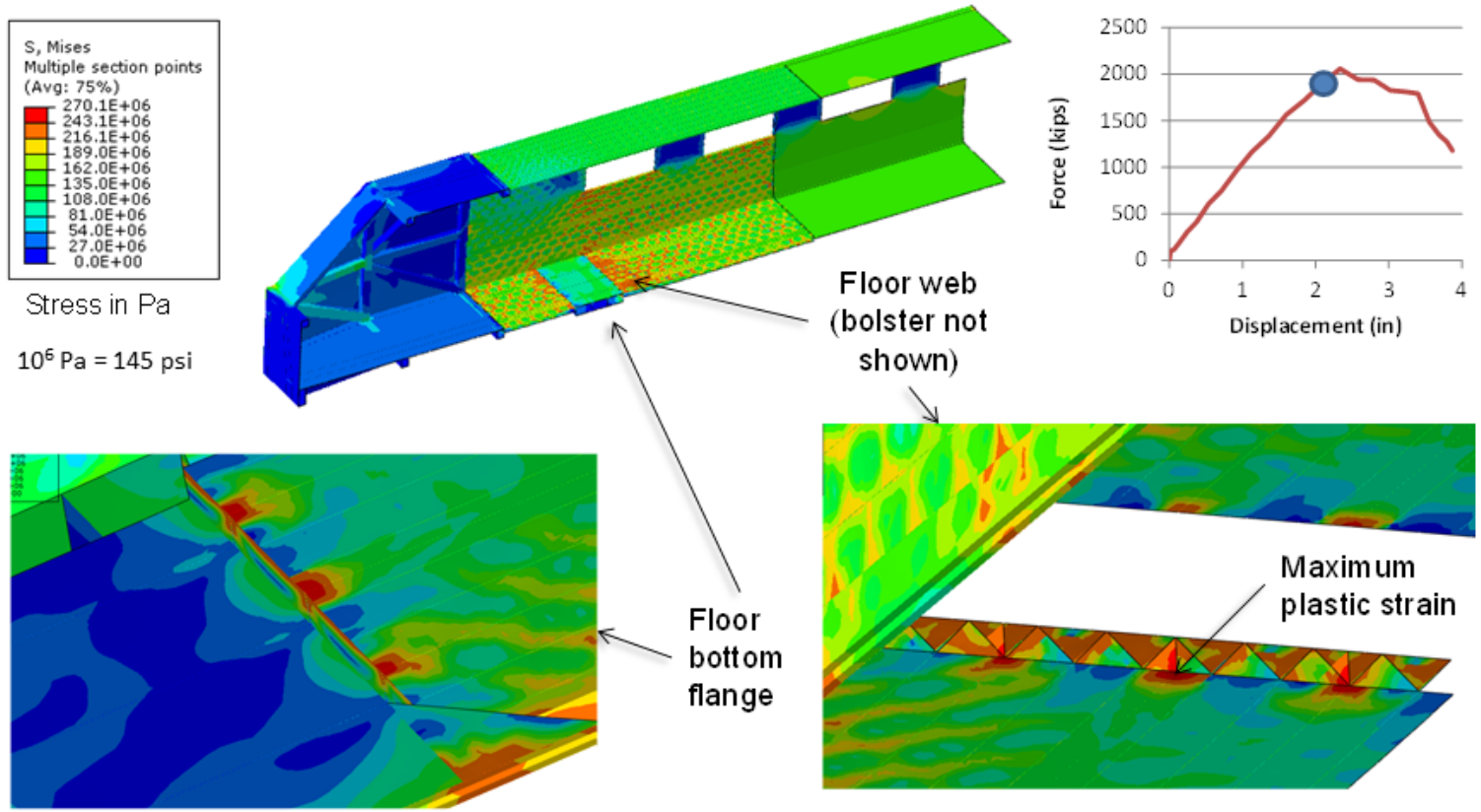

Figure 18. Stress contours of the baseline model at the first occurrence of 5 percent plastic strain

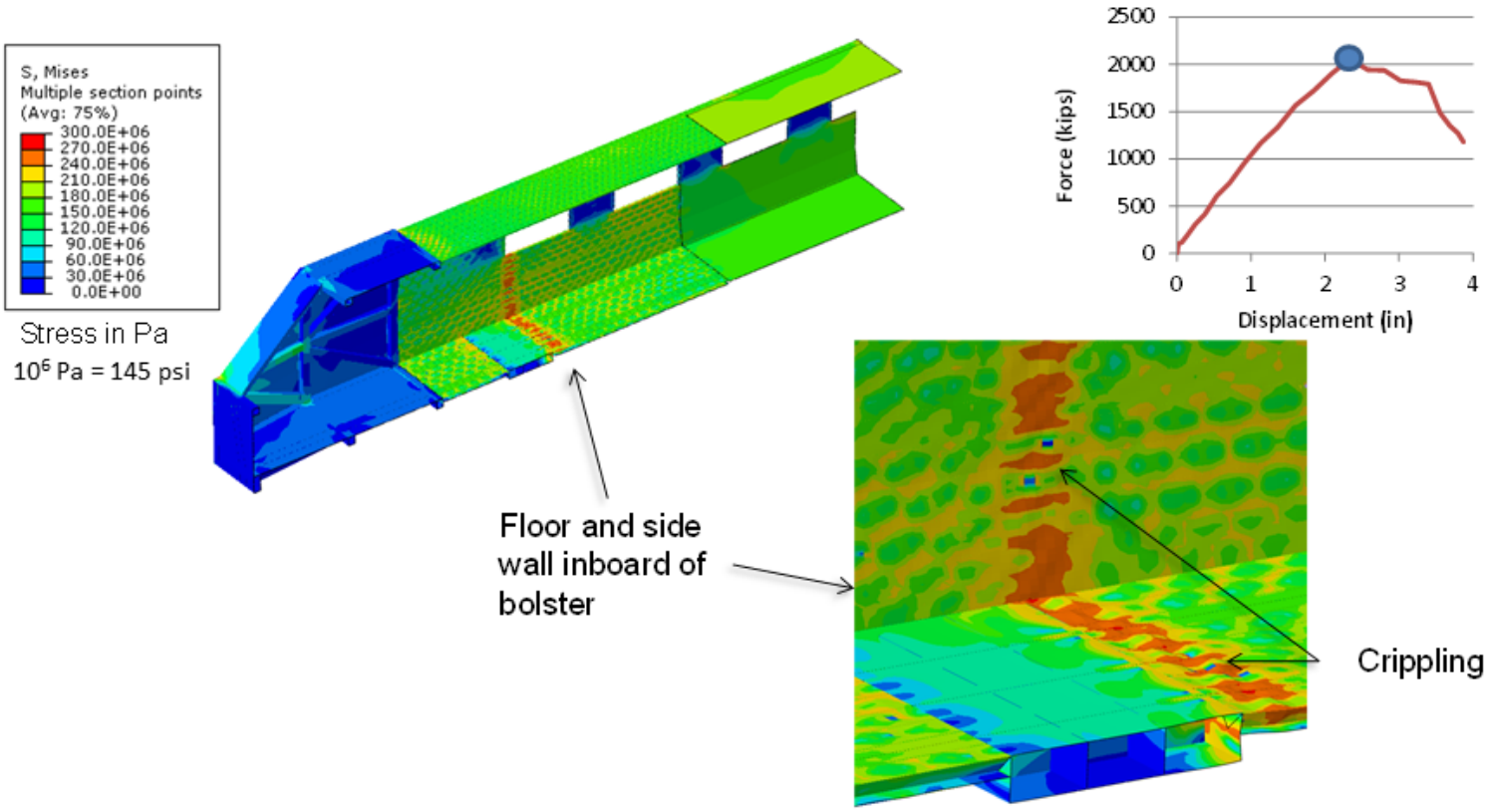

Figure 19. Stress contours of the baseline model at maximum compressive load

3.4.2 Analyses for Higher Occupied Volume Strengths

The results of the baseline analysis were used to develop models for three additional analyses to develop a relationship between occupied volume strength and carbody structural weight. For each analysis, the primary change was made to the thickness of the floor extrusions (flanges and diagonal members.) These were increased in 0.5 mm increments (i.e., from 2.5 mm for the baseline model to 4.0 mm for the third and final iterative analysis). The floor section was selected as the primary variable for the analyses because aluminum extrusions in the floor controlled each of the Tier III criteria for the baseline model. In some cases, it was also necessary to increase the thickness of other members to ensure that the extrusions in the floor controlled each of the Tier III criteria.

Table 7 identifies key variables for the baseline model and the three additional analyses. The locations that controlled each of the three Tier III occupied volume strength measures were the same as for the baseline case, and so contour images are not shown here.

Table 7. Aluminum section thicknesses for each analysis model

Floor section thickness **mm (in.)**	Weight **kg (lbs)**	Remarks
2.5 (0.098)	4,283 (9,442)	Baseline model
3.0 (0.118)	4,547 (10,025)	
3.5 (0.138)	4,814 (10,612)	Bolster gusset plate thickness increased from 3.0 mm to 4.0 mm so that first yield would not occur in gusset.
4.0 (0.157)	5,174 (11,408)	Bolster flange and stiffener thickness increased from 8.0 mm to 10.0 mm so that maximum compressive strength would not be controlled by bolster.

Figure 20 shows occupied volume strength, using the first yield criterion, plotted against added vehicle weight (i.e., the baseline case is zero added weight). Note that structural weight encompassed all of the assumed occupied volume (i.e., the weight of the quarter-symmetric model is multiplied by four). The plot shows that increasing the weight of structural members by 21 percent increases the compressive load at yield by 39 percent. Figure 21 shows compressive load at 5 percent plastic strain and maximum compressive load plotted against added vehicle weight. The plot shows that increasing the structural weight by 21 percent increased the compressive load at 5 percent plastic strain and at the maximum compressive load by 41 percent and 36 percent, respectively. Note that the relationship between maximum compressive strength and added weight was approximately linear for the models considered in this study.

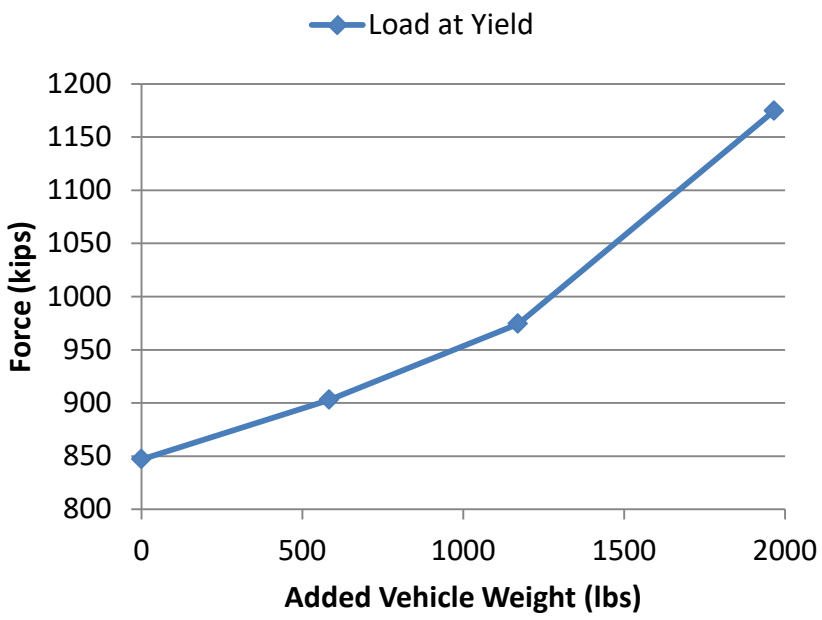

Figure 20. Compressive load at first yield, plotted against added vehicle weight

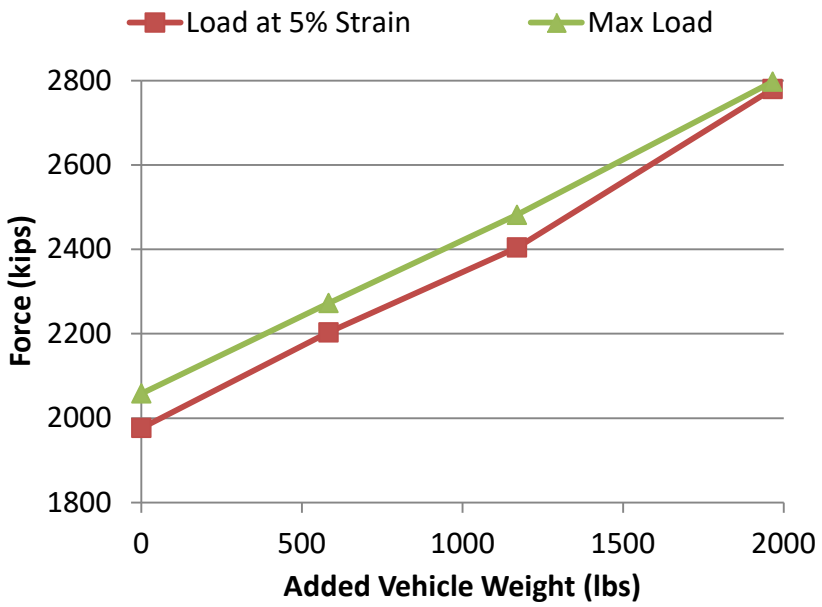

Figure 21. Compressive load at 5 percent plastic strain and maximum compressive load, plotted against added vehicle weight

3.5 Discussion

The absence of detailed public information about the structural design of high-speed trains required the development of an approximate model for this study. The model used here included some of the features known to be common to high-speed trains: aluminum extrusions and elements to represent two of the key structural discontinuities: bolsters and windows. The

thickness of the extrusions appeared to be lower than those in European construction, but this was necessary to obtain an occupied volume strength at first yield close to the Tier III requirement. This suggested that other discontinuities in the carbody of actual high-speed trains control yield. Nevertheless, the purpose of the model was to obtain an approximate relationship between car shell weight and occupied volume strength, and the baseline model served this purpose. The weight of the baseline model car shell, about 4,300 kg (9,440 lbs) was close to but lower than the weights reported by the car builders (likely because of the absence in the model of attachments (including welds) and other details).

The results obtained appeared consistent with those reported in the ETF by car builders. Most reported that it was easier to achieve the required occupied volume strength according to the 5 percent and ultimate load criteria than the first yield criterion. The shape of the load-crush curves was also similar to those reported at the ETF. For reference, the load to first yield, 847 kips, was also substantially lower than the simple uniaxial compression strength (the product of the cross-sectional area on a plane through a window and the yield strength) of 3,490 kips.

All of the models examined in this study exhibited local buckling to some extent in the aluminum extrusions once the yield strength was exceeded; for example, see the undulating appearance in Figure 18. Local buckling of an element, such as the flanges and webs of the extrusions, was controlled by the b/t ratio; where b is a component's free span length and t is its thickness, as shown in Figure 22. Components with larger b/t ratios were more susceptible to local buckling. Structural engineering codes (e.g., [4]) required a b/t ratio less than about 33 (for 6005A aluminum) to avoid local buckling. The b/t values of the floor extrusion in this study varied from 64 for the baseline model to 40 for the third iteration model; the maximum b/t value for any model in this study was 75, which occurred in the lower portion of the side wall.

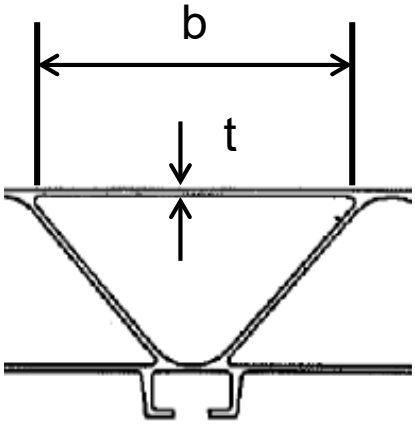

Figure 22. Schematic showing the physical meaning of b/t ratio

The results of the analyses indicated that increasing occupied volume strength by 25 percent by any of the three measures required about a 1,200-1,300 lb weight increase, or a weight increase of just under 15 percent above the baseline.

4. Energy Absorbers

The weight of the crush zone in a high speed train (or any train) varies substantially depending on the particular design approach and the amount of energy to be absorbed. The proposed Tier III requirements include a collision between the subject train and a defined locomotive-led train at 20 mph. The amount of energy that the subject high speed train must absorb is given approximately by the formula:

$$E_c = \frac{1}{2}\frac{m_1 m_2}{m_1 + m_2}(\Delta V)^2$$

where m_1 and m_2 are the masses of the colliding trains and ΔV is the closing speed. The mass of a typical, eight-car high-speed train is about 950,000 lbs; the mass of the locomotive-led train in the Tier III requirements is 735,000 lbs. This results in a collision energy at 20 mph of $E_c = 5.5 \times 10^6$ ft-lbf. This energy must all be absorbed by the subject train, because, by definition, the locomotive-led train absorbs no collision energy. Figure 23 shows the amount of energy that must be absorbed in the Tier III collision scenario configuration as collision speed is increased. Note that an additional 3.2×10^6 ft-lbf of energy absorption is required if the collision speed is increased from 20 to 25 mph.

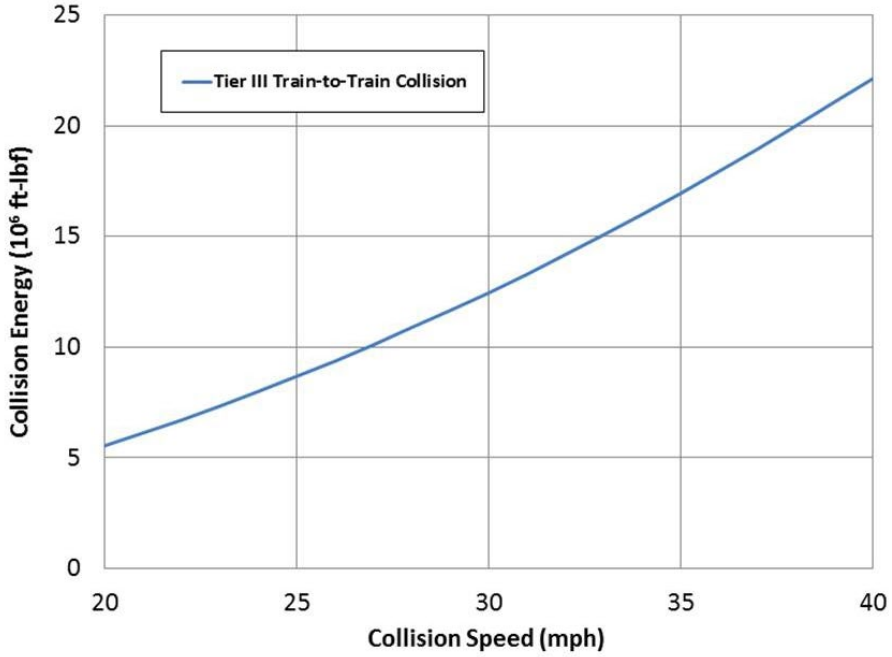

Figure 23. Plot of the estimated energy that a high speed train must absorb in the required Tier III collision scenario (high-speed train mass = 950,000 lbs)

Most high-speed trains with crush zones incorporate several elements to provide energy absorption, and each contributes to the overall weight of the crush zone. These elements include crushable elements, an energy-absorbing push-back coupler, structure needed to carry the loads of the absorbers into the carbody, and the outer skin or shell. The skin or shell of the crush zone would normally be required anyway and, therefore, adds essentially no weight. Figure 24 shows an example of a crush zone (not high-speed) with these elements [5].

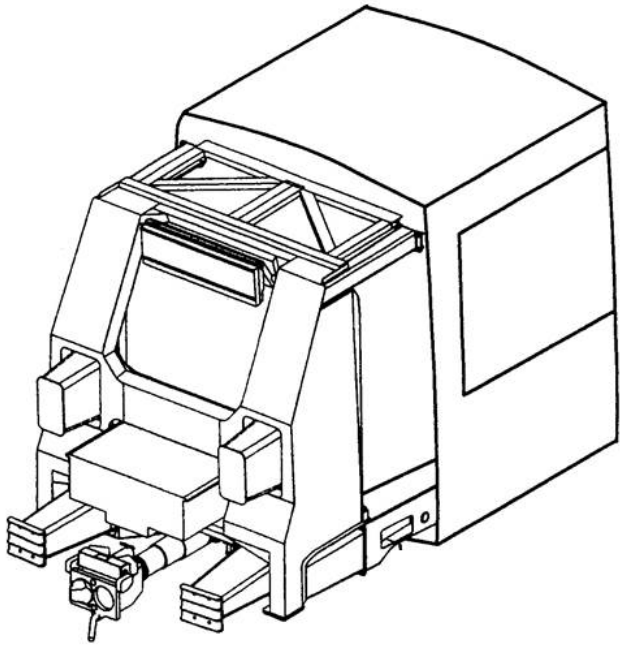

Figure 24. Layout of energy absorbers in a railcar end crush zone [5]. The outer nose mask is not included in this image.

There are a variety of push-back coupler designs being used in high-speed trains. Some of these are proprietary to the car builder, but some are from third-party suppliers. Voith produces an energy-absorbing push-back coupler that has been widely adopted for different types of operations in the U.S. It is a candidate for use on U.S. Tier III high-speed trains because it can accommodate a Type-H Tightlock coupler making it compatible with other U.S. couplers. This type of coupler is also compatible with and takes advantage of the type of train-to-train collision scenario to which Tier III high-speed trains must be designed; it can push back substantially on interaction with the protruding coupler of the locomotive in that scenario. The weight of the main energy absorber of this coupler is about 800 lbs and it can absorb over 1 million ft-lbf (1.35 MJ) of energy.

The most common type of crushable energy absorber is referred to as a progressive buckling tube; Figure 25 shows an example [6]. These have lengths from about 10 to 60 inches and thin walls relative to the circular or rectangular cross-sectional dimensions. They are generally fabricated from carbon steel, but there are examples made from aluminum and stainless steel. There is no standard absorber design, partly because the car builders must adapt the shapes of the absorbers to accommodate the space available and the manner in which they want the force-crush response to proceed. Some third parties provide off-the-shelf absorbers, but these are commonly used for side-buffers in European trains. The weight of a progressive buckling tube absorber varies considerably. The weight of the absorber shown in Figure 25 is about 50 lbs and absorbs about 70,000 ft-lbf of energy.

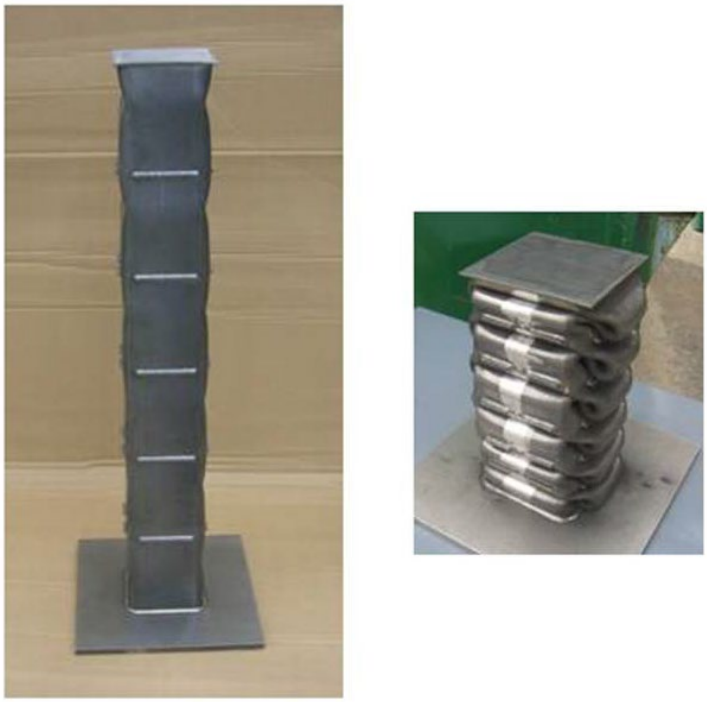

Figure 25. Carbon steel progressive buckling tube energy absorber (left – undeformed; right – completely crushed) [6]

In fact, it is possible to characterize energy absorbers in terms of their efficiency: energy absorbed per unit weight. Figure 26 shows a plot of energy absorption efficiency for different energy absorption material technologies [7]. This is a generalized plot – the actual efficiencies depend on the absorber and support condition details – but the overall trend is correct. Of particular note is the substantially higher efficiency potential (with respect to weight) of carbon fiber-reinforced plastics. According to the plot in Figure 26, CFRP absorbers can be a factor of 10 more efficient than steel absorbers. (Note that the CFRP absorbers deform more by a fiber fracture mechanism than the folding accordion mode of metal tubes.)

These results can be used to estimate the weight increase associated with a higher train energy absorption capacity and an associated higher collision speed requirement. Figure 27 shows a plot of the weight increase as a function of speed in the Tier III collision scenario based on a material change only. Note that an increase of 5 mph results in a weight increase of 1,600 lbs when steel absorbers are used, but only about 200 lbs if CFRP absorbers are used. Of course, the actual added weight could be substantially greater, as described below.

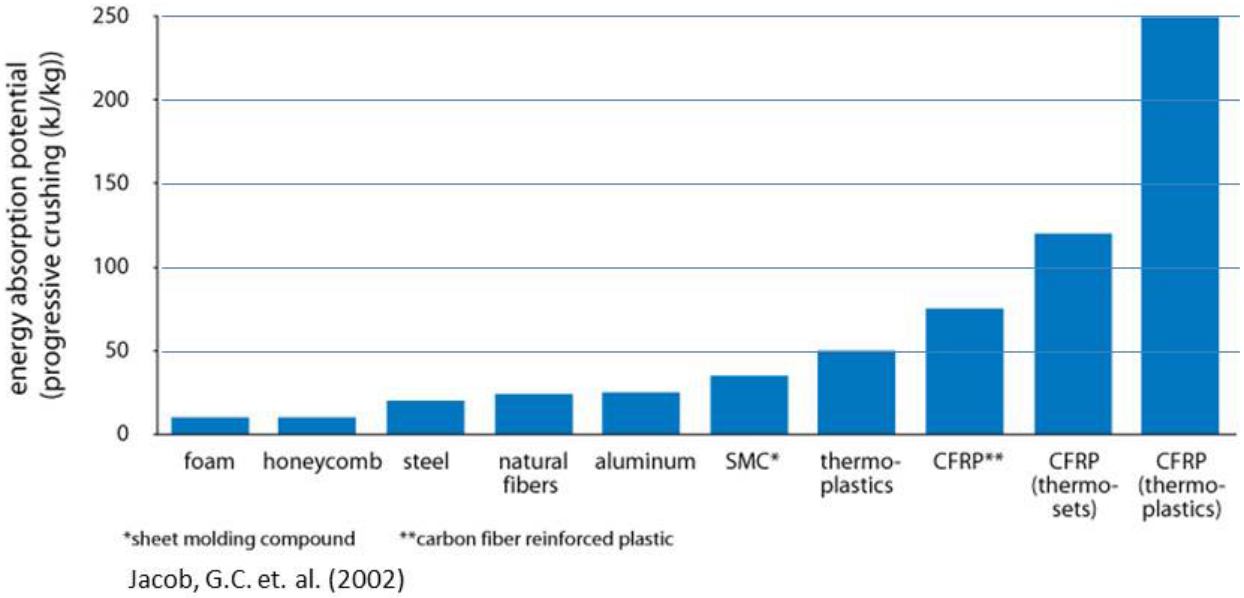

Figure 26. Energy absorber efficiency by material type [7]

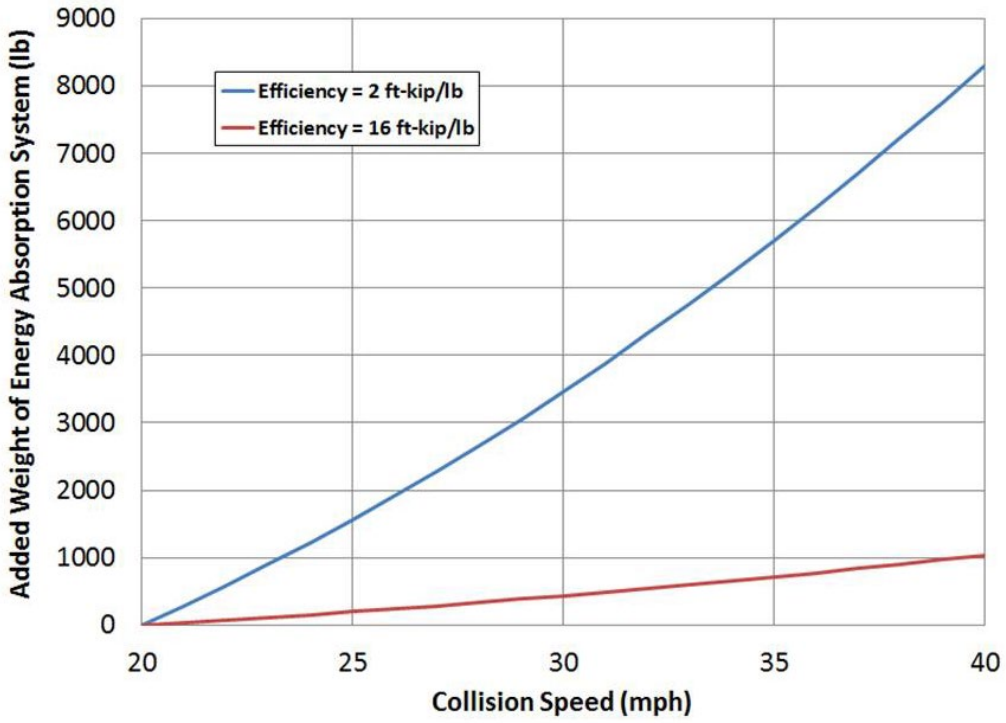

Figure 27. Additional weight required to achieve higher collision speeds in the Tier III train-to-train collision scenario; subject train weight is 950,000 lbs

The apparent, clear benefit of using carbon fiber-reinforced polymer absorbers depicted in Figure 26 must be tempered by such factors as cost and repeatability. These types of composites cost

10-40 times more than metallic tubes. In addition, it is much more difficult to predict the response of composite absorbers for different crash conditions due to the effect of loading rate and processing conditions on composite deformation and fracture behavior. The ability to reliably calculate response is important in design and validation of crush zone performance.

Greater energy absorption for a train system can be achieved in various ways, including these combinations:

- Include crush zones in more vehicle ends in the high-speed train.
- Increase the length (and therefore the stroke) of the crush zone.
- Increase the average crush force of the crush zone.

The physics of collisions limits the extent to which multiple vehicle ends can participate in energy absorption. It is more difficult to absorb energy the further the crush zone is from the impacted end. This is why so many designs place the majority of energy absorption at the impacted end. (There is also more space at the impacted end, because there is no need for a door and passage to other cars in a high-speed train.)

Increasing the length of the crush zone is generally the approach taken when more energy absorption is needed, because the crush force and the associated support structure need not be increased. However, increasing the crush zone length also has the effect of decreasing space available for occupants or the services provided to passengers, because the length of rail cars is generally fixed. The substantial disadvantage of increasing the crush force is the need for stronger support structure and occupied volume, the weight implications of which were discussed in the previous section.

It is thus difficult to estimate the increase in train weight associated with an increase in overall energy absorption. Suppose the energy absorption were increased at the lead end only to accommodate an increase in collision scenario speed of 5 mph. This corresponds in the example above to an increase of just over 3.2×10^6 ft-lbf of energy, or about 56 percent. If this additional energy absorption were achieved only through an increase in crush force, then the strength of the occupied volume would also need to be increased by 56 percent. This, in turn, would result in an occupied volume weight increase of over 2,000 lbs, using the relationship from Figure 20 of the previous section. Thus, the total weight increase (by this simplified methodology) would be 3,600 lbs if using steel progressive buckling tube absorber technology.

The calculation just presented is intended only to illustrate the potential weight increase associated with requirements of a higher collision speed in the Tier III scenario.

5. Passenger Seats

Passenger seats are important components on a train. They provide the primary interface between the customers and the train itself. Therefore, they must be comfortable and provide some useful functions as well as be safe.

They also represent a significant component of the weight of high-speed train. The number of seats in each car depends on the car builder and class of operation, but a typical value is about 60. The weight of each seat also varies, but seat manufacturers report a typical weight of 35 lbs (16 kg) per passenger. Thus, passenger seats can account for over 2,000 lb in a high-speed rail car. In contrast, a typical coach class seat weight for a current U.S. commuter train can be as much as 70 lbs.

Calculations were conducted to obtain an approximate relationship between seat crashworthiness performance and seat weight. The approach was to simulate the secondary impact of seated passengers into the back of a forward-facing seat, evaluating both the structural integrity of the seat structure and attachments and the injury potential to the occupant.

First, descriptions are provided of the current seat structural requirements and current designs.

5.1 High-Speed Train Seat Requirements

There currently appear to be no universal requirements for the structural integrity of high-speed train seats. A review of high-speed train seat information, including communications with suppliers, reveals that many standards have been used; the most common of these are listed in Table 8.

Table 8. Standards for high-speed train seats

Standard	Title	Comments
UIC 566	Loadings of coach bodies and their components	Includes static load and equivalent dynamic load requirements
NF F31-119 (in French)	Railway rolling stock material – behavior of seats for static, fatigue, vibration, and impact	Contents of this standard were not reviewed.
AV/ST9001	Vehicle interior crashworthiness	Has static strength requirements and refers to GM/RT2100 for dynamic impact requirements
GM/RT2100	Requirements for rail vehicle structures	Supersedes AV/ST9001; has static and dynamic strength requirements

The UIC standard is an older one from 1990, but is still referenced in some of the seat supplier literature. It includes the following loads that should not cause permanent deformation:

- Longitudinal load of 1500 N anywhere on the seat back
- Vertical upward load of 1200 N on the front edge of the seat

- Dynamically equivalent static loads of 5g longitudinal, 1g transverse, and 3g vertically of the dead weight of the seat

NF F31-119 is a French standard referred to in some of the seat supplier literature. It does not seem to be in widespread use, and so a translation of this standard was not obtained. The standard AV/ST9001 has been superseded by GM/RT2100, but it is still referenced in high-speed train seat product literature. Its structural requirements include the following loads, with the criterion of no permanent deformation:

- Longitudinal load of 1500 N on the center of the uppermost part of the seat back
- Vertical upward load of 1200 N on the front edge of the seat

AV/ST9001 also requires the following test with the criterion that the seat must remain fixed to its mountings and fail in a manner which itself is not likely to cause injury:

- A dynamic sled test with a 95th percentile Hybrid III male anthropomorphic test device (ATD) in each seating position; a test pulse that falls between two curves (these curves are nearly identical to those shown in Figure 28 below for GM/RT2100, except the plateau of the lower limit is 5.67g and the plateau of the upper limit is 8g.).

GM/RT2100 is increasingly being adopted for seats in high-speed trains. As stated previously, it has superseded AV/ST9100. Parts of GM/RT2100 have also been adopted by the Engineering Task Force of the Railroad Safety Advisory Committee for seats in U.S. Tier III trains.

The failure criteria in GM/RT2100 for seats under the specified loadings include:

- Attachments to the primary structure must remain intact.
- A continuous load path must be maintained with no abrupt changes in force levels.
- No sharp fracture surfaces may be produced.

There are also general requirements about the conditions under which some permanent deformation is allowed; for example, permanent deformation must be due to plastic deformation.

The load cases required by GM/RT2100 include:

- Longitudinal load of 1500 N on the center of the uppermost part of the seat back.
- A lateral displacement of the complete seat assembly of 100 mm without failure (ultimate load case). In the case of a bodyside attachment configuration (a common configuration for high-speed trains), the displacement may be applied to the side attachment component of the seat.
- A dynamic sled test with a 95th percentile male ATD in each seating position; a test pulse that falls between the two curves in Figure 5.1 below and one that produces ATD free flight velocity of at least 5 m/s.

The loads are applied simultaneously to each seat in the case of multiple seats.

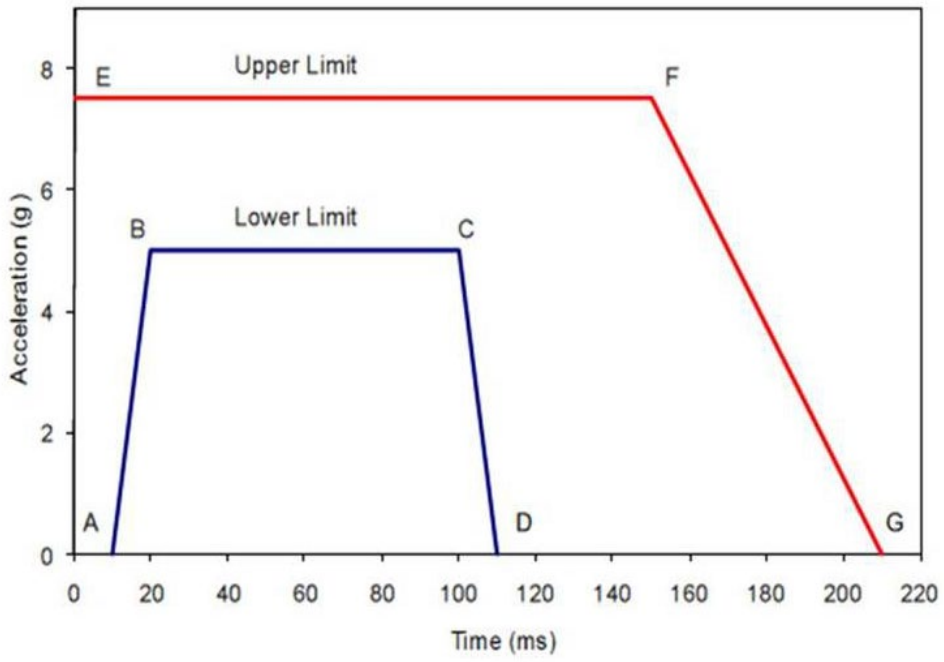

Figure 28. Crash pulse envelope from GM/RT2100

5.2 Existing High-Speed Train Seat Designs

The seat designs for several high-speed trains were reviewed in terms of materials, geometry, method of attachment, and standards to which they are designed. The products varied widely and appeared to be tailored in some form for each train, so it was difficult to identify specific seat models. The seat suppliers for high-speed and other trains contacted as part of this study are listed in Table 9.

Table 9. High-speed train seat suppliers

Seat Supplier	Website
Saira	www.sairaeurope.com
Grammer	www.grammer.com/en/
Clerprem	(no apparent web site)
Kiel	www.kiel-sitze.de
Compin	www.compin.com
Kustom Seating	www.kustomseating.com

Figure 29 illustrates a common configuration for attaching seats to the aluminum carbody of a high speed train. A pair of seats in this train has two attachment points – one to the floor and one to the side. One method of attachment is into a channel that is part of the carbody aluminum extrusion (Figure 30). The implications of this particular attachment approach on strength are discussed below.

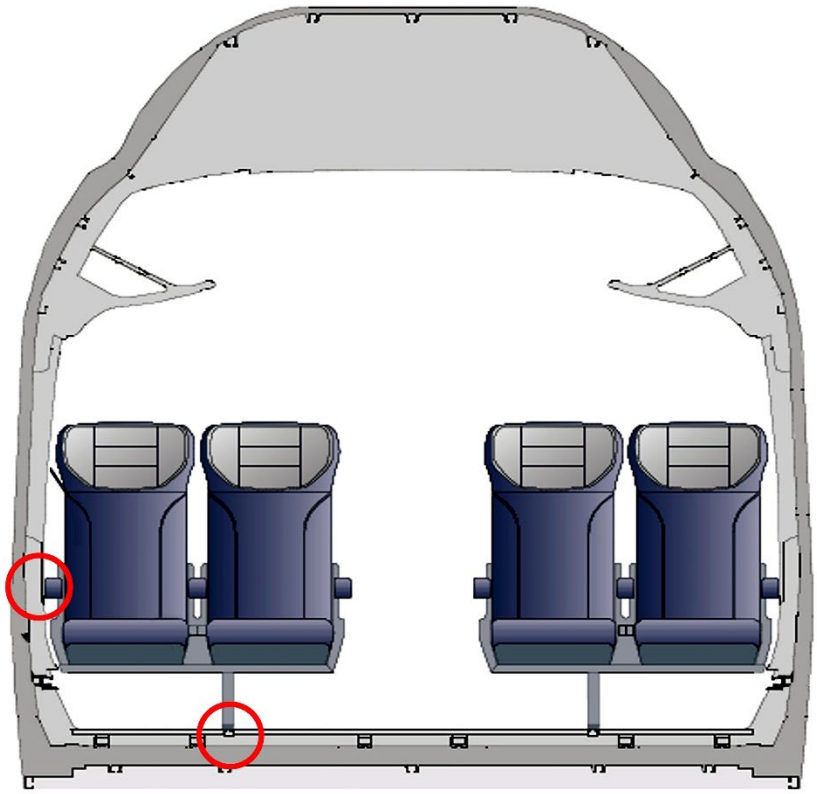

Figure 29. One method of attachment configuration for high-speed train seats

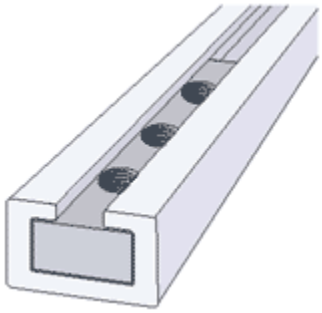

Figure 30. Detail of a seat attachment approach in a high-speed train

An example of a high-speed train seat from the supplier Compin, used in some Alstom high-speed trains, is shown in Figure 31. The seat structure (not the cushions and fabric) is generally made from aluminum castings (e.g., A383). A383 has yield and tensile strengths of approximately 22 and 45 ksi, respectively. Magnesium cast alloys are also used for high-speed train seats. Magnesium is lighter than aluminum (density of 0.065 lb/in^3 vs. 0.097 lb/in^3), but with comparable or superior strength to aluminum. (Note that it is difficult to make comparisons on strength because of its strong dependence on the heat treatment.) Magnesium is generally substantially more expensive than aluminum. Some seat suppliers are conducting research on fiber-reinforced composite seat structures, but evidently there are no such seats in existing or

planned high-speed trains. Note that the Compin seat is attached at the base near the aisle and at the side wall.

Figure 31. Example of a Compin high-speed train seat

The weight of a high-speed train seat varies and increases substantially as equipment (e.g., trays, reclining features, etc.) is added. Typical high-speed train seat weight (unequipped; e.g., no amenities) is about 15 kg (33 lbs). Apparently, the percentage of this weight corresponding to the structural frame is about 30 percent, or about 4.5 kg (about 10 lbs). The weight of these high-speed train seats is considerably less than that for seats for conventional trains. For example, the recent PRIIA specification being adopted by Caltrans utilizes a single-passenger (total) seat weight of 55 kg (120 lbs).

The discussions with suppliers of high-speed trains and high-speed train seats indicate that the general trend in seating design, in addition to the strength requirements just mentioned, include: lower cost, lighter weight, and reduced spacing to increase the number of passengers in the train.

5.3 Aircraft Seat Design

Weight is particularly critical in the aircraft industry, so it makes sense to review that technology for insight into what could be done for high-speed rail vehicles.

Structural requirements for aircraft seats are covered in FAR 25.561 and 562. The strength requirements are similar in form to those for rail vehicles. For example, the equivalent static loads on the seat are:

- 3.0g upward
- 9.0g forward
- 4.0g sideward
- 6.0g downward
- 1.5g rearward

Seats are also required to pass a sled test with the conditions shown in Table 10. The test uses a 170-lb ATD. These requirements are intended to provide protection in the event of an emergency landing.

Table 10. Dynamic sled test conditions for commercial aircraft seats

Section (from 25.562)	Seat configuration	Minimum change in velocity (ft/s)	Minimum acceleration (g) in maximum time (s)
(b)(1)	Floor 60° to the horizontal	35	14, 0.08
(b)(2)	Floor level, seat yawed 10° to the longitudinal	44	16, 0.09

The second test in Table 10 is most similar to the requirements for rail vehicle seats and is depicted in Figure 32 with the corresponding target crash pulse used. Unlike rail vehicle seat testing standards, the ATD is restrained in the test for aircraft seats. The strength-related requirements are that the seat remains attached at all points of attachment and that the permanent deformation does not impede evacuation of the aircraft.

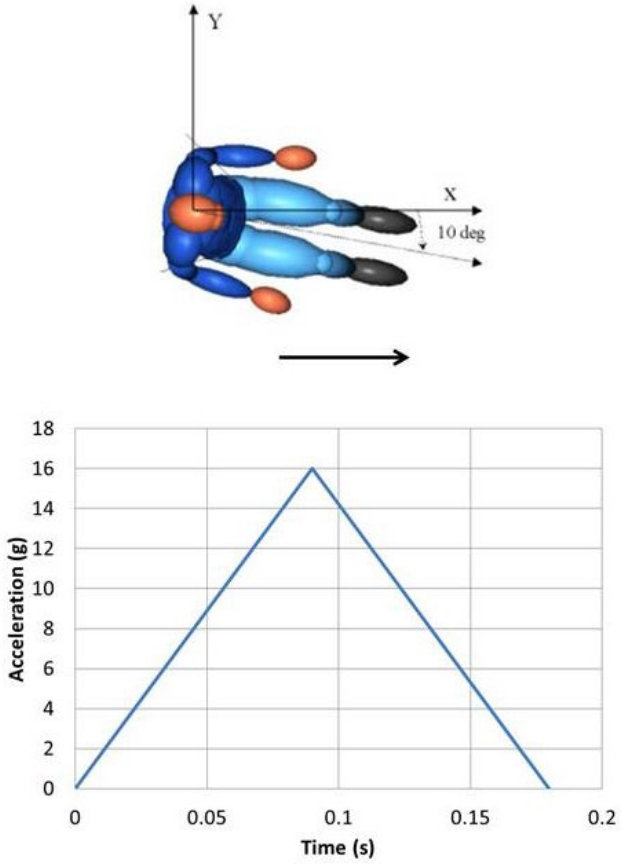

Figure 32. Illustration of the dynamic seat test for commercial aircraft seats

Aluminum alloys are the primary materials being used for aircraft seat frames, including 2000, 6000, and 7000 series materials; e.g., 2024-T3511, 6082, 7075. Strength, modulus, and damage tolerance (fracture toughness) are issues. Some seats use energy-absorbing devices in the seat tracks to satisfy dynamic test requirements. Telephone conversations with aircraft seat suppliers indicate that a typical aircraft seat weight is 20 lbs (9 kg).

5.4 Comparison of crash pulses from different standards

It is interesting to examine the extent to which the structural requirements for seats differed between conventional (U.S.) and high-speed trains and for commercial aircraft. Figure 33 shows a comparison of the different crash pulses used in tests for the seats. Table 11 compares the calculated secondary impact velocities taking into account, approximately, differences in seat pitch, which were estimates. Note that the free flight distance was smaller when the dimensions of the ATD were included. In addition, the values of ΔV were based on the assumption that the ATD was not restrained, which was not the case for aircraft seats. For aircraft seats, the ΔV may be considered approximate for the head form.

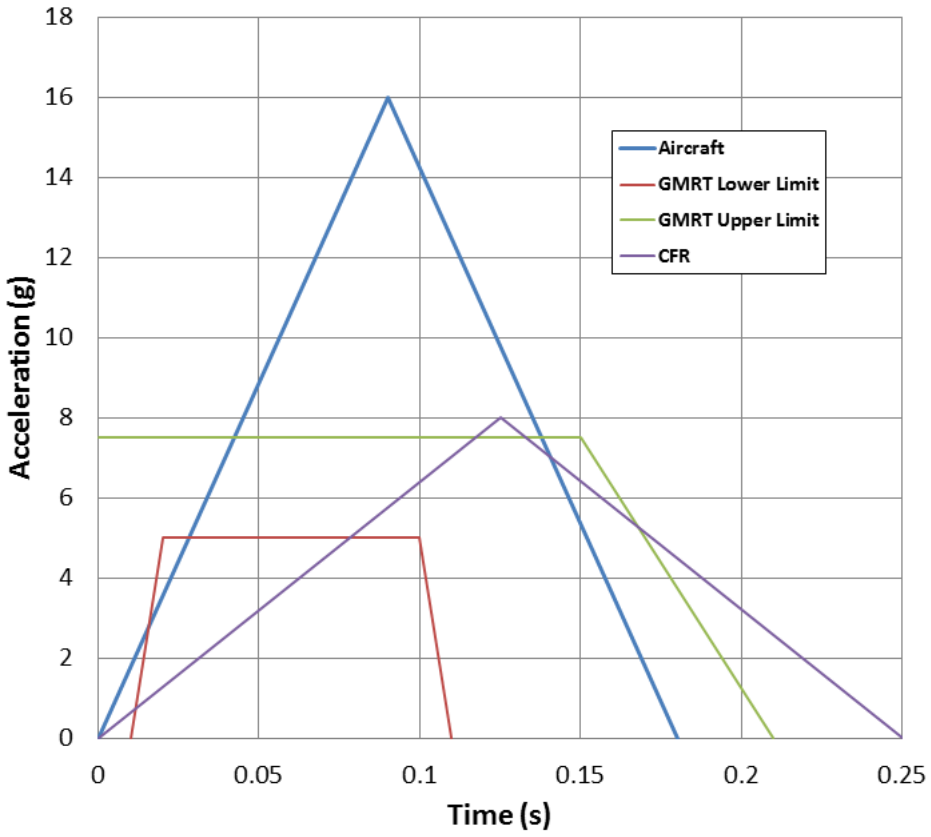

Figure 33. Comparison of the crash pulses used for rail vehicle and aircraft seats

Table 11. Estimates of impact velocity for different dynamic seat tests

	Pulse	ΔV for pulse (ft/s)	Seat pitch (ft.)	ΔV accounting for seat pitch (ft/s)
Aircraft	Aircraft	46.4	2.5	42.3
High-speed train	GMRT lower	14.5	3.3	14.5
	GMRT upper	43.5	3.3	39.5
	8g	32.2	3.3	31.7

Note that, according to the assumptions used, the dynamic test for aircraft seats resulted in a higher impact velocity. This was probably offset to some degree by the differences in the weight of the test dummies: 170 lbs (77 kg) for the aircraft seat test and 223 lbs (101 kg) for the rail vehicle test. Nevertheless, it appeared that the tests were generally comparable, so that the aircraft industry has been able to design very light seats that meet crash requirements.

5.5 Calculating the Effect of Performance on Weight

The objective of the work described in this section was to estimate the increment of seat weight associated with changing crashworthiness performance requirements, in particular from those of GM/RT2100 to those of the current APTA standard, the so-called 8g, 250 ms requirements. The approach was to use a finite element model of an idealized high-speed train seat, to develop two configurations of this model, one that meets the 8g, 250 ms requirement and one that met GM/RT2100, and to calculate the difference in weight.

The model was developed using the FEA program ABAQUS/Explicit. It included a seat pair, connections representing the attachment to the rail car, and two rigid bodies to represent occupant head forms. The seat included seat backs, headrests, a seat base-frame, and a pedestal. Connections were made to simulate floor and wall mountings. The impact scenario and the effective mass of the rigid impactors were meant to correspond to sled-testing of forward-facing seats. The parameters calculated were attachment point loads, seat deformation, and the head impact criterion (HIC) for the two rigid masses.

5.5.1 Model Description

A model was constructed for a two-passenger seat based on photographs of actual seat structures and prior experience developing a prototype crashworthy seat design. The effective mass of an impacting head was estimated using data from sled tests of a forward-facing seating system that were conducted on a prototype crashworthy seat in another project [8].

The seat FEA model featured side frames that were representative of cast aluminum seat structures in certain high-speed trains, as shown in Figure 34. The frame had a lateral depth of 3.0 inches and was about 18 inches long and 33.5 inches high, angled back by about 9 degrees.

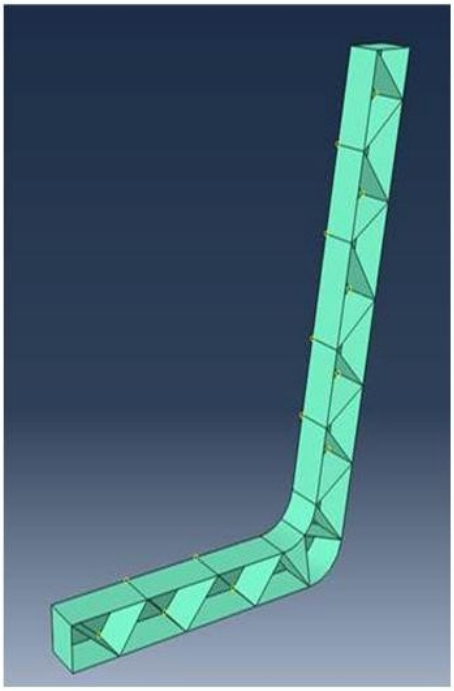

Figure 34. FEA side frame model

The remainder of the two-passenger seat structure, shown in Figure 35, was constructed based on prior experience by adding additional components, namely:

- Seat back sheets, 18 inches wide by 31.4 inches high
- Seat back braces, 17 inches wide by 3 inches high
- A seat pan, 41 inches long by 18 inches deep, stiffened by four longitudinally oriented L-shaped brackets, 3 inches wide and 1 inches deep, located under each of the four seat side frames and two vertical plates, 41 inches long by 1 inch deep at the front and back of the seat pan so as to form a box open at the bottom
- A pedestal, 10 inches high, 10 inches deep, and 2 inches wide, closed on all sides except for a 6 inch wide by 10 inch high window to provide access to the floor mounting bolts
- A wall mount, 10 inches long by 4 inches wide
- A headrest, 13 inches high by 10 inches wide
- A headrest frame, 10 inches high by 8 inches long by 1 inch deep side closed box

All sheet structures were modeled as aluminum, with an elastic modulus of 10×10^6 psi, and a stress-plastic strain curve for which the stress was 22 ksi at zero plastic strain and 30 ksi at a plastic strain of 10 percent.

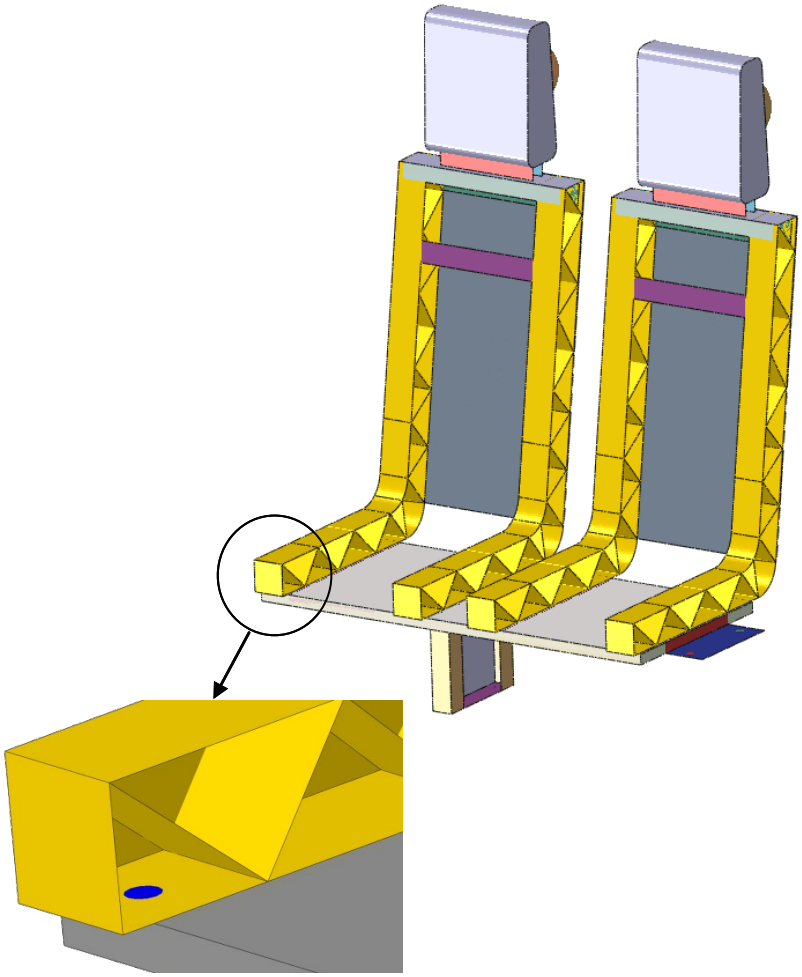

Figure 35. FEA model of the two-passenger seat structure with detail illustrating one of the seat pan-to-seat side frame connector locations.

Each of these components was modeled as plates using ABAQUS type S4R shell elements. The exception was the headrest, which was modeled with 3-D elements (ABAQUS type C3D8R). The baseline model had the thickness values listed in Table 12; the seat side frame and back were defined to be 0.080 inch (2 mm) thick, and most regions of the other components were defined to be 0.125 inch (3.2 mm) thick. In a few locations—the top of the seat back, the top of the pedestal, the seat pan-to-wall mount connection, the regions around the seat side-frame to seat connections—additional thickness was added to provide stiffening.

Table 12. Baseline seat component weights (seat pair)

Component	Thickness (in)	Weight (lb)
Seat Side Frames	0.08	24.8
Seat Back Sheets	0.08	9.4
Seat Pan	0.125	12.0
Seat Pan Stiffeners	0.25	5.4
Seat Back Braces	0.125	0.9
Pedestal	0.125	4.1
Wall Mount	0.25	1.3
Headrest Frame	0.125	7.6
Headrest Support Plates	0.25	3.2
Headrest	n/a	3.9
Total		72.6

The model employs approximately 300,000 elements, with a characteristic element length of about 0.2 inch. The inset detail in Figure 35 highlights (in blue) one of many connector regions – in this case a connector between the seat side frame and the seat pan. These connector regions are described in more detail below.

To properly model the stiffness of the various components, the plates that formed the seat back, seat side frame, seat pan and pedestal were modeled as distinct and separated by half the sum of their respective thicknesses. Interactions between these components were modeled through contact and through definition of bolted connections. The bolted connections were modeled by specifying corresponding regions (specifically 0.75 inch diameter disks) in each of the plates that were being connected, directly opposite one another. These disks were then defined to be rigid and connected to one another. ABAQUS type CARTESIAN connector elements were used for this purpose, with the spring stiffness defined to be 1×10^6 lbf/in. in each direction, making the connection also effectively rigid. Connections between the pedestal and the floor and the wall mount plate to the wall were modeled in a similar manner, in this case with one end of the connector completely fixed.

Figure 36 shows rear and bottom views of the seat, with the connector locations highlighted. Table 12 lists the plate thicknesses noted above and the calculated weights of the model seat components. The weight per seat was 36 lbs.

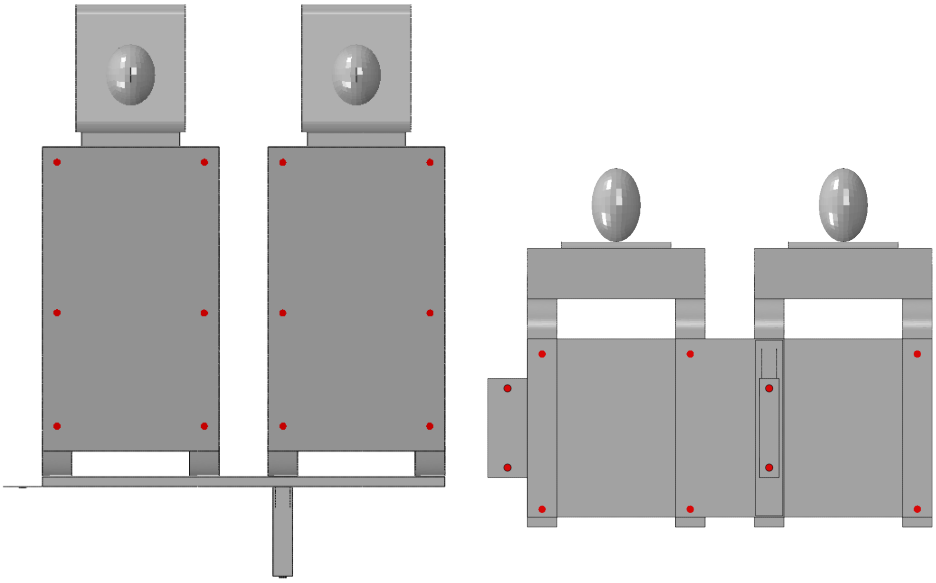

Figure 36. View of the seat model from behind (left) and from underneath (right), with connector locations highlighted

The headrest was modeled as a viscoelastic foam using ABAQUS material model *HYPERFOAM, with sub-options *UNIAXIAL TEST DATA used to define the quasi-static compression behavior of the foam and *VISCOELASTIC to model the rate dependence of foam. This material model was previously developed specifically to simulate the impact of a foam-based headrest and used test data from foam commonly used in headrests [9]. Figure 37 illustrates the model of the headrest and the headrest frame.

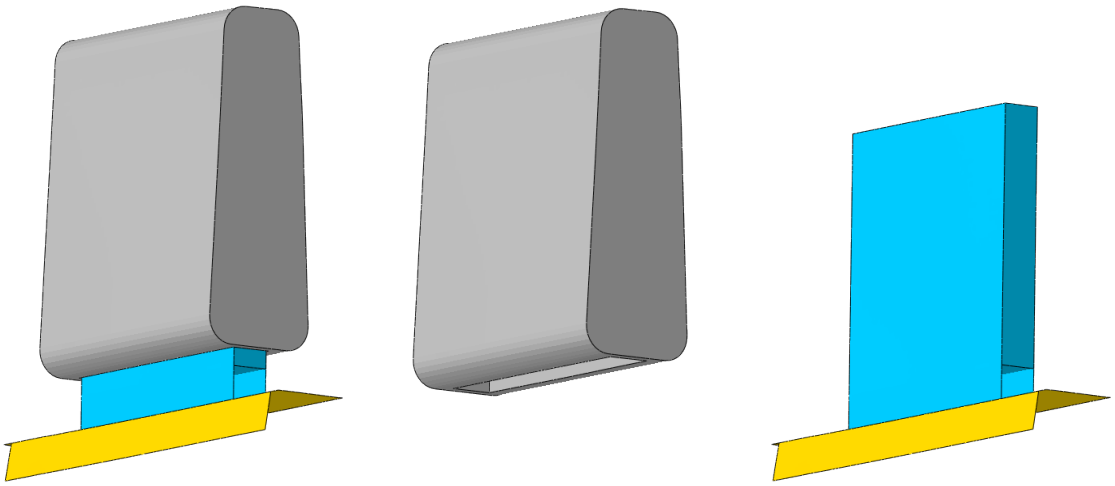

Figure 37. Model for the headrest only: complete headrest with frame (left); headrest foam only (middle); headrest frame only (right)

Figure 38 shows the seat model from the side and from the back. The impacting heads were simulated using ellipsoid-shaped rigid bodies. Based on sled test results for the crashworthy

commuter seat [8], they were positioned 51 inches above the floor at the left/right centers of the respective headrests.

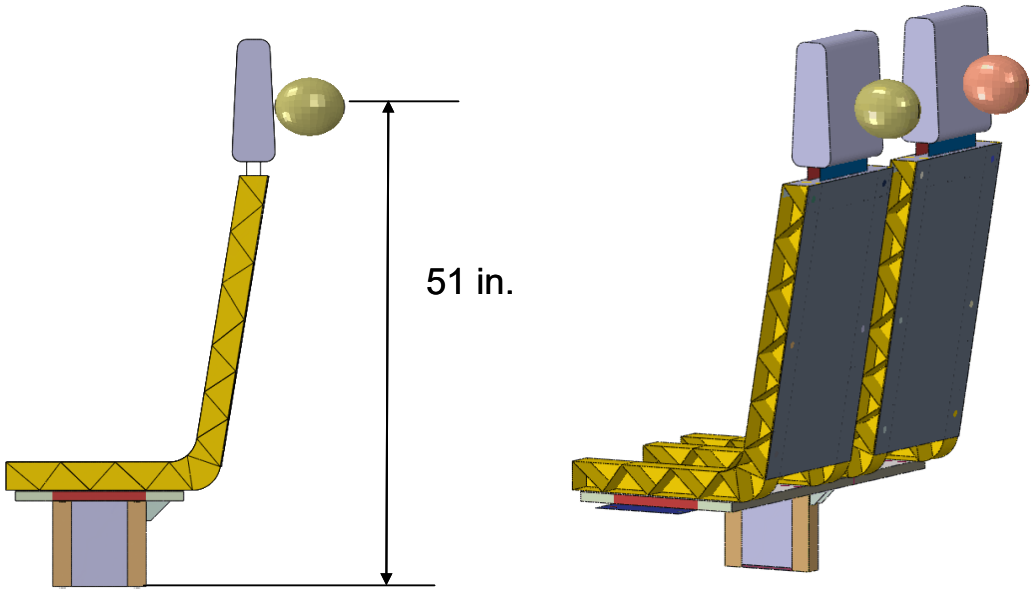

Figure 38. Side view (left) and rear isometric view (right) of the seat model with the moment arm between the impacting rigid bodies representing passenger heads and the floor indicated

Prior work [8] was also used to select the mass of the headform in the seat impact analysis for this project. Results from forward-facing impact tests of a three-passenger crashworthy commuter seat indicated that there were two primary impacts between the passengers and the seat backs in front of them in the 8g, 250 ms scenario. The first impact was between the passengers' knees and the seat bolster. Following this impact, the passengers continued to move forward, with some forward rotation of their bodies, until the fronts of their heads impacted the backs of the headrests. Because the travel distance was greater, and because the moment arm with respect to the floor and wall connections was greater, test results indicated that this impact was more severe, despite the fact that the effective mass that participates in the impact was smaller.

The energy that is imparted to the seat by an impacting head can be substantially larger than the kinetic energy of the head itself, due to forces that are transmitted from the rest of the body through the neck. To estimate an effective mass that would impart an equivalent amount of energy when isolated from the rest of the body, the research team examined data from a sled test. Figure 39 illustrates the manner in which this estimate was made. The total longitudinal force measured at load cells attached to the seat connection points and the longitudinal accelerations measured at the centers of gravity of the aisle and window ATD headforms were plotted versus time. The first peak in the force curve corresponds to knee impact and the second corresponds to head impact. As is evident, the ATD headform acceleration pulses line up perfectly with the second peak in longitudinal force (the middle-seat headform was not instrumented in the test [8]).

If it is assumed that the second peak in force arises primarily from head impact, then the effective mass of the impacting headforms can be estimated by dividing the longitudinal force per headform (6,900 lbf/3 = 2,300 lbf) by the average peak acceleration (100g). This yielded an effective mass of 23 lbm (about twice the actual mass of a typical head). This value was adjusted upwards to account for the fact that the tests were performed using a 50th percentile male ATD, and the GM/RT2100 standard calls for use of a 95th percentile male ATD. The difference in mass between the respective headforms was about 13 percent, so the effective mass was adjusted to 26 lbm.

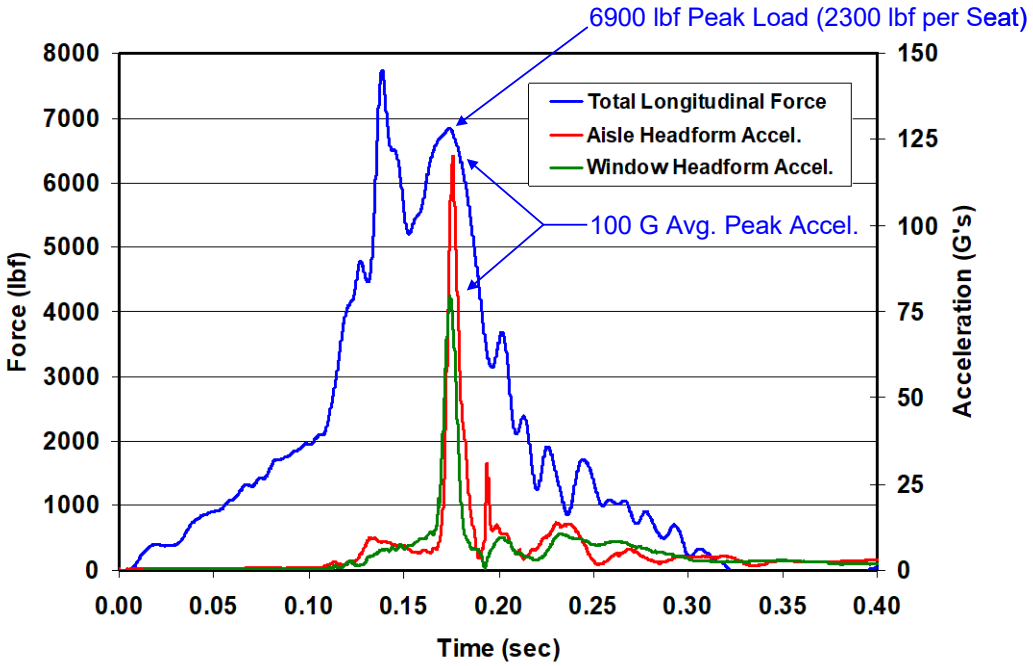

Figure 39. Measured time-histories (from [9]) of total longitudinal force and longitudinal ATD headform accelerations for the forward-facing test of the crashworthy commuter seat

5.5.2 FEA Results

8g, 250 ms crash pulse

The first analysis was performed by specifying a headform impact speed of 32.2 ft/s (9.81 m/s). This is the maximum secondary impact velocity that can arise from the 8g, 250 ms pulse. Note that this was a conservative assumption, as it was likely that the headform did not reach this velocity, due to the limited travel distance to the back of the headrest (see Table 11). However, it was also true that, with respect to seat stresses and reaction forces, the deceleration of the seat itself was being neglected; this effect alone can generate several hundred pounds of force on the connections.

The calculated deceleration time-histories for the respective impacting headforms for the baseline seat structure and the 8g/250 ms pulse are shown in Figure 40. Note that the initial pulses for the two headforms are essentially identical, as one might expect given that these pulses are primarily due to compression of the headrest foam. The duration of both initial pulses was about 0.02 second, consistent with the test results for the crashworthy commuter seat (see Figure

39). The headforms rebound off the headrests after about 0.02 seconds and made contact again after about 0.04 seconds and 0.06 seconds, respectively. The time lag for the second aisle-side headform pulse with respect to the second window-side headform pulse arose because the aisle seat back deformed more extensively than the window seat back, the motion of which was restricted by its stiff connection to the wall.

The calculated head impact criterion (HIC) for both pulses was about 490. This value was a little less severe than the value measured in the crashworthy commuter rail seat sled test for the window-side headform (560 for a 120-g peak pulse) and more severe than the value measured for the aisle-side headform (258 for an 80-g peak pulse); see [8].

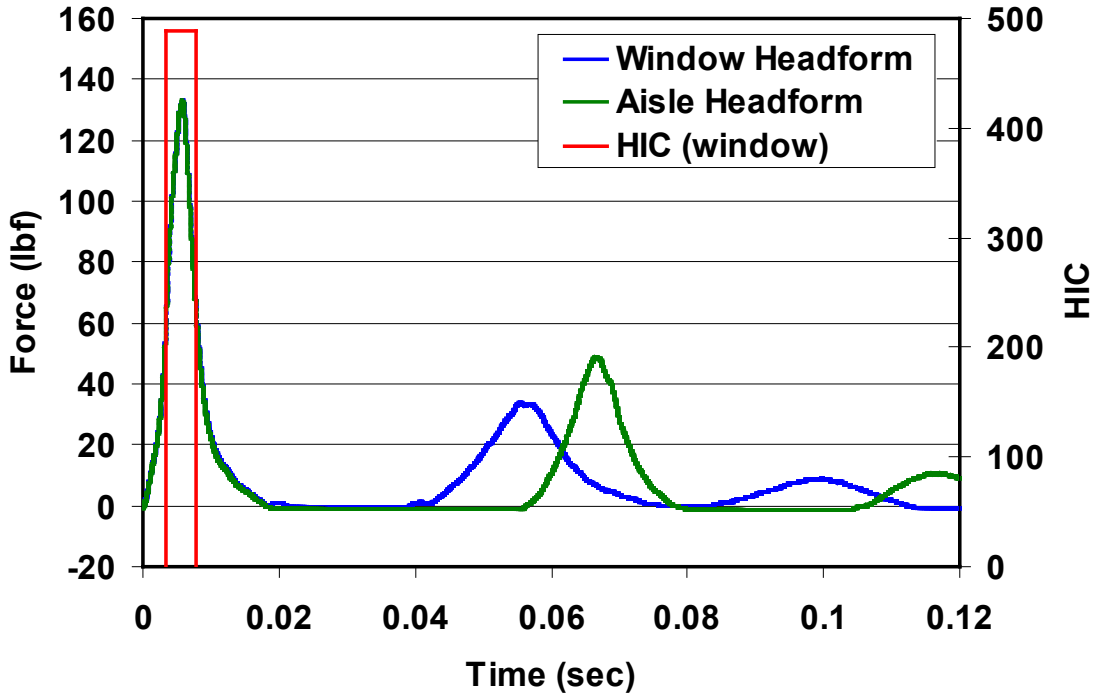

Figure 40. Calculated deceleration pulses for the aisle and window impacting headforms for the baseline seat structure with the 8g/250 ms pulse. The calculated HIC of 489 is shown in red, with the width of the box corresponding to the time duration (3.4 ms) over which the HIC attains its maximum value.

The predicted final deformation of the seat is shown in Figure 41. As noted above, the aisle-side seat deformed further than the window-side seat. It was effectively cantilevered off one side of the pedestal, and it appeared that deformation of the seat pan contributed significantly to its compliance. The maximum longitudinal deformation of the aisle-side seat back was about 8 inches The window-side seat back deformed about 2 inches less.

Figure 42 shows the calculated force versus displacement for the window-side headrest. The peak force of 3,500 lbf occurred when the headform displacement was about 2 inches. Note that, as indicated in the figure, the seat frame had deformed very little at this point. The subsequent deformation of the seat frame was due to the impulse transmitted into the headrests by the headforms.

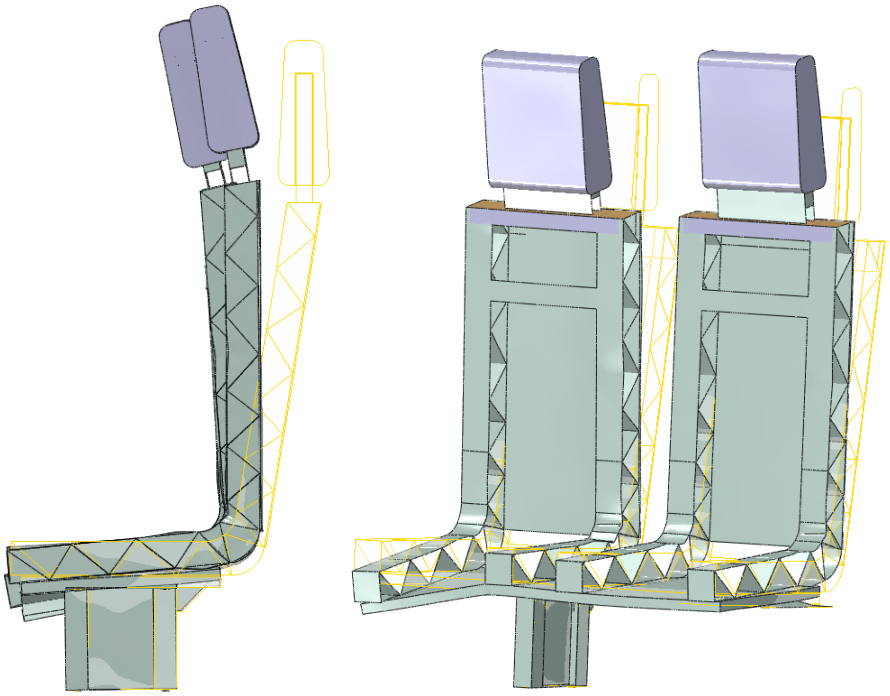

Figure 41. Side (left) and isometric (right) views showing the final deformation of seat frame for the baseline seat structure with the 8g/250 ms pulse. The initial position of seat frame is shown outlined in yellow.

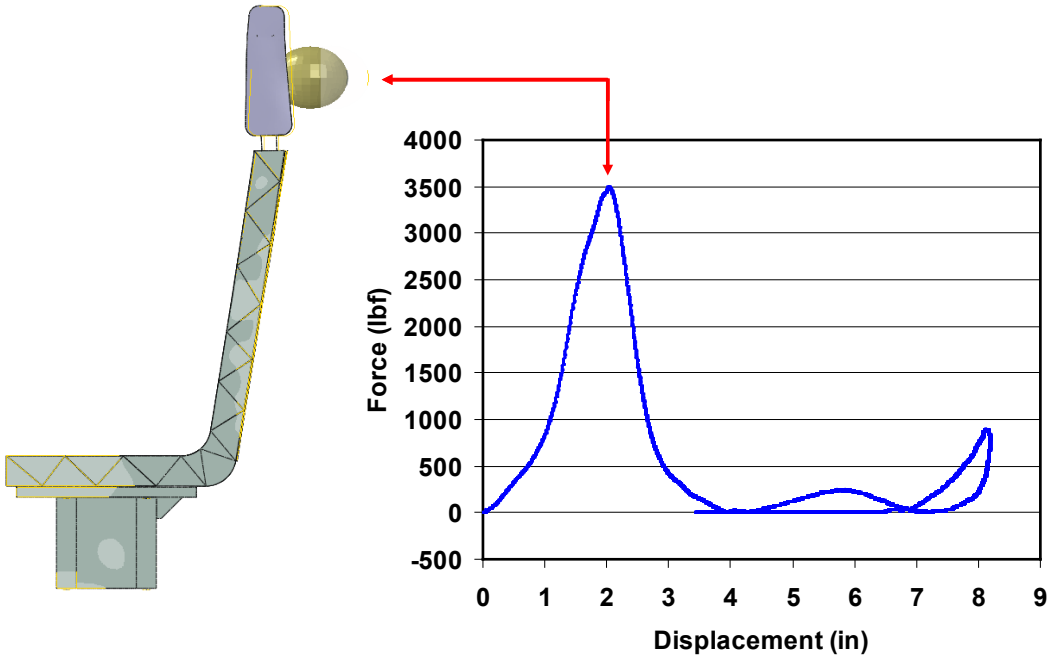

Figure 42. Force vs. displacement for the window-side headform for the baseline seat structure with the 8g/250 ms pulse. The peak displacement of about 2 in. occurs after only 0.006 seconds, with very little deformation of seat structure.

The calculated vertical reaction forces at the floor and the wall are plotted in Figure 43. These forces are important factors for the structural integrity of the seat, as the large moment applied by headform impact creates very large vertical force magnitudes. As was evident, the forces at the floor attachment points were highest, reaching a maximum magnitude of almost 5,000 lbf at the rear attachment location. This negative reaction force implied a strong upward force at this location that could promote failure of the bolted connection. The attachment hardware in the carbody and the lower seat structure must be strong enough to support such high loads.

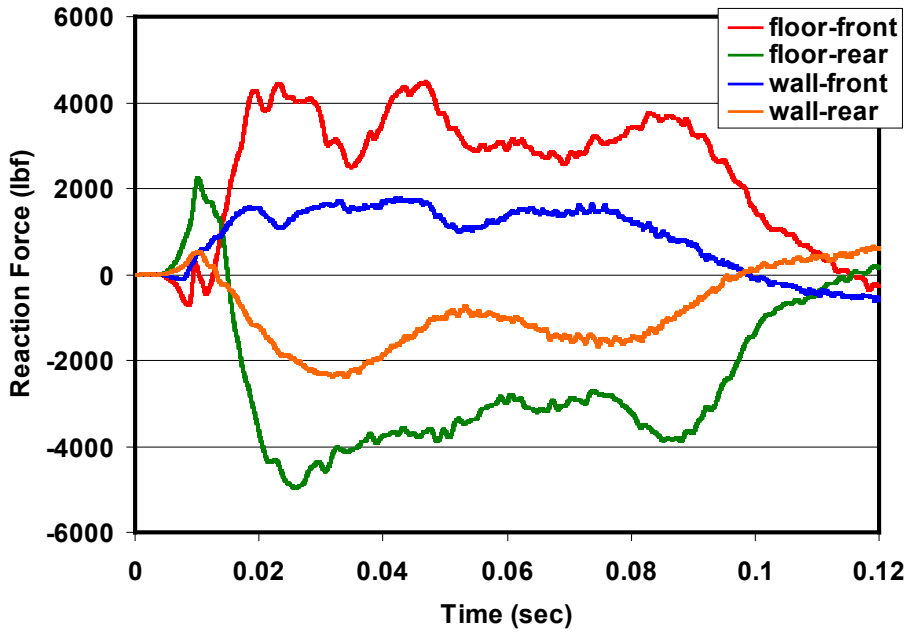

Figure 43. Vertical reaction forces vs. time for the four seat frame attachment points of the baseline seat structure with the 8g/250 ms pulse

GM/RT2100 crash pulse ($\Delta V = 5$ m/s)

A second simulation for this same seat model was conducted using an initial headform impactor velocity of 5 m/s (16.4 ft/s). This is the minimum impact speed specification in GM/RT2100. Note that the initial kinetic energy for this analysis was only about 26 percent of the energy of the 8g, 250 ms crash pulse.

The predicted headform deceleration time-histories are shown together with the predicted final deformation of the seat in Figure 44. Because the crash pulse was much less severe, the peak headform accelerations dropped by over 65 percent. And because the HIC calculation is very sensitive to the magnitude of the acceleration, it dropped by even more. The deformation of the seat back decreased substantially—to only 3.4 inches on the aisle-side—because much less of an impulse was given to the seat from the headform.

The vertical forces on the attachment points were still quite high, however, as illustrated in Figure 45. The magnitude of the peak force at the rear floor attachment point was about 4,000 lbf, only 20 percent less than it was for the 8g, 250 ms crash pulse.

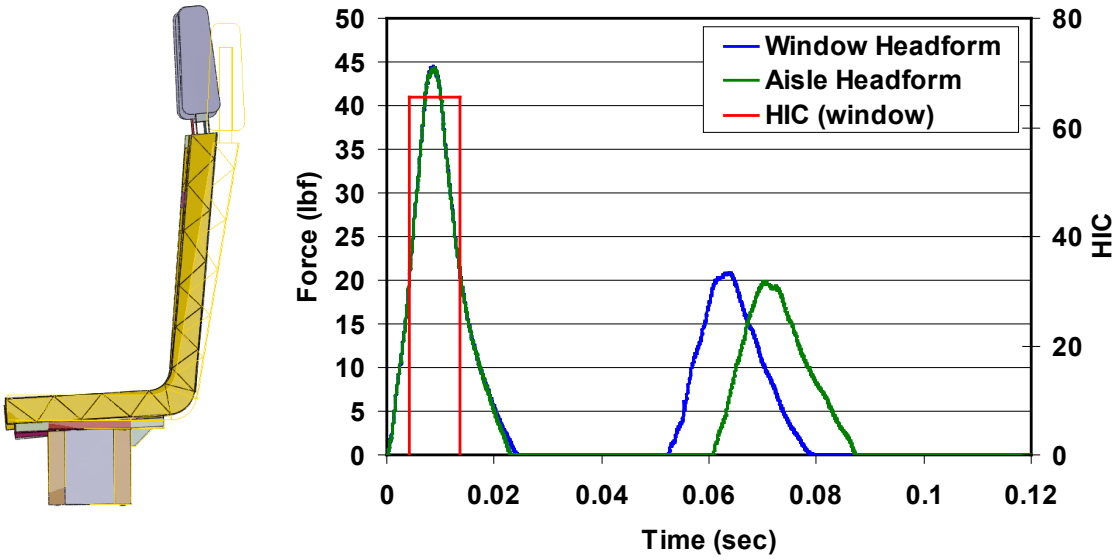

Figure 44. Calculated deceleration pulses (right) for the aisle and window impacting headforms for the ΔV = 5 m/s crash pulse. The calculated HIC of 65 is shown in red (time duration = 9.4 ms). The final deformation of the aisle-side seat back decreases to only 3.4 inches, as shown at left.

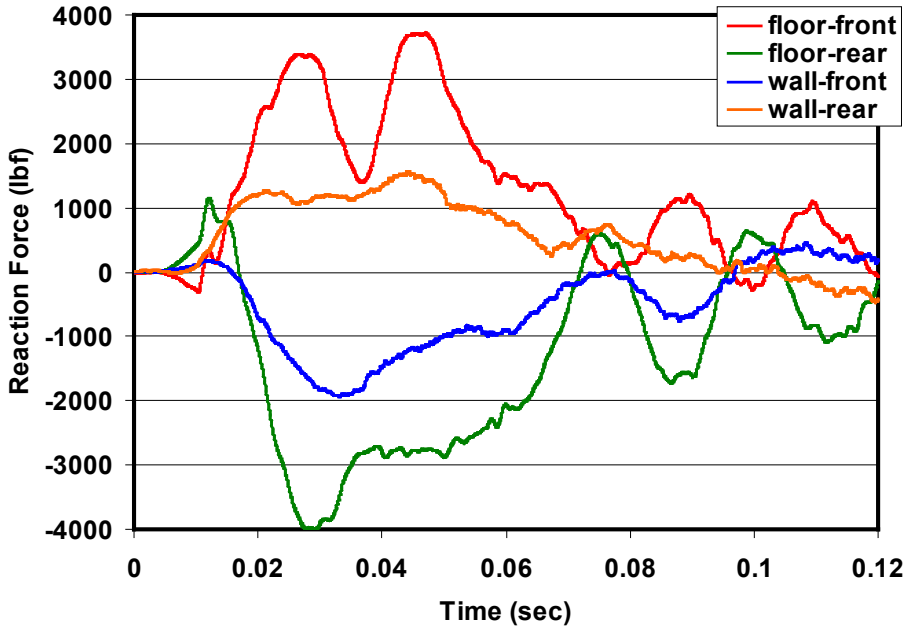

Figure 45. Vertical reaction forces vs. time for the four seat frame attachment points for the ΔV=5m/s crash pulse

Modified Seat Frame/GM/RT2100 Crash Pulse (ΔV = 5 m/s)

As discussed above, a primary objective of this analysis activity was to assess how much less the seat structure can weigh if it was designed to the less stringent GM/RT2100 specification rather than the 8g/250 ms specification (or, equivalently, how much more structural weight was required to meet the more stringent specification).

The analysis of the baseline seat configuration suggested that it would likely meet the requirements of the APTA specification:

- The calculated HIC of 489 was less than both the threshold value of 700 specified in CFR 49 Part 571, Standard No. 208 and referenced in APTA PR-CS-S-016-99, Rev. 2 and the threshold value of 500 specified in GM/RT2100.
- The deformation of the seat (maximum 8 in.) and the associated plastic strains (isolated and generally less than 10 percent except in very small regions) were not likely to cause failure of seat structures.
- This extent of deformation was similar to what was observed in the forward-facing test of the crashworthy commuter seat [8], a test in which compartmentalization of the passengers was determined to be acceptable.
- The calculated attachment forces were large but could be accommodated through design of both robust attachment features and lower seat structure.

The results from the second analysis clearly indicate that all measures of crashworthy performance are much better when the seating system is subjected to the less energetic ΔV = 5 m/s secondary impact velocity specified in GM/RT2100 rather than the full ΔV = 9.81 m/s secondary impact velocity that can be reached using the APTA 8g, 250 ms pulse specification.

If the thickness of the seat structural elements (and thus the overall seat weight) is decreased, most of the measures of crashworthy performance listed above would likely continue to decrease: the headform acceleration pulse and the HIC would likely be much smaller, and the loads on the seat structure would also likely be smaller. Only the seat deformation is likely to get larger.

To estimate the weight reduction achievable by using the less stringent GM/RT2100 standard, the seat back deformation was used as the limiting measure of crashworthy performance. An additional analysis was then conducted using the lower impact speed to estimate the weight difference of a seat structure that deformed to roughly the same 8 inches that was determined in the first analysis (the original structure, but with the higher impact speed). In this third analysis, the thickness was decreased by 50 percent for all of the shell-based structural elements, and the density and strength of the foam was decreased by 50 percent. This resulted in a seat weight of 18 lbs/seat compared to the baseline value of 36 lbs/seat.

The results of the analysis are summarized in Figure 46 and Figure 47. Figure 46 shows the predicted headform acceleration versus time curves, the calculated HIC, and the final deformation of the seat back. Because the seat was much more compliant, the accelerations were smaller, with the peak for this crash pulse decreasing from 45g to 25g and the associated HIC decreasing from 65 to 16. The deformation of the seat back increased, however, to about 8.5

inches, a little more than was calculated for the original seat structure and the more stringent 8g, 250 ms crash pulse. Figure 47 shows the vertical reaction forces, with the magnitude of the force at the rear floor connection decreasing substantially, from 4,000 lbf to 1,600 lbf.

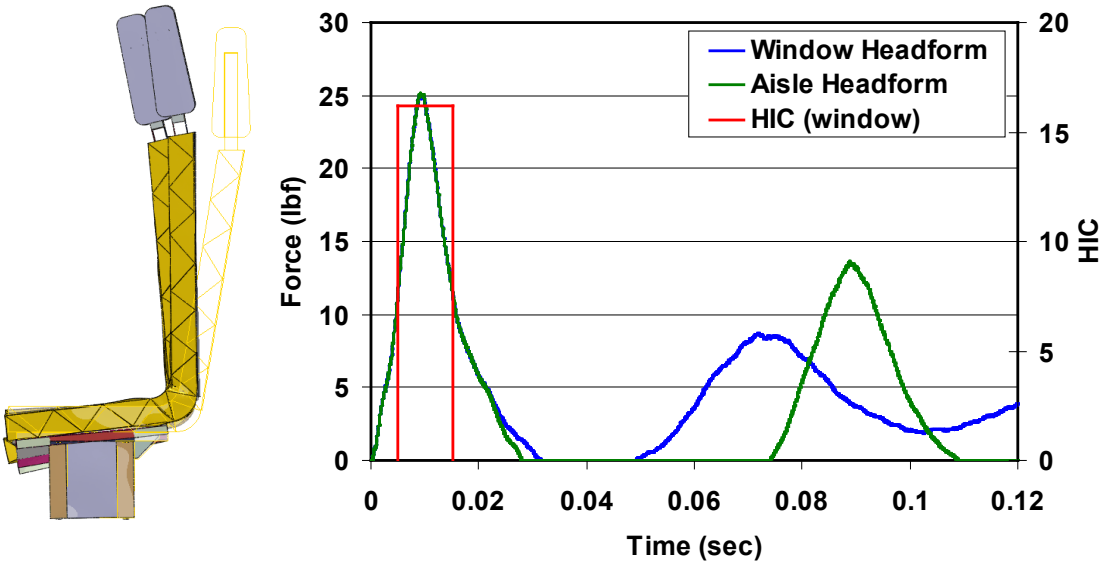

Figure 46. Modified seat design: calculated deceleration pulses (right) for the aisle and window impacting headforms for the ΔV = 5 m/s crash pulse. The calculated HIC of 16 is shown in red (time duration = 10.2 ms). The final deformation of the aisle-side seat back is about 8.5 in., as shown at left.

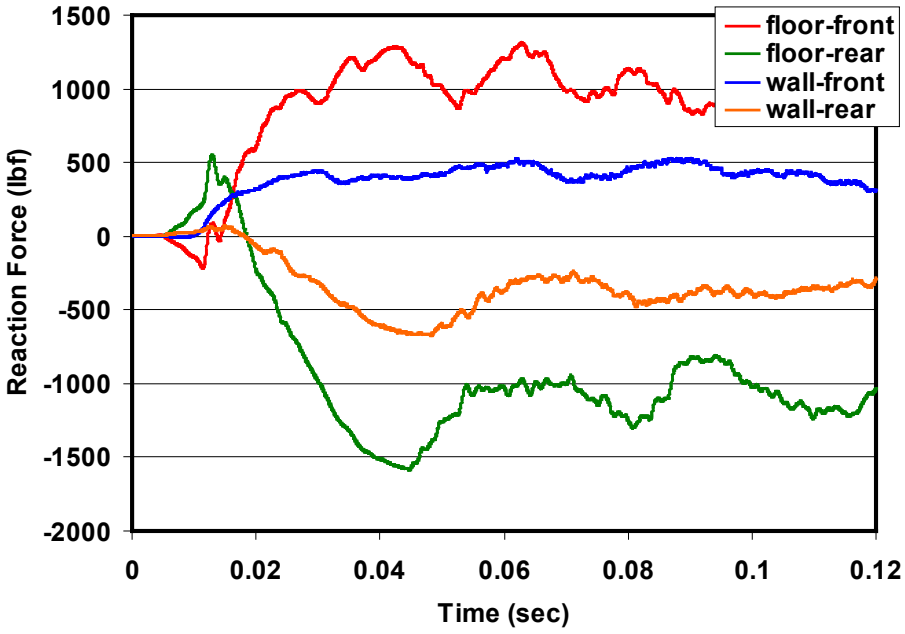

Figure 47. Modified seat structure: vertical reaction forces vs. time at the four seat frame attachment points for the ΔV = 5 m/s crash pulse

5.6 Seat connection strength

More stringent seat crashworthiness requirements lead to higher required seat attachment strength, and so it was of interest to determine whether this also leads to higher weight. As a means to investigate this issue, a calculation was conducted for one type of seat attachment: use of additional channel attachment points that were part of the aluminum profiles, as shown in Figure 48. There are two components that determine the attachment strength (not including the seat itself): the channel and the hardware. Fasteners can be obtained in a wide variety of sizes and strengths, so it was unlikely that they would significantly control weight and cost.

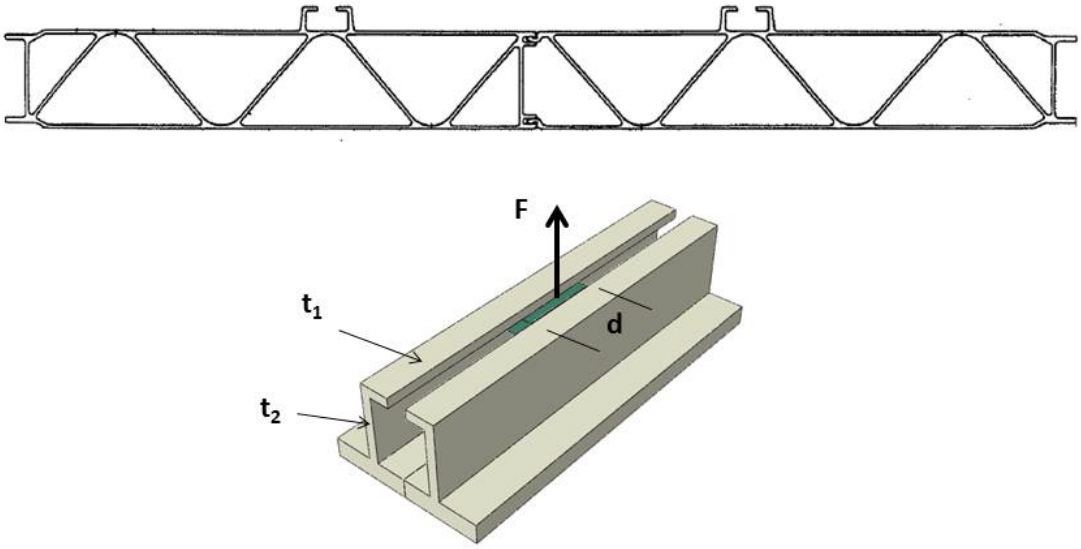

Figure 48. Schematic illustration for use in estimating rail seat attachment strength

The shear strength of the aluminum channel in the configuration shown in Figure 48 is approximately given by:

$$F_u = 2(0.6\sigma_u)(t_1)(d)$$

where, σ_u is the ultimate tensile strength of the aluminum extrusion, t_1 is the thickness of the channel, and d is the length over which the attachment nut or block bears on the channel. A typical value for the tensile strength is 37 ksi (255 MPa) for a 6005A-T6 alloy. The thickness of the aluminum in the channel is about 0.125 inch. (3 mm) The length over which the load is effectively distributed is a matter of judgment in a hand calculation. If this value is taken as 1 inch (25 mm), then the strength of one attachment point is F_u = 5500 lb (24.5 kN). This is comparable to the loads calculated in the previous sections. If a factor of two is required on strength then additional hardware would be needed, possibly adding a few pounds of weight.

5.7 Discussion

The analyses presented in this section indicated that application of the less stringent GM/RT2100 standard, in comparison to the 8g/250 ms requirement, resulted in a seat structure that was lighter by about 50 percent and still satisfied crashworthiness requirements. Looked at from the opposite viewpoint, requiring the seats to satisfy the more stringent 8g/250 ms standard may

require a seat structure that is up to twice as heavy—about 18 additional pounds per passenger seat. This conclusion was based on a compartmentalization measure of crashworthiness. No attempt was made to optimize the seat for measures of strength and injury criteria. Nevertheless, the results indicated that as the design crash pulse becomes more severe, the injury requirements and strength of attachment points will become more important, eventually governing the design.

It is likely that careful design with crashworthiness considerations would lead to a lower weight penalty to meet the more stringent requirements. For example, meeting the injury requirements for the more severe crash pulse may be achieved through more efficient design of energy-absorbing headrests and seat bolsters, with little impact on overall seat weight. Likewise, it is evident that the reaction forces at the various seat attachment points will be greater for seating systems designed to the more stringent crashworthiness standard; however, it is likely that connections and lower seat structure could also be designed to take these higher loads without a substantial weight penalty.

6. Fire Protection Analysis

High-speed train car builders have reported difficulty meeting the U.S. CFR structural fire resistance requirements for their lightweight aluminum structures. Aluminum has a substantially lower melting temperature than carbon or stainless steel (610 °C vs. 1500 °C), and the floor structures tend to be lighter than in U.S. cars, partly because of the lower buff strength requirement normally used for the design of high-speed trains. This section of the report provides a summary of the current U.S. structural fire requirements, a review of various approaches to improve fire protection (with consideration of their effect on weight), and an assessment using FEA of the ability of high-speed train cars to meet the structural fire requirements with and without added protection.

6.1 Structural Fire Resistance Requirements

Appendix B of CFR 49 Part 238.103 contains fire protection requirements for materials used in passenger cars and locomotive cabs. Part (c) of this appendix states that the structural floor system shall have a fire resistance rating per the testing requirements of ASTM E 119 (Standard Test Methods for Fire Tests of Building Construction and Materials [10]) that is the greater of the following:

- Twice the maximum expected time period under normal circumstances for a vehicle to stop completely and safely from its maximum operating speed, plus the time necessary to evacuate all the vehicle's occupants to a safe area.
- 15 minutes

Part (c) of Appendix B also states that the fire resistance period required shall be consistent with the safe evacuation of a full load of passengers from the vehicle under worst-case conditions.

The primary requirement of ASTM E119 is a test of a representative structural member or assembly in a furnace with prescribed temperature versus time characteristics and structural support conditions. The test article is usually a full-width section of the railcar that is long enough to represent the car structure. It need only include part of the side structure—again, enough to represent the structural response of the floor. The temperature versus time history to which symmetrically distributed thermocouples located 12 inches below the test article bottom surface are to be exposed is shown in Figure 49.

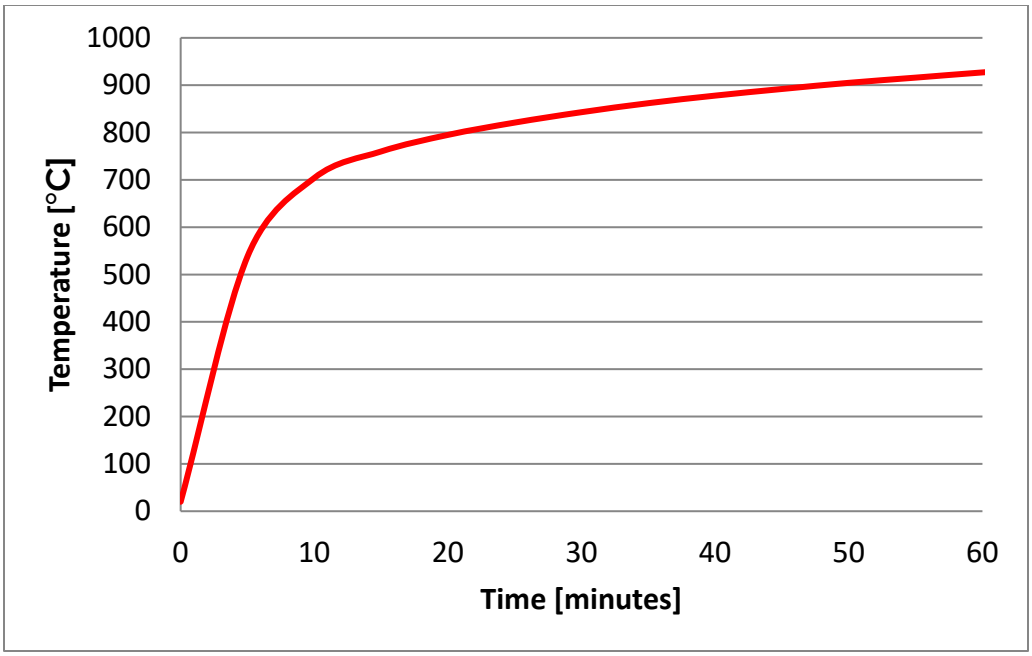

Figure 49. ASTM E 119 temperature-time curve (up to 1 hour shown)

The requirements to pass the test are:

- The temperature on the unexposed surface shall not be more than 139 °C (250 °F) average or 181 °C (325 °F) at a single point.
- There shall be no passage of flame or gases hot enough to ignite cotton waste on the unexposed surface of the assembly.
- The test article must be able to support the applied loading.

ASTM E 119 does not specify a deflection magnitude and/or rate as indicative of the inability of the structure to carry loading. In practice, test operators monitor the deflection history of the assembly and stop the test when the deflection is deemed excessive, based on judgment.

Testing per ASTM E 119 dates back to the early 20th century and remains mostly unchanged from that time. The temperature-time history of the furnace exposing the structural specimen was originally developed to simulate a cellulosic fire exposure. There are only a few laboratories in the U.S. that conduct standard fire-resistance testing.

Another U.S.-based standard used for assessing the structural fire resistance of railcars is NFPA 130 (Standard for Fixed Guideway Transit and Passenger Rail Systems [11]). This standard has requirements similar to 49 CFR Part 238.103, except it includes the following:

- A minimum fire-resistance rating of 30 minutes for the structural floor system
- The test floor assembly shall be at least 3.7 m (12 feet) long by the normal width of the given rail vehicle.
- The test floor assembly shall have a loading applied that is consistent with the vehicle design and accounts for equipment and a crush load of passengers (AW2 loading).

- Support of the test floor assembly shall be limited to the transverse ends of the assembly only.

Evidently, many train operators in the U.S. (none high speed) require these NFPA 130 requirements in their new car specifications.

Other standards used for structural fire resistance of railcar floors are the British standard, BS6853, Code of Practice for fire precautions in the design and construction of passenger carrying trains [12], and the European standard, EN45545-3, fire-resistance requirements for fire barriers [13]. These standards have a structural test and temperature-time history very similar to that of E119, but the allowable surface temperature and the time to reach this temperature differ, as shown in Table 13.

Table 13. Comparison of some requirements from different structural fire resistance codes and standards

	CFR (ASTM E 119)	NFPA 130	EN 45545-3	BS 6853
Loading	Maximum loading condition	Equipment and AW2 loading	Realistic loading	No applied loading
Heat Transmission Failure	139 ˚C (average); 181 ˚C (spot) (temperature on unexposed surface)	139 ˚C (average); 181 ˚C (spot) (temperature on unexposed surface)	No requirement except ignition (any material through the floor or on the unexposed surface)	250 ˚C (average); 300 ˚C (spot) (any surface through the floor or on the unexposed surface)
Required Rating	15 minutes	30 minutes	15 minutes	20 minutes

6.2 Rail Vehicle Floor Structure

The floor structure of a high-speed train that would be subjected to a structural fire test usually consists of a double-walled aluminum extrusion, such as shown in Figure 50 and described in Section 3 of this report. The geometry shown in Figure 50 was selected as the structural segment to evaluate here for baseline and additionally protected configurations. This segment was essentially repeated to achieve a total width of 2.9 m (9.5 feet), a typical vehicle width.

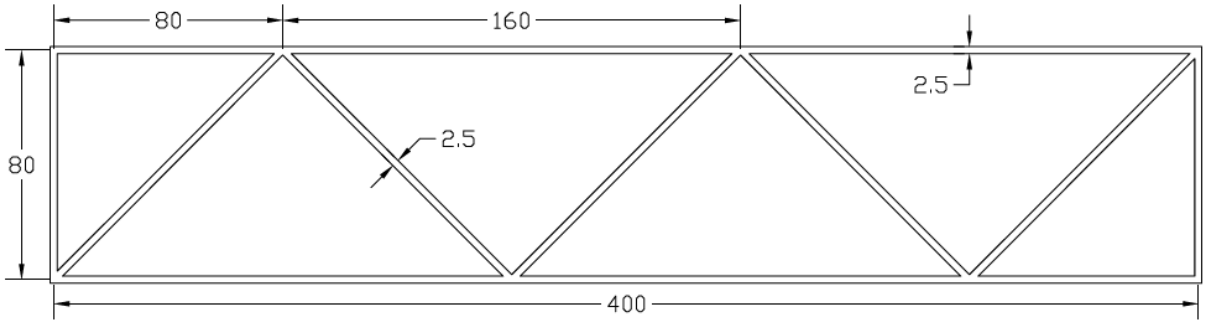

Figure 50. 2-D profile of floor extrusion (repeating segment) (mm)

The RSAC ETF has proposed including underfloor equipment and the bottom cover to represent the additional fire resistance that would exist for fires originating on the track. However, because the cover would not provide protection of the floor system from a fire within its cavity space (e.g., equipment fire), it was not included in this study.

The floor extrusion modeled here was assigned the properties of 6005A aluminum alloy. Table 14 lists the room temperature thermal properties of 6005A aluminum alloy compared to those for carbon steel. The temperature dependence of the material's thermal conductivity and specific heat were decreased linearly by 10 percent between ambient and 600 °C. The variation of elastic modulus with elevated temperature was included in the structural model using the values shown in Figure 51; the elastic modulus declined rapidly for temperatures above 500 °C until the melting point of the aluminum was reached.

Table 14. Thermal properties of 6005A aluminum alloy [14]

Thermal Property	6005A Aluminum Alloy	Steel
Density (kg/m^3)	2,700	7,850
Thermal Conductivity (W/m°C)	167	53
Specific Heat (J/kg°C)	900	440
Emissivity	0.1 (oxidized)	0.8 (oxidized)

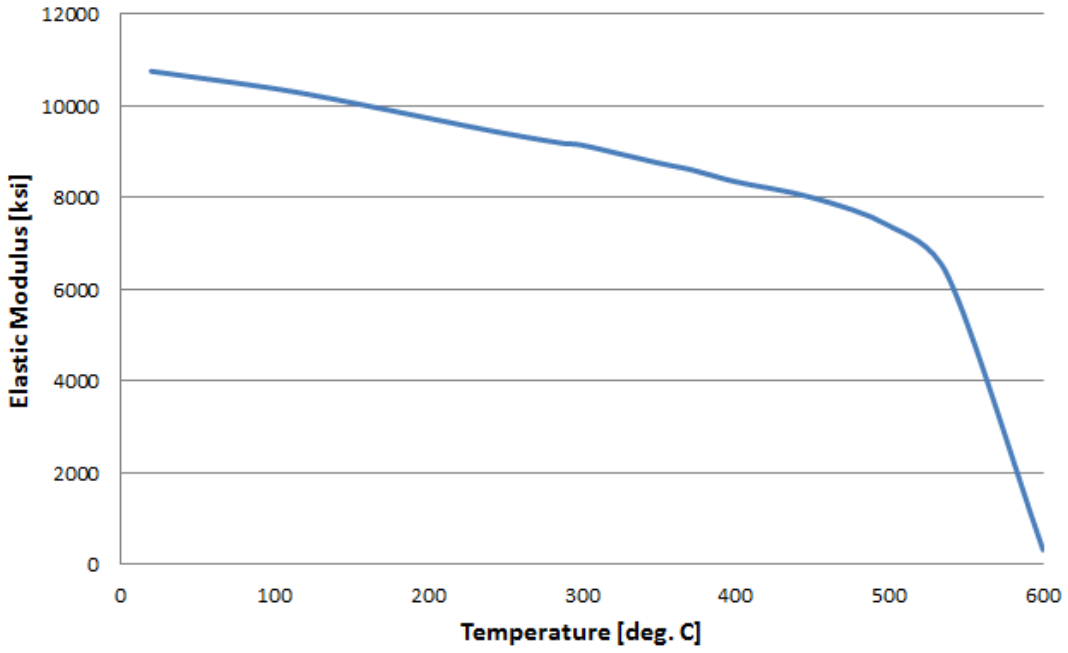

Figure 51. Temperature-dependent elastic modulus of aluminum 6005A alloy [15]

6.3 Methods to Increase Fire Resistance

Analyses of the baseline structure of Figure 50 showed that without additional protection, the top surface temperature of the floor extrusion would exceed the allowable value in less than the required 15 minutes of the CFR and, certainly, within the 30 minutes of NFPA 130. Accordingly, various means to increase the floor's fire resistance were investigated to limit the rise of

temperature on its unexposed surface and to help maintain its load-carrying capacity. The various approaches studied are listed in Table 15, and the analysis results for these options are presented in Section 6.5.

Table 15. Fire protection approaches in this study

Approach	Basis of added protection
Fill the spaces of the extrusion with insulating material.	• Reduces heat transfer through cavity radiation
Include a top, ply-metal floor panel.	• Requires more time for heat conduction • Provides an opportunity for adding a layer of different thermal conductivity
Add bottom protective layers: • Blanket • Board • Intumescent coating	• Provides an insulating layer
Include an active fire suppression system.	• Put the fire out once detected.

6.3.1 Insulation of Extrusion Void Spaces

The first option considered was filling the void spaces of the floor extrusion with insulation. There are two modes of heat transfer from the bottom flange of the extrusion to the top flange: conduction through the angled, metal webs, and heat transfer through the spaces between the flanges primarily by radiation. Insulation would reduce the latter mechanism of heat transfer. The effect this could have been analyzed by simply eliminating the radiation heat transfer within the cavities, simulating an ideal insulator.

6.3.2 Inclusion of Ply-Metal Floor

A ply-metal floor is normally included as part of a railcar floor structure to meet performance objectives related to acoustics and floor stiffness. Ply-metal floors are typically comprised of a plywood sheet or aluminum honeycomb sandwiched between two thin aluminum layers with a total thickness of around 0.375 to 0.5 inch (9.5-12.7 mm.) The ply-metal functions as an additional thermal insulator, and this was analyzed as a configuration. In reality, this could be viewed as the baseline, since it is almost always the case that a ply-metal floor is included in the construction.

The configuration shown in Figure 52 was analyzed. The thermal properties used for the inner layer are for plywood and are listed in Table 16. The plywood would not be exposed to radiation heating or cooling, since it was sandwiched between thin aluminum layers; therefore, the emissivity of plywood was not considered.

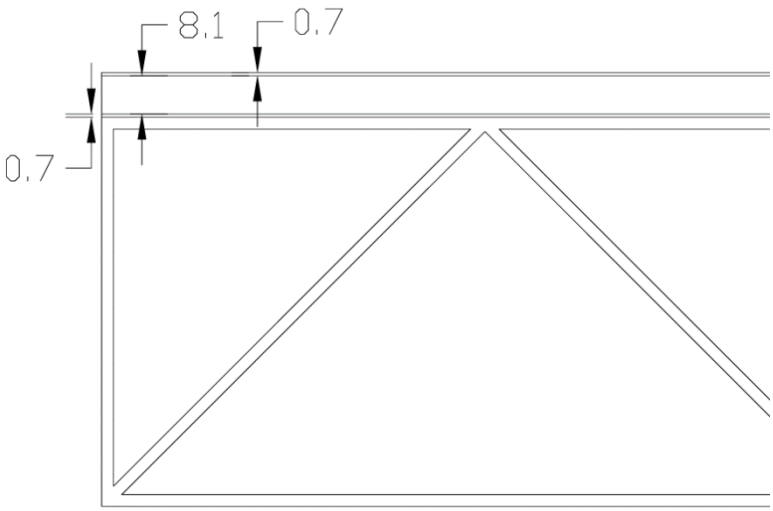

Figure 52. Schematic of the ply-metal floor model (dimensions in mm)

Table 16. Thermal properties of plywood [16]

Thermal Property	Value
Density (kg/m^3)	545
Thermal Conductivity (W/m°C)	0.12
Specific Heat (J/kg°C)	1,215

Note that if a ply-metal floor were included as part of the test specimen, the thermocouples would be located on the top surface of the ply-metal floor as opposed to the top surface of the floor extrusion.

6.3.3 Fire Protection Materials

Three general types of applied fire protection materials were investigated to limit the temperature rise of the top surface of the floor extrusion: fire-resistant blankets, fire-resistant boards, and intumescent coatings. Each was applied to the underside of the extrusion. Table 17 lists the thickness values that were analyzed together with the added weight per railcar for each of the materials investigated. The following sections provide descriptions for each material.

Table 17. Applied Fire Protection Materials.

Technology	Thickness (mm)	Estimated Weight Per Railcar* (lbs)
Fire-resistant blankets	25	350
Fire-resistant boards	13	1000
Intumescent coating	5	750

* Based on a 21.3 m (70 ft.) long by 3.1 m (10 ft.) wide rail car

6.3.3.1 Fire-Resistant Blankets

Fire-resistant blanket products are widely used in the building industry. They are commonly composed of mineral wool, available in thicknesses as low as 25 mm (1 inch). They have good insulating properties and are relatively light, but hardware is generally required to attach the blanket to the structure, and that would certainly be the case for the underside of the rail vehicle. There may also be issues of blanket and attachment durability for the vibration environment of rail vehicle operation and possibly from weathering, depending on outside exposure.

Figure 53 and Figure 54 show the temperature-dependent conductivity and specific heat of mineral wool, respectively; these are the curves that were used in the finite element model for this configuration. Values for density of 160 kg/m^3 and emissivity of 0.9 were also used in the analysis.

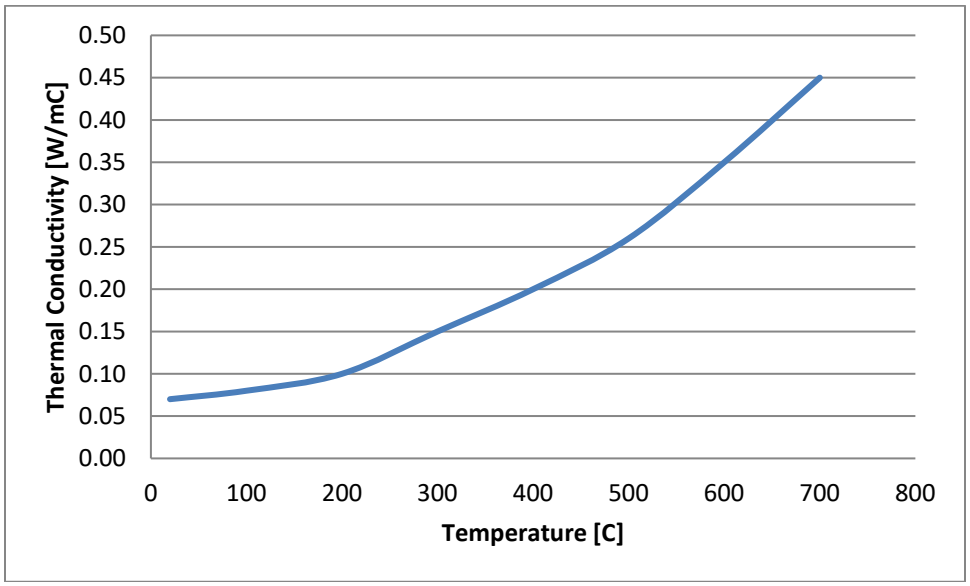

Figure 53. Temperature-dependent thermal conductivity of mineral wool [17]

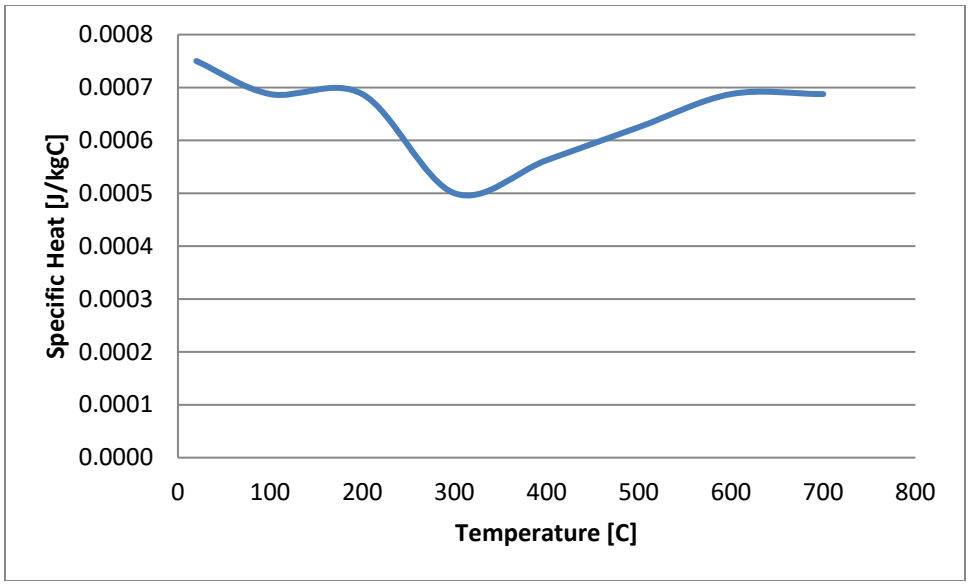

Figure 54. Temperature-dependent specific heat of mineral wool [17]

6.3.3.2 Fire-Resistant Boards

Fire-resistant boards are commonly composed of gypsum which undergoes an endothermic (calcination) reaction when heated; that is, it absorbs heat. Type X, an ASTM designation, is one type of gypsum board that also has special additives to enhance this heat-absorbing characteristic, and it is commonly available in thicknesses of 9.5 mm (0.375 inch) and 13 mm (0.5 inch) Figure 55 through Figure 57 show the temperature-dependent conductivity, specific heat, and density of Type X gypsum board, respectively, used in the analysis. The endothermic reaction of the gypsum was evident in the dramatic increase in specific heat between 100 and 200 °C (Figure 56). An emissivity of 0.7 is characteristic of this material and was used in the analysis.

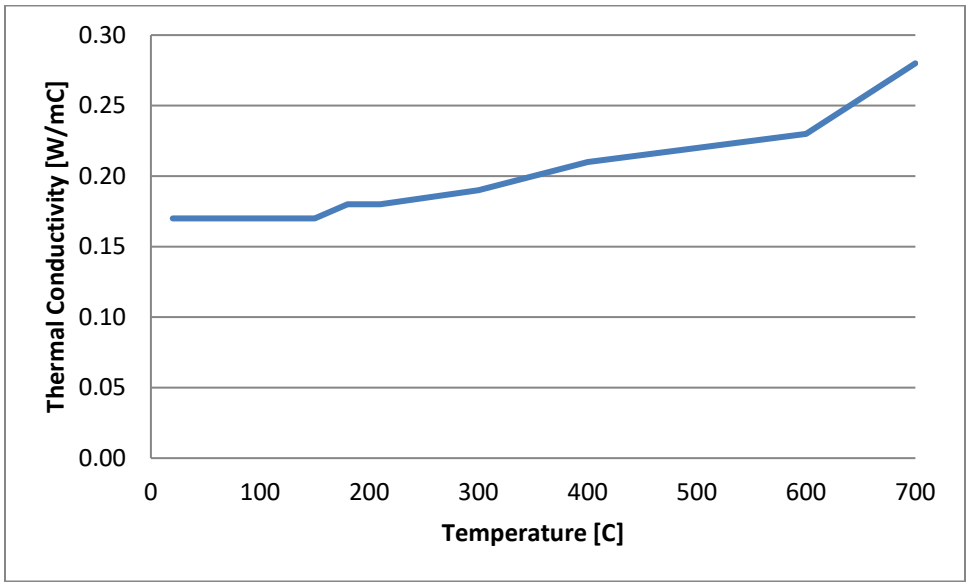

Figure 55. Temperature-dependent thermal conductivity of Type X gypsum board [18]

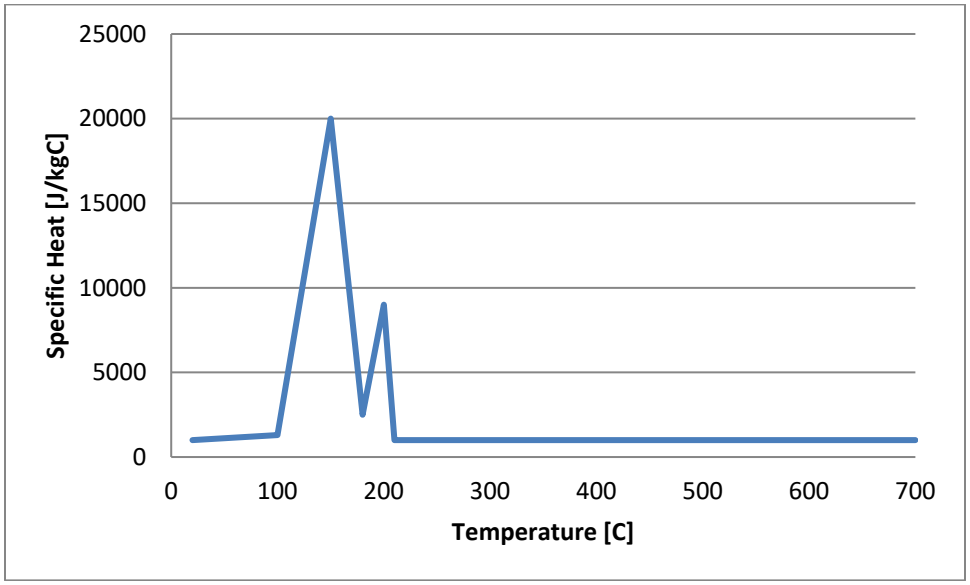

Figure 56. Temperature-dependent specific heat of Type X gypsum board [18]

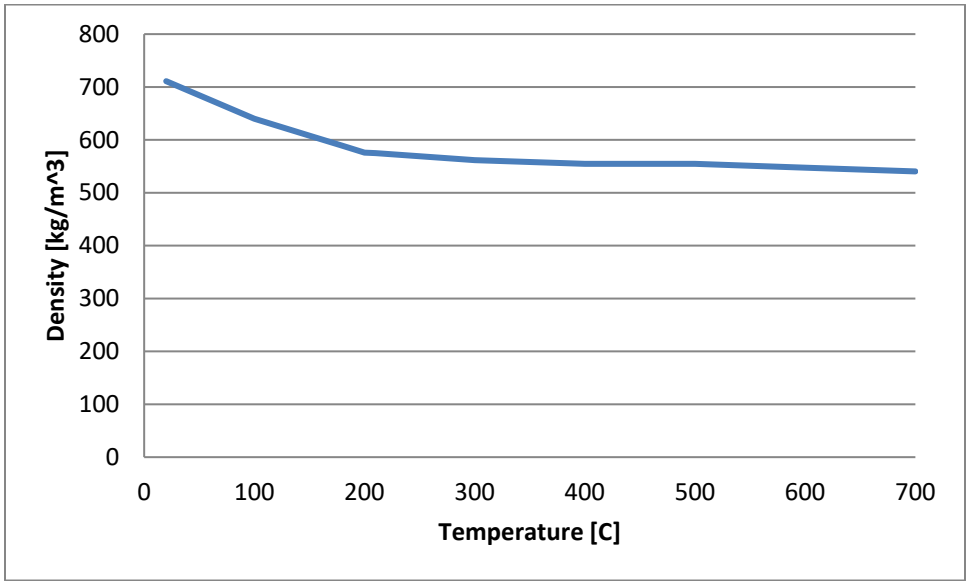

Figure 57. Temperature-dependent density of Type X gypsum board [18]

6.3.3.3 Intumescent Coatings

Intumescent coatings are often used for providing fire protection to structural members. They can be spray- or trowel-applied to the surface. When exposed to fire, it significantly expands and forms an insulating char layer. There is also an associated endothermic reaction that forms a char that absorbs heat energy. Intumescent coatings are classified as two general types: water-

and epoxy-based. An epoxy-based intumescent coating is necessary for the rail vehicle application because of its enhanced durability; for example, these coatings are used for harsh exterior applications (e.g., oil rigs). Epoxy intumescent coatings release smoke when activated by fire, but this would likely not pose a hazard to occupants inside the cabins if the vehicles are properly sealed.

Epoxy intumescent coatings typically range from 5 mm (0.2 inch) to 25 mm (1 inch) thick, depending upon the level of protection required. The minimum thickness of 5 mm (0.2 inch) is usually set by the manufacturer to allow for the inclusion of a reinforcing metal mesh at mid-thickness. However, the need for such a mesh in the rail vehicle application is not clear and would need to be investigated. In any case, it would add little weight.

Selection of intumescent coating thermal properties for use in the FEA was difficult because of the phase change with temperature. Data from [16] were used to estimate the temperature-dependent conductivity, specific heat, and density, respectively, used in the analysis, as shown in Figure 58 through Figure 60. The transformation of the original material into char between about 300 and 400 °C was evident in the dramatic decrease in thermal conductivity, shown in Figure 58, and the temporary increase in specific heat, as seen in Figure 59. An emissivity of 0.9 was used for this material.

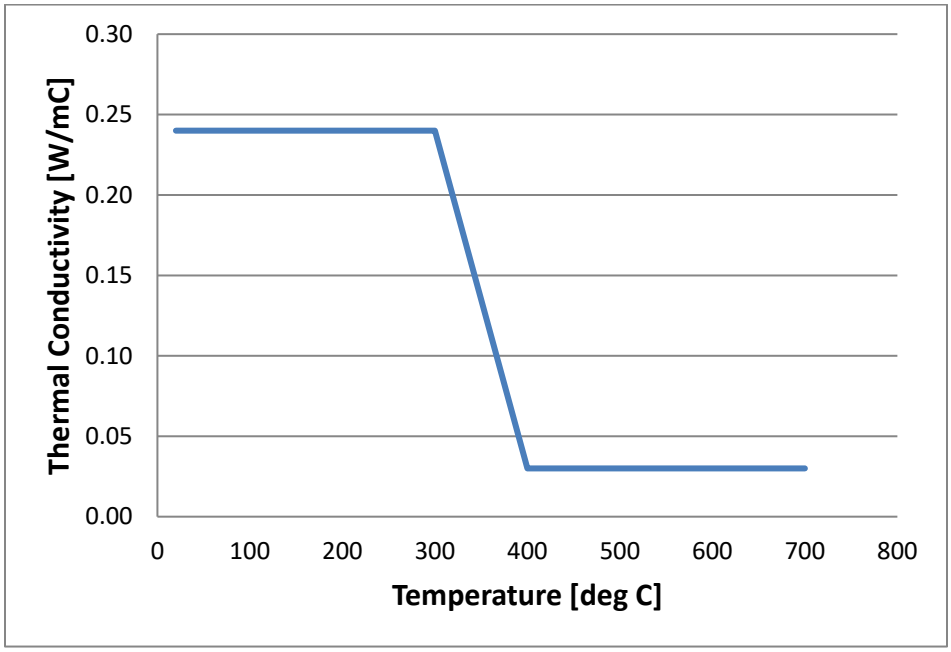

Figure 58. Temperature-dependent thermal conductivity of epoxy intumescent [19]

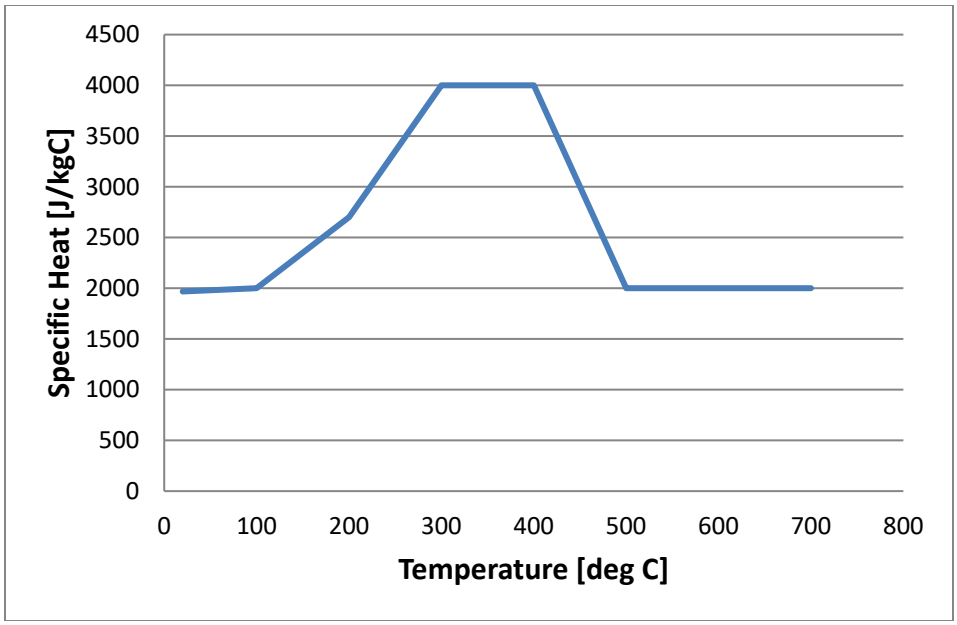

Figure 59. Temperature-dependent specific heat of epoxy intumescent [19]

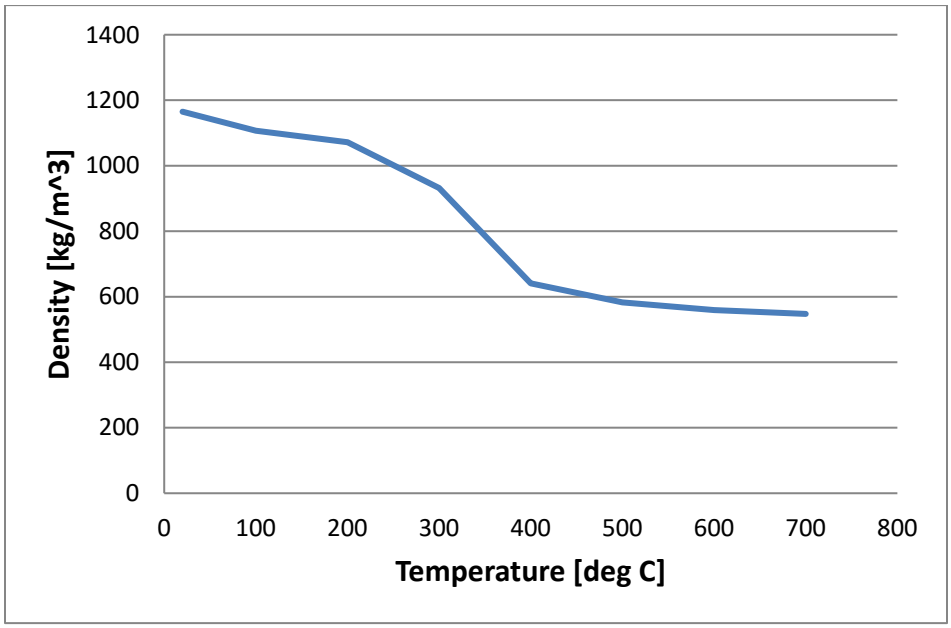

Figure 60. Temperature-dependent density of epoxy intumescent [19]

6.3.4 Clean Agent Fire Suppression System

Clean agent suppression involves the release and containment of inert gases or chemical agents to suppress fire. Such a system together with the railcar could be engineered to function within the cavity space between the railcar floor and the underside cover. In this case, high-pressure-rated piping and clean agent storage tanks would be required, as well as a fire detection system.

The weight of the piping and storage tanks alone would likely be over 1,000 lbs per rail car. Such a system can be very effective but has reliability issues, particularly in the dynamic environment of the rail vehicle. It is a viable fire protection approach but was not investigated further in this study.

6.4 Performance Analysis Approach

Two modeling approaches were used to evaluate the effects of different fire protection approaches on performance: a thermal model and a structural model. The thermal model is used to calculate the temperature as a function of time at the top surface of the floor configuration. The temperature at this location must be less than 139˚C at 15 minutes according to the CFR and less than 139˚C at 30 minutes according to NFPA 130. The structural model is used to calculate the floor assembly deflection as a function of time. The E119 standard does not specify the allowable deflection, but the model is used to determine when deflections increase rapidly with time. Both types of analysis were conducted using the finite element software Abaqus/Standard Version 6.12-1.

The thermal finite element model used the configuration previously shown in Figure 50. It was 2-dimensional with a width of 0.4 m (1.3 feet) The mesh consisted of 8-node, biquadratic, diffusive 2-dimensional heat transfer elements that allowed a nonlinear temperature gradient through each element. A typical element size of 1.25 mm (0.05 in.) was used, which allowed for two elements through the thickness of the extrusion web plates and top/bottom flanges. The thermal properties of 6005A aluminum alloy described in Section 6.2 were used for the analysis. The E119 furnace conditions were simulated by including radiation and convection heat transfer at the bottom surface of the assembly being analyzed. The time-varying sink temperature in this case was the E119 curve shown in Figure 49. Emissivity depends on the material and the values used are listed in the sections on the particular configuration. The convection heat transfer coefficient was 25 $W/m^2°C$ for the bottom (exposed surface) and 5 $W/m^2°C$ for the top surface. Additionally, cavity radiation within the extrusion void spaces was included. Perfect thermal contact was modeled for cases in which layers of material were included at the top or bottom surfaces of the extrusion.

The structural model included the full span of the floor extrusion (2.88 m (9.5 feet.)) with depth of 1 m (3.3 feet), shown in Figure 61. It consisted of six units of the cross-section used for the thermal model and one central section to create symmetry about the center line. The mesh was comprised of conventional 4-node structural shell elements (Abaqus S4). The temperature-dependent elastic properties described in Section 6.2 were used in the structural model.

The temperature-time history from the thermal analysis for the 0.4 m wide configuration was used as input for the structural model in the following manner. In the structural model, there were three regions of spatially constant temperature: the bottom flange, the angled webs, and the top flange. The time-varying temperature from the thermal model used for each region was taken from the corresponding center point in the 0.4 m long model. The support conditions at the lateral ends of the panel were pinned and a 34 lb/ft^2 uniform load was applied to the top surface corresponding to an AW2 loading condition. (AW2 corresponded to the weight of the rail car with all seats occupied and some standing passengers.) Use of a unit depth was acceptable since the floor acted primarily as a one-way member between span supports.

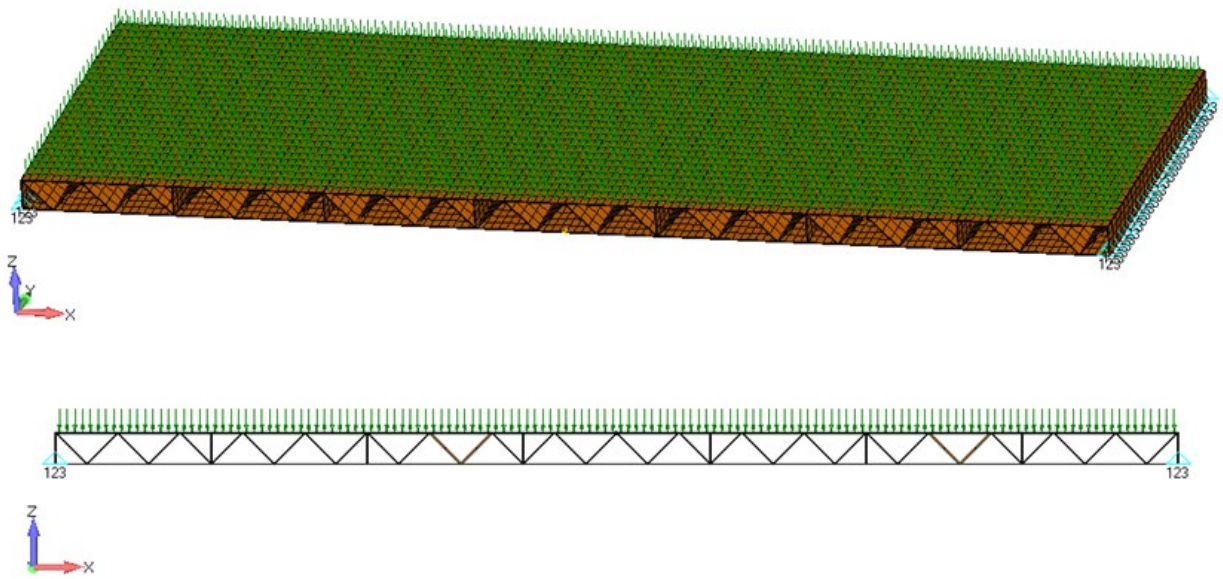

Figure 61. Structural model with applied loading (top: isometric view; bottom: elevation view)

The AW2 loading was applied to the structural model under ambient conditions as a first step. After the loading was applied, the standard furnace exposure history, seen in Figure 49, was simulated by applying the temperature histories of the floor extrusion derived from the corresponding thermal model. Over the course of the simulation, the mid-span deflection of the floor extrusion panel was monitored to provide an indication of when the floor extrusion was no longer able to support the applied loading.

The following effects were neglected for the structural analysis: thermal expansion, plastic deformation, and creep. Neglecting thermal expansion in the analysis was reasonable since the floor would likely be tested in an unrestrained condition (i.e., supports would offer minimal resistance to thermal expansion). The stresses in the panel from the AW2 loading were very low, less than 2 ksi, so yielding and creep would not become important until the metal approached its melting temperature.

6.5 Performance Analysis Results

6.5.1 Unprotected Assembly Performance

The first analysis was for the case in which the double-walled aluminum extrusion had no additional material and radiation heat transfer was permitted within the cavities of the extrusion. Figure 62 shows a plot of the calculated temperature histories of the floor extrusion at its bottom surface, mid-height, and top surface. The failure limit, 139 °C, for the top surface temperature is also represented.

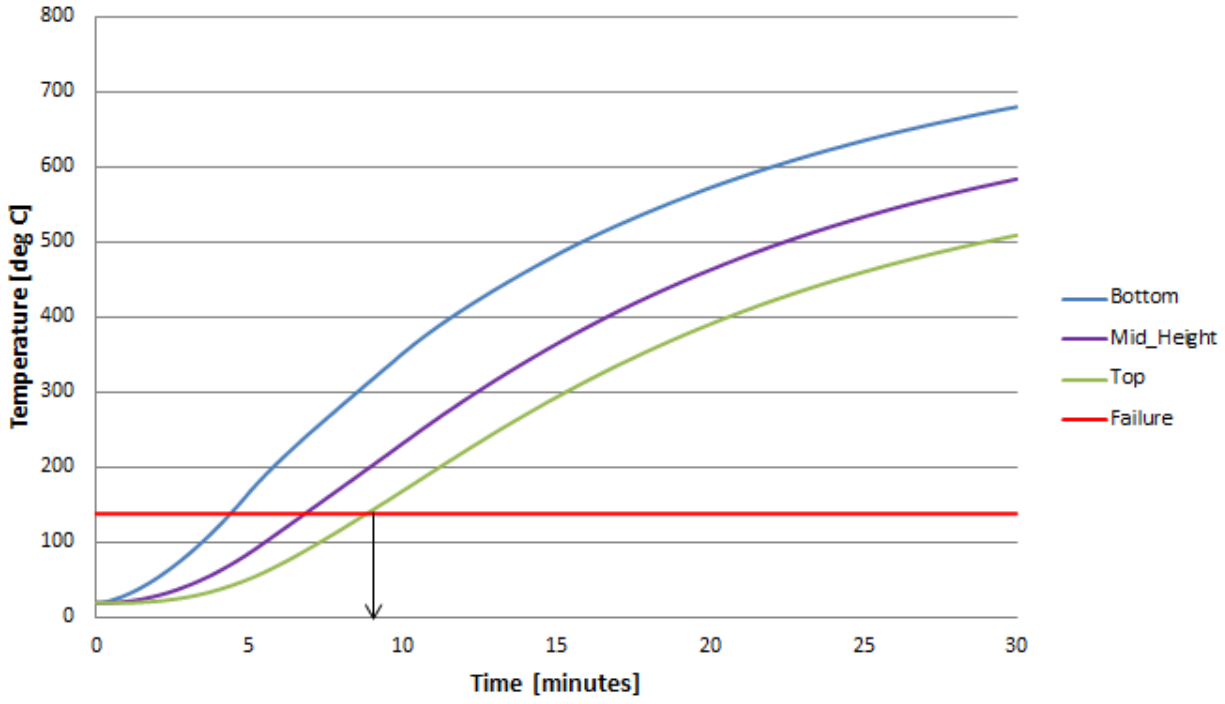

Figure 62. Temperature-time histories of the double-walled aluminum extrusion without addition of other materials and with internal cavity radiation heat transfer

These results indicated that the failure criterion was reached in approximately 9 minutes, well below the 15 minute limit of E119 and the 30 minute limit of NFPA 130. In fact, the calculated temperature of the bottom surface at 30 minutes exceeded the melting temperature of the aluminum, 610 °C.

Figure 63 shows the temperature distribution through the floor extrusion after 9 minutes of exposure. At this point in the analysis, the temperature of the bottom flange of the floor extrusion was approximately twice that of the top surface.

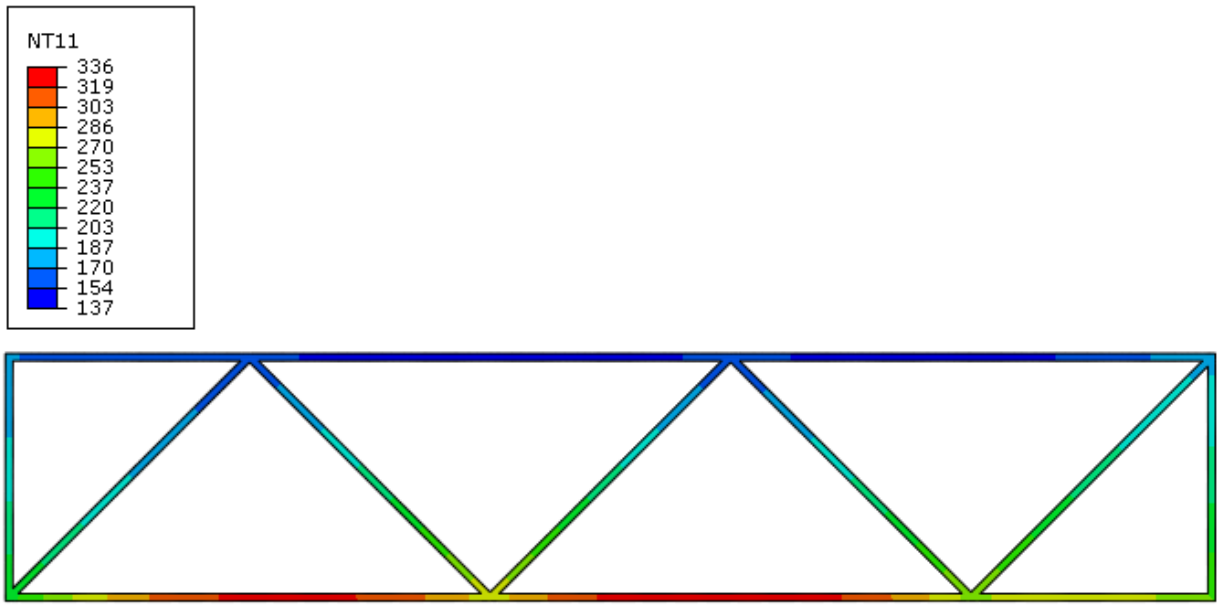

Figure 63. Temperature distribution in the double-walled aluminum extrusion without addition of other materials and with internal cavity radiation heat transfer after 9 minutes of exposure [˚C]

Figure 64 shows the mid-span vertical deflection after the initial AW2 load application and subsequently during the standard furnace exposure. The deflection history increased rapidly at approximately 21 minutes of exposure. Therefore, the thermal response governed the fire resistance performance of this baseline configuration.

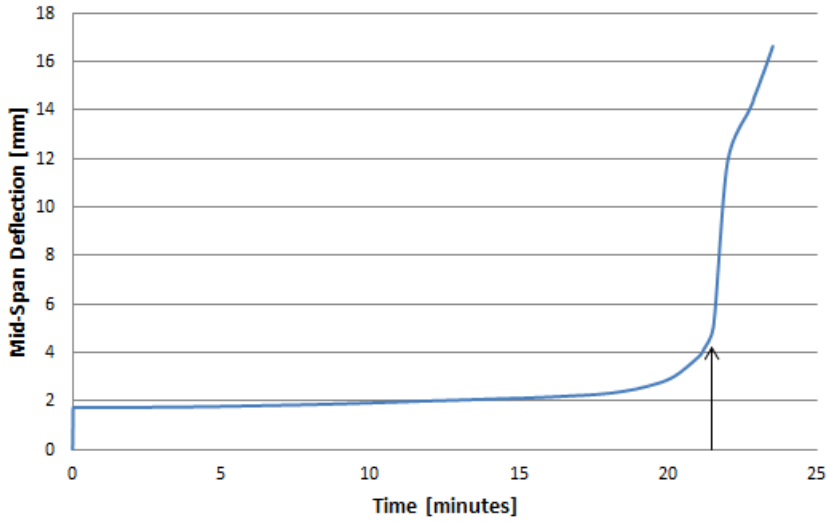

Figure 64. Mid-span vertical deflection history of the double-walled aluminum extrusion without addition of other materials and with internal cavity radiation heat transfer

6.5.2 The Effect of Insulating Floor Extrusion Voids

Filling the void spaces of the floor extrusion with insulation eliminated or greatly reduced heat transfer in these spaces, primarily from radiation. Figure 65 compares the calculated temperature histories of the baseline configuration, Section 6.5.1, to the case in which the radiation heat transfer in the void spaces was not simulated; convection in the spaces was not significant and was not simulated in either case. There was essentially no difference in results demonstrating that the primary heat transfer from bottom to top flange was through conduction through the angled webs. Adding insulation to these spaces had very little benefit; the air already provided substantial insulation.

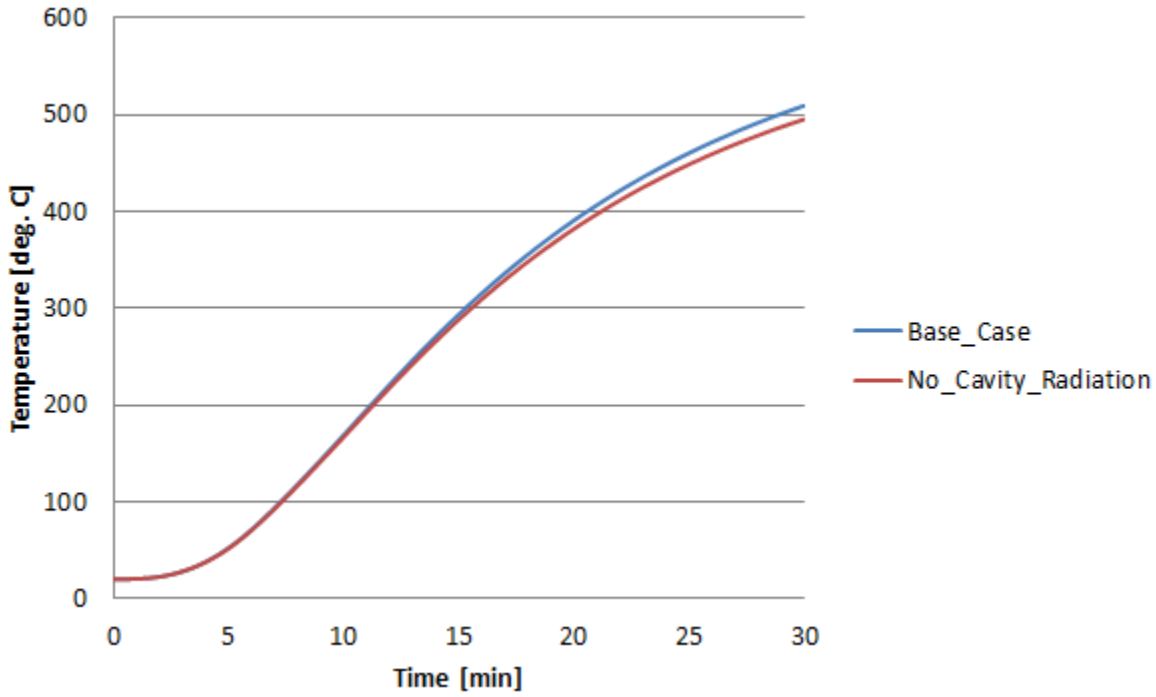

Figure 65. Top surface temperature histories with and without cavity radiation in the extrusion spaces to investigate the effect of insulation within the extrusion

6.5.3 The Effect of Inclusion of a Ply-metal Floor

The results of the analysis in which a top surface ply-metal floor was included are shown in Figure 66; the characteristics of the layer were provided in Section 6.3.2. The temperature in this case was taken from the top surface of the ply-metal layer.

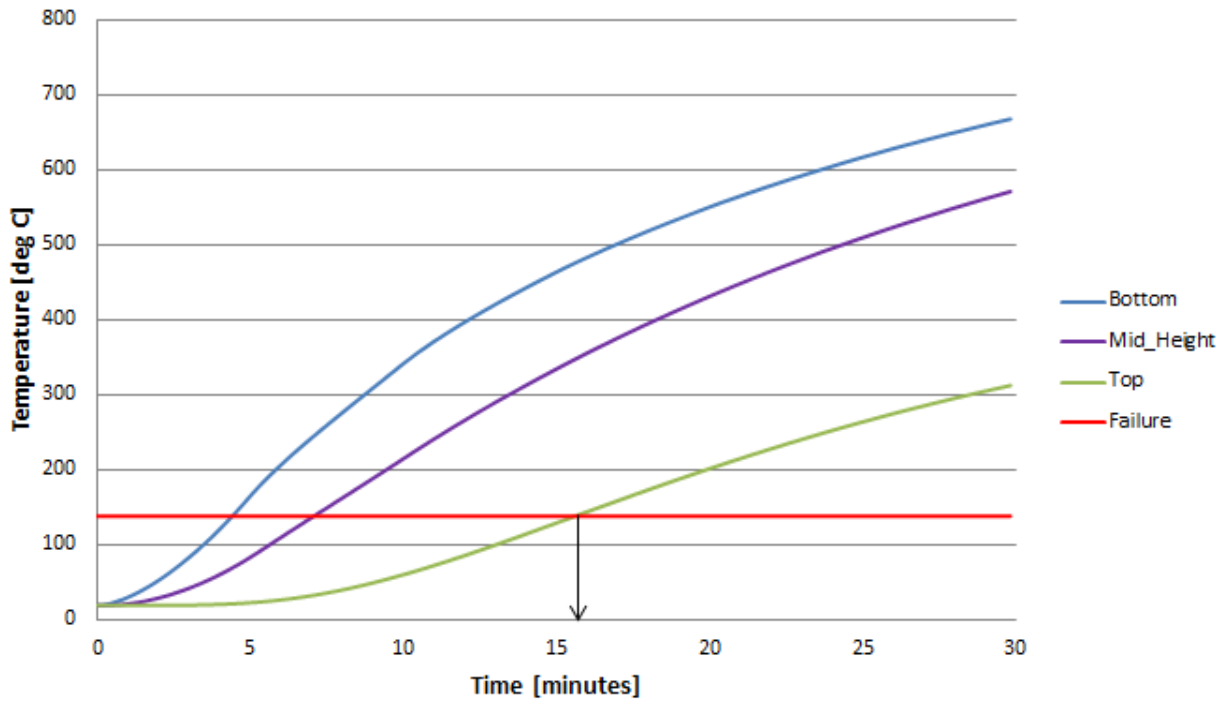

Figure 66. The temperature-time histories of the double-walled aluminum extrusion with a top surface ply-metal layer

The time at which the temperature of the top surface reached the thermal failure criterion was approximately 16 minutes. Note that the bottom surface temperature at this time was about 500 ˚C, within about 100 ˚C of the aluminum melting temperature when the structural integrity of the system would be completely compromised. The calculated temperature of the bottom surface exceeded the aluminum melting temperature at 30 minutes, as was the case when the ply-metal floor was not included.

6.5.4 Benefit Provided by Applied Fire Protection Materials

The next three sections describe the results of simulating the inclusion of an insulating material on the bottom surface of the double-walled aluminum extrusion. In each case the ply-metal floor layer was included. The reported top surface temperature corresponded to the top of the ply-metal floor and the bottom surface temperature corresponded to the bottom of the aluminum profile.

6.5.4.1 Fire Resistant Blanket

The results for the case in which a 25 mm (1 inch) thick fire resistant blanket was attached to the underside of the floor extrusion are shown in Figure 67; the characteristics of the blanket layer are provided in Section 6.3.3.1. The time at which the temperature of the top surface reached the thermal failure criterion was approximately 28 minutes. Furthermore, the temperature of the bottom flange of the aluminum extrusion at this time was only about 350 °C, well below the melting temperature. Figure 68 shows the temperature distribution through the assembly after 28 minutes of standard furnace exposure. The deflection of the assembly was low at 28 minutes.

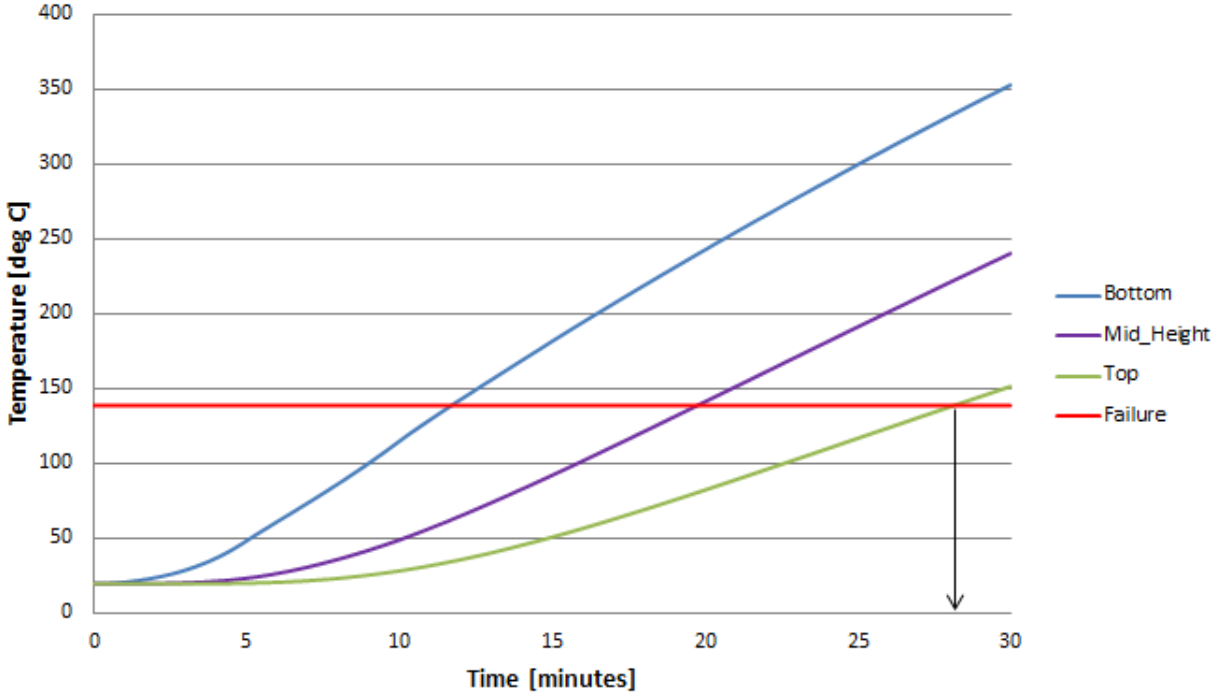

Figure 67. The temperature-time histories of the double-walled aluminum extrusion with an insulating bottom blanket layer and a top surface ply-metal layer

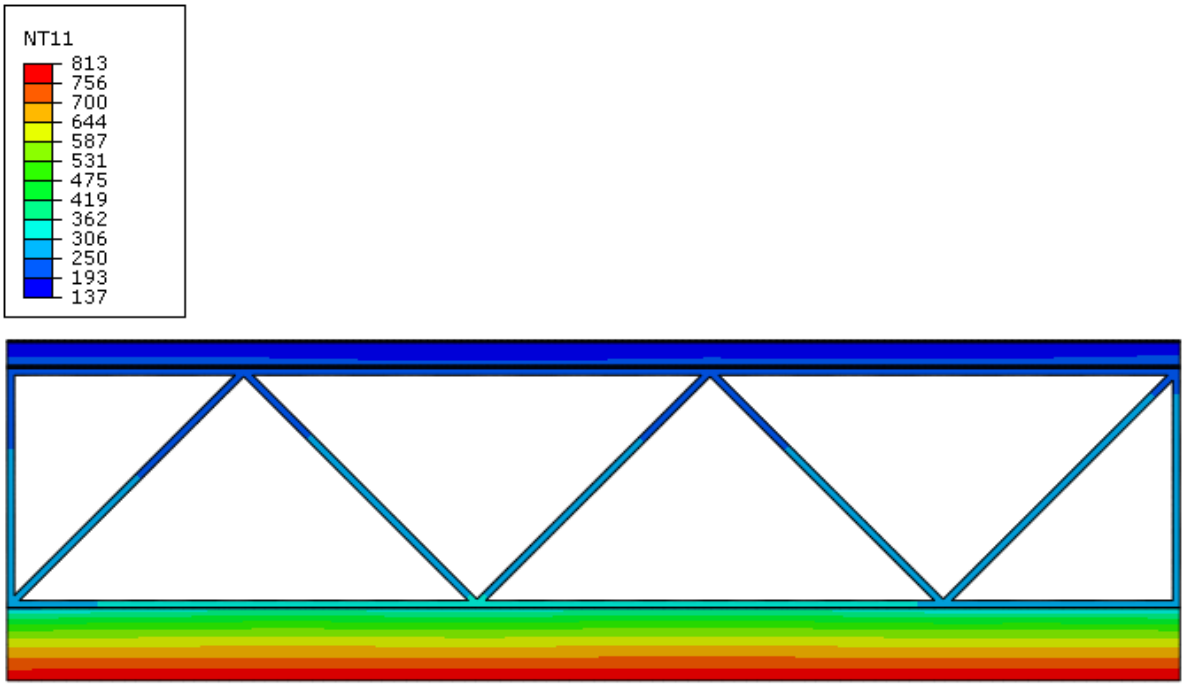

Figure 68. The temperature distribution after 28 minutes of the double-walled aluminum extrusion with an insulating bottom blanket layer and a top surface ply-metal layer [˚C]

6.5.4.2 Fire Resistant Boards

Figure 69 shows the results of the thermal analysis for the case in which a 13 mm (0.5 inch) thick Type X gypsum board was attached to the underside of the floor extrusion; the characteristics of the board layer are provided in Section 6.3.3.2. The time at which the temperature of the top surface reached the thermal failure criterion was greater than 30 minutes; the analysis was only conducted to simulate 30 minutes of exposure. Again, the temperature of the bottom flange of the aluminum extrusion at this time was only about 350 ˚C, well below the melting temperature.

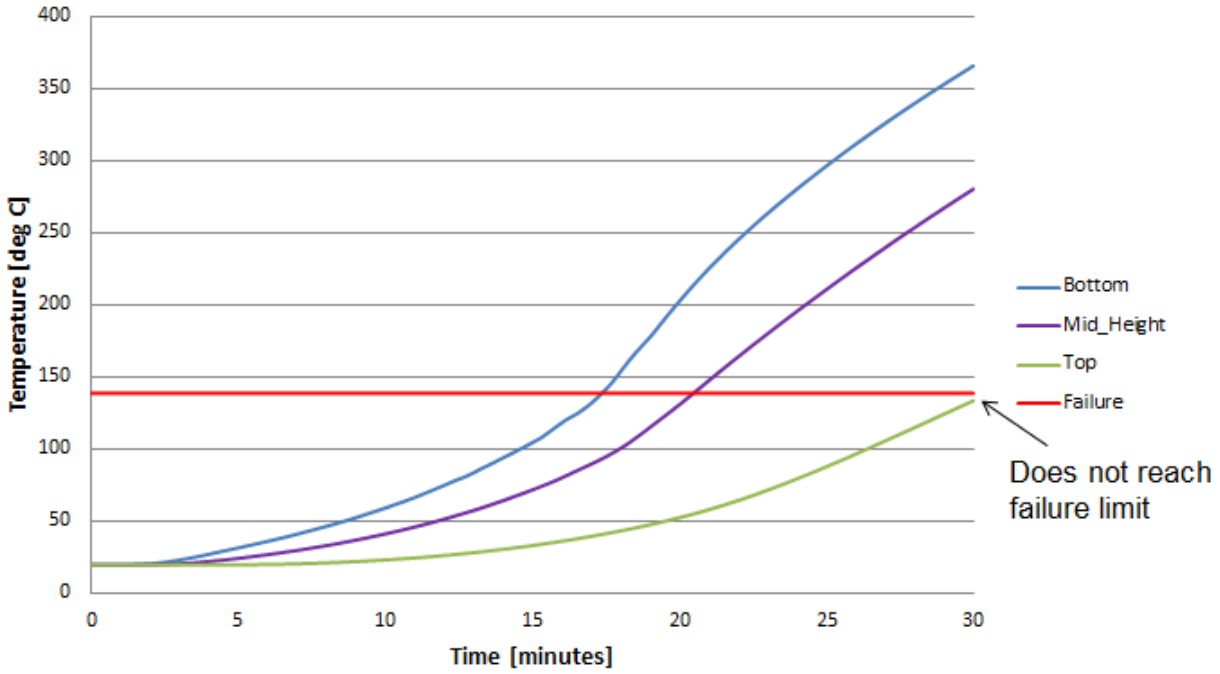

Figure 69. The temperature-time histories of the double-walled aluminum extrusion with an insulating bottom board layer and a top surface ply-metal layer

6.5.4.3 Epoxy Intumescent

Figure 70 shows the results of the thermal analysis for the case in which a 5 mm (0.2 inch) thick epoxy intumescent coating was applied to the underside of the floor extrusion; the characteristics of the intumescent layer are provided in Section 6.3.3.3. The time at which the temperature of the top surface reached the thermal failure criterion was approximately 23 minutes.

The expansion of the epoxy intumescent coating when it formed a char layer was not simulated (i.e., a constant thickness was considered). This expanding char layer was difficult to simulate and there was no publicly available data on which to base the model. Inclusion of this effect would increase the time required to reach the failure limit temperature on the top surface.

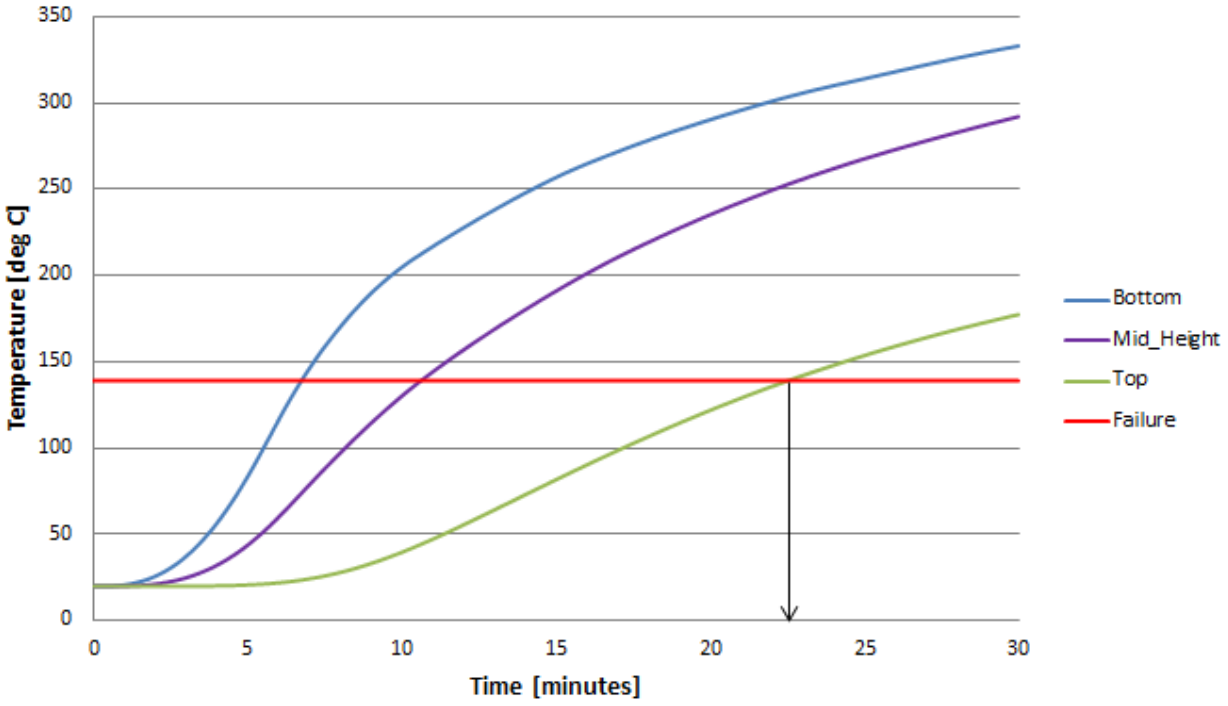

Figure 70. The temperature-time histories of the double-walled aluminum extrusion with an insulating intumescent coating on the bottom surface and a top surface ply-metal layer

6.6 Discussion

The results of the thermal analysis of double-walled extrusion configurations supported the general expectation that it is difficult to meet the requirements of Appendix B of CFR 49 Part 238.103, in which a floor assembly is exposed to the ASTM E119 temperature-time history without having its top surface temperature exceed 139 ˚C and without structural failure in a 15 minute period. The analysis indicated that failure to comply with the standard was due to exceeding allowable surface temperature rather than structural failure. However, the results did suggest that the bottom surface of the extrusion approached the melting temperature.

The inclusion of bottom insulating materials can greatly increase the performance of the aluminum floors. Table 18 provides a summary of the analysis results.

Table 18. Performance of assembly with ply-metal floor and applied fire protection

Configuration	Estimated Fire Resistance Rating of the Assembly (minutes)
No additional layers	9
No heat transfer within internal spaces	9
With ply-metal floor	16
Mineral wool blanket	28
Type X gypsum board	>30
Epoxy intumescent coating	23

Each of the three simulated protective bottom layers provided protection beyond the 15 minutes required by the Code of Federal Regulations and exceeded or approached the required 30 minutes of NFPA 130. It was likely that the mineral wool blanket and intumescent coating thicknesses and properties could have been adjusted to achieve a 30-minute rating.

The additional weight per railcar associated with these layers varied from approximately 350 lbs for the blanket material to 1,000 lbs for the board material. An active fire suppression system would also likely add over 1,000 lbs per rail car. All of these systems would need to be engineered to ensure sufficient durability over the life of the car, or for reasonable maintenance periods, for a vehicle that experiences a substantial vibration environment.

7. Conclusion and Discussion

The work reported here had the objective of determining the effect on weight of increasing crashworthiness performance of high-speed trains. Weight is a particularly critical factor for high-speed trains because of the effect it has on acceleration and on the overall wear-and-tear of both rail vehicles and infrastructure, each of which are finely tuned in high-speed operations to provide safe and comfortable service to customers.

The work focused on four vehicle subsystems: occupied volume (car shell), energy absorbers, seats, and structural fire protection systems. In each case, a baseline model was generated that was approximately representative of current high-speed trains. This model was selected to meet the recently proposed Tier III requirements, but with little or no margin. Variations on this baseline model were then generated to provide greater crashworthiness performance and the weight associated with the changes was determined. FEA was used to evaluate the performance in each case, except for energy absorbers.

Key results are summarized in Table 19. None of these incremental increases in weight were substantial compared to the overall weight of a high-speed rail car (about 120,000 lbs with all equipment, but no passengers.) The occupied volume can be strengthened by using extrusions with thicker wall sections and by adding reinforcement at locations of stress concentration.

Table 19. Summary of the increase in weight with increased crashworthiness performance

System	Baseline performance	Adjusted performance	Incremental weight increase per car
Occupied volume	800 kip strength along the crush zone load path, no yield	1,000 kip strength along the crush zone load path, no yield	1,500 lbs
Energy absorbers	5.5×10^6 ft-lbf (corresponded approximately to a 20 mph collision scenario)	8.7×10^6 ft-lbf (corresponded approximately to a 25 mph collision scenario)	1,600 lbs
Seats	GM/RT2100 minimum crash pulse ($\Delta V = 5$m/s)	8g/250ms crash pulse	18 lbs/seat (about 1,100 lbs/car)
Structural fire protection	E119 temperature-time history for 15 minutes	E119 temperature-time history for 30 minutes	350 lbs

The estimated weight penalty associated with increasing the required collision scenario speed by 5 mph was comparable to that required to increase the occupied volume strength by 25 percent. However, this assessment was complicated by a few factors. The result given in Table 19 was based on the assumption that all additional energy absorption must have occurred in the impacted end of the lead vehicle. In reality, it may be possible at a higher collision speed to achieve greater contribution from the existing energy absorbers at the coupled interfaces if they are present. On the other hand, if some of the additional required energy absorption is achieved by using higher crush forces, rather than additional car length, the strength of the occupied volume will need to increase, and this will also lead to greater weight. If the occupied volume strength were increased by 25 percent anyway, then there would probably be no more weight penalty for energy absorption than that given in Table 19; that is, the weight penalty for both changes would be about 3,200 lbs. A substantially lower increase in absorber weight could be achieved if

carbon fiber-reinforced polymers were used instead of metal, but the cost would be much higher and it would be more difficult to ensure repeatable behavior.

The weight penalty estimated for seats given in Table 19 was based on compartmentalization and, effectively, seat strength measures of crashworthiness improvement; the results suggested that the injury measures were probably not controlling. In effect, seat stiffness in this study was modified by simply increasing the thickness of the model elements. Seat stiffness could be modified with a lower weight penalty by changing the depth of sections or using alternative materials, such as fiber-reinforced polymers. Such changes would affect meeting spatial and cost requirements. Higher seat connection strength is also required with more severe crashworthiness requirements, but these can likely be accommodated without a substantial weight penalty.

The results of the study of fire protection supported the general belief that it is difficult for cars built from aluminum extrusions to meet the current U.S. structural fire resistance requirements, particularly if a 30-minute duration is specified. Nevertheless, it seems likely that the requirements could be met with the addition of a layer of fire protection material on the underside of the aluminum floor structure. The additional weight in this case could be as low as 350 lbs/car if a mineral wool blanket system were used and if the attachment approach were sufficiently robust.

In closing, note that a methodology of simply changing a baseline configuration to meet new requirements and calculating weight differentials ignores the elements of the actual design process. In reality, a high-speed train will have limitations on the weight, usually expressed in terms of axle load, and the systems incorporated into the train must be adjusted to meet this weight budget. If additional energy absorption is required and it can only be achieved by adding weight, then some other system or systems will be modified to reduce their weight for an even balance. Such changes promote innovation and the pursuit of alternate equipment. Thus, one may also view the results of this study as being indicative of the degree of difficulty created by requiring higher crashworthiness performance.

8. References

1. Vanolo, P., Magnani, A., Debbia, E., Gugliesi, C., Cencio, L., and Gerbaudo, L. (1995). Body Structure for Railway Vehicles. U.S. Patent 5383406.
2. Stringfellow, R.G., Mayville, R.A., and Fulton, C.C. (2002). Modeling the Crush Behavior of Welded Aluminum Extrusions. *World Congress on Computational Mechanics.*
3. Tsuruda, H., Hattori, M. Okazaki, M., Yamada, H., Kikumoto, K., Watanabe, T., Takayama, R., and Okuno, S. (1993). Vehicle body construction having longitudinally elongated extruded panels and continuous welds joining the panels. U.S. Patent 5267515.
4. The Aluminum Association. (2010). Aluminum Design Manual. Arlington, VA: The Aluminum Association.
5. U.S. Patent and Trade Office. Buffer Cars; Arrangements or Construction of Railway Vehicles for Protecting Them in Case of Collisions [B61G 11/10].
6. Mayville, R.A. Rail Vehicle Component Impact Tests and Analysis. *80th Shock and Vibration Symposium,* October 25-29, 2009, San Diego, CA.
7. Jacob, G.C., Fellers, J.F., Simunovic, S., and Starbuck, J.M. (2002). Energy Absorption in Polymer Composites for Automotive Applications. *J. Composite Materials, 36*(7), 813-850.
8. Severson, K., Perlman, A.B., and Stringfellow, R.G. Quasi-static and dynamic sled testing of prototype commuter rail passenger seats. *Proceedings of the 2008 IEEE/ASME Joint Rail Conference,* April 22-23, 2008, Wilmington, DE.
9. Federal Railroad Administration. Development of Prototype Commuter Rail Passenger Seats for Use in CEM Passenger Rail Cars [forthcoming]. Washington, DC: U.S. Department of Transportation.
10. ASTM International. (2012). ASTM E119-12: Standard Test Methods for Fire Tests of Building Construction and Materials.
11. National Fire Protection Association. (2010). NFPA 130: Standard for Fixed Guideway Transit and Passenger Rail Systems.
12. British Standards. (2002). BS6853:1999: Code of Practice for Fire Precautions in the Design and Construction of Passenger Carrying Trains.
13. European Committee for Standardization. (2013). EN45545-3: Railway Applications – Fire Protection on Railway Vehicles – Part 3: Fire Resistance Requirements for Fire Barriers.
14. American Society for Metals. (1998). Metals Handbook, Desk Edition (2nd ed.).
15. Brommer, J.A. and Percival, C.M. (1970, June). Elevated Temperature Elastic Moduli of 2024 Aluminum Obtained by a Laser-Pulse Technique. *Experimental Mechanics.*
16. Incropera, F.P., and D.P. DeWitt, D.P. (2002). *Introduction to Heat Transfer* (4th ed.). Hoboken, NJ: John Wiley & Sons.
17. SP Research Institute. (2004). Measurement of Thermal Properties of Elevated Temperatures. Brandforsk Project 328-031. SP Report 2004:46.

18. Manzello, S.L., Park, S.H., Mizukami, T., and Bentz, D.P. Measurement of Thermal Properties of Gypsum Board at Elevated Temperatures. *Proceedings of the 5th International Conference on Structures in Fire, National Institute of Standards and Technology,* 2008, 656-665.

19. Koo, J.H. (1997). Thermal Characteristics Comparison of Two Fire Resistant Materials. *Journal of Fire Sciences, 15,* 203-221.

Abbreviations and Acronyms

Abbreviation or Acronym	Name
ATD	Anthropomorphic Test Device
ETF	Engineering Task Force
FRA	Federal Railroad Administration
OVI	Occupied Volume Integrity
RSAC	Railroad Safety Advisory Committee